



**Wear Behavior of Hardfacing on 3.5% Chromium Cast Steel by Submerged Arc
Welding**

Hein Zaw Oo

**A Thesis Submitted in Fulfillment of the Requirements for
the Degree of Master of Engineering in Materials Engineering
Prince of Songkla University
2018**

Copyright of Prince of Songkla University



**Wear Behavior of Hardfacing on 3.5% Chromium Cast Steel by Submerged Arc
Welding**

Hein Zaw Oo

**A Thesis Submitted in Fulfillment of the Requirements for
the Degree of Master of Engineering in Materials Engineering**

Prince of Songkla University

2018

Copyright of Prince of Songkla University

Thesis Title Wear Behavior of Hardfacing on 3.5% Chromium Cast Steel by
Submerged Arc Welding
Author Mr. Hein Zaw Oo
Major Program Materials Engineering

Major Advisor

.....
(Asst. Prof. Dr. Prapas Muangjunburee)

Examining Committee:

.....Chairperson
(Dr. Somjai Janudom)

.....Committee
(Asst. Prof. Dr. Prapas Muangjunburee)

.....Committee
(Asst. Prof. Dr. Thawatchai Plookphol)

.....Committee
(Dr. Kanit Tapasa)

The Graduate School, Prince of Songkla University, has approved this thesis as fulfillment of the requirements for the Master of Engineering Degree in Materials Engineering.

.....
(Prof. Dr.Damrongsak Faroongsarng)
Dean of Graduate School

This is to certify that the work here submitted is the result of the candidate's own investigations. Due acknowledgement has been made of any assistance received.

..... Signature

(Asst. Prof. Dr. Prapas Muangjunburee)
Major Advisor

..... Signature

(Mr. Hein Zaw Oo)
Candidate

(4)

I hereby certify that this work has not been accepted in substance for any other degree, and is not being currently submitted in candidature for any degree.

..... Signature

(Mr. Hein Zaw Oo)
Candidate

Thesis Title	Wear Behavior of Hardfacing on 3.5% Chromium Cast Steel by Submerged Arc Welding
Author	Mr. Hein Zaw Oo
Major Program	Materials Engineering
Academic Year	2017

ABSTRACT

Hardfacing is an economical process for maintaining or repairing the engineering components due to wear problems. In this project, twelve samples of 3.5% Cr steel plates were hardfaced using austenitic stainless-steel buffer electrodes and martensitic steel hardfacing electrodes with a twin-wires submerged arc welding process. Identical welding procedures were repeated in all samples. The main objective of this research is to maximize wear resistance obtained in the hardfaced layer obtained by optimizing the welding parameters. The heat inputs for single layer and three layers hardfacing were varied using three different welding currents: 500A, 600A and 700A while keeping welding voltages and travel speeds constant; and two different welding polarities (AC and DC+). Single buffer layer was deposited on the base metal and preheating on the base metal plate at 350 °C was kept constant for all experiments. An optical microscope was used to analyze macrostructures and microstructures of the base metal, heat affected zone, buffer layer and hardfacing layers. The structures of single layer and three layers hardfacing and worn surfaces of the wear tested samples of three layers hardfacing were also taken using a scanning electron microscope (SEM). Chemical compositions of phases seen on SEM images were also determined using EDX. The amounts of martensite phase seen in the cross-sections and top surfaces optical micrograph of three layers hardfacing and dilution percentage of all samples were determined using Image J software. A Vickers hardness tester was used to measure microhardness values of the cross-sectional and top surface of the hardfaced samples. Wear resistance based on mass loss of the hardfaced samples was tested using a dry sand rubber wheel machine according to A of ASTM G65 standard procedure. The microstructural examinations showed absence of welding defects and good bonding between layers. Wear resistance results showed lower wear were found in samples welded using AC polarity. Also, those samples

showed higher hardnesses, dilution, the volume fraction of martensite phase compared to samples welded using DC+ polarity. Percent dilution correlated with hardness and microstructure of hardfaced layers. The microstructures and amount of martensite phase present influence the wear resistance of hardfaced layers. In addition, the abrasive mass loss of single layer hardfacing was higher than that of three layers hardfacing because the microstructure of single layer hardfacing showed higher amount of austenite phase due to the effect of dilution with austenitic buffer layer. In summary, the optimum procedure to get hardfacing wear resistance is to use 15 KJ/cm heat input obtained using 500A with AC polarity for both single layer and three layers hardfacing.

ACKNOWLEDGEMENTS

No thesis of this sort is possible without sympathetic advice, constructive criticism, kindness and innovative ideas from my advisor, Assistant Professor Dr. Prapas Muangjunburee. I would like to deeply thank him as he has been giving me the opportunity to study my Master of Engineering degree since when he interviewed me for consideration of the fully funded scholarship.

I am beholden to Mr. Buntoeng Srikarun, Ph.D. student at Department of Mining and Materials Engineering, Prince of Songkla University, for supporting my experiments and providing beneficial ideas and suggestions.

I am also grateful to the thesis examining committee: Dr. Somjai Janudom, Asst. Prof. Dr. Prapas Muangjunburee, Asst. Prof. Dr. Thawatchai Plookphol and Dr. Kanit Tapasa, for their precious time and fruitful recommendation.

I am obliged to the Higher Education Research Promotion and Thailand's Education Hub for Southern Region of ASEAN Countries Project Office of the Higher Education Commission for giving me a chance and allowing me to earn Master of Engineering Degree here, at Prince of Songkla University, with the full scholarship.

I would fully appreciate the kind suggestions and ideas of Dr. Salita Petchsang, Lecturer at Department of Mining and Materials Engineering, Prince of Songkla University as well.

My sincere thanks also go to the Department of Mining and Materials Engineering, Prince of Songkla University for providing all necessities of my experiments and supporting equipment and valuable facilities.

Finally, I would greatly love to acknowledge, and my most profound debts are to my beloved parents, U Tin Htun Oo and Daw Yee Yee Shein, and then my lovely sister, Miss Khaing Wutt Yee Htun, for their eternal love, endless support and optimistic encouragement.

I would never do such a great work without you all.

Hein Zaw Oo

Table of Contents

	Pages
Title page	(1)
Approval page	(2)
Certification	(3)
Abstract	(5)
Acknowledgements	(7)
Table of Contents	(8)
List of Tables	(12)
List of Figures	(13)
List of Abbreviations	(18)
Chapter 1 Introduction	1
1.1 Background and motivation	1
1.2 Objectives	2
1.3 Benefits of research	2
1.4 Research scope	2
1.5 Research plans	3
Chapter 2 Theories and Literature Reviews	4
2.1 Theory of wear	4
2.1.1 Abrasive wear	5
2.2 Protection against wear	6
2.2.1 Welding hardfacing	7
2.3 Submerged arc welding	8
2.3.1 Principles of operation	9
2.3.2 Welding current	11
2.3.3 Welding arc voltage	11
2.3.4 Electrode stick-out	12
2.3.5 Travel speed during welding	12
2.3.6 Wire diameter	13
2.3.7 Heat input	13
2.4 Metallurgy of welding	14

Table of Contents (Continued)

	Pages
2.4.1 Heat affected zone (HAZ)	14
2.4.2 Preheating	15
2.4.3 Dilution	16
2.5 Hardfacing materials	17
2.5.1 Type of electrodes	17
2.5.2 Hardfacing filler metals	18
2.5.3 Martensitic alloys	19
2.5.4 Austenitic alloys	19
2.6 Hardness testing	20
2.7 Abrasive wear testing	21
2.8 Literature reviews	22
Chapter 3 Experimental Procedures	26
3.1 Materials and equipment	26
3.1.1 Base metal (3.5% Cr)	26
3.1.2 Electrodes	27
3.1.3 Flux	28
3.1.4 Power source	28
3.1.5 Thermocouple and data logger	29
3.1.6 Flexible ceramics pad heaters	29
3.1.7 Band saw	30
3.1.8 Abrasive cut-off machine	30
3.1.9 Vertical milling machine	31
3.1.10 Metallographic polishing	31
3.1.11 Etching reagents	32
3.1.12 Microscopes	33
3.1.13 Micro Vickers hardness tester	35
3.1.14 Abrasive wear testing instrument (ASTM G65)	35
3.1.15 Precision balance	36
3.1.16 Other equipment	37

Table of Contents (Continued)

	Pages
3.2 Research procedures	37
3.3 Sample preparation for welding	38
3.4 Preheating	38
3.5 Deposition using submerged arc welding	40
3.6 Macro/microstructural characterization	42
3.7 Phase analysis on microstructure by ImageJ	45
3.8 Hardness testing	49
3.9 Abrasive wear testing	50
Chapter 4 Results and Discussion	52
4.1 Base metal	52
4.2 Welded sample	53
4.3 Macrostructural analysis	53
4.4 Microstructural characterization	56
4.4.1 Heat affected zone	56
4.4.2 Buttering	58
4.4.3 Single layer hardfacing	61
4.4.4 First of three layers hardfacing	62
4.4.5 Second of three-layer hardfacing	63
4.4.6 Third of three layers hardfacing	64
4.4.7 Top surface	66
4.4.8 SEM images	69
4.4.9 Emission-dispersive x ray result (Point Scan)	74
4.4.10 Emission-dispersive x ray result (Point Scan)	76
4.5 Amount of martensite phase in the micrographs	79
4.6 Phases identified by X-ray diffraction (XRD)	79
4.7 Dilution	81
4.8 Hardness distributions	83
4.8.1 Cross-sectional hardness	83
4.8.2 Top surface hardness	85

Table of Contents (Continued)

	Pages
4.9 Abrasive mass loss	88
Chapter 5 Conclusions and recommendations	91
5.1 Conclusions	91
5.2 Recommendations	92
References	93
Appendix A: Single layer hardness data	97
Appendix B: Three layers hardness data	110
Appendix C: Emission-dispersive X-ray spectroscopy results of Single and Three layers hardfacing	129
Appendix D: List of Publications	134
Vitae	156

List of Tables

Tables	Pages
3.1 Chemical composition of the base metal	26
3.2 Chemical composition of wire electrode for hardfacing (Martensitic)	27
3.3 Chemical composition of wire electrode for Buffer (Austenitic)	27
3.4 Chemical composition of flux for Submerged Arc Welding	28
3.5 Standard parameters of ASTM G65	36
3.6 Fixed welding conditions	41
3.7 Variable parameters of the experiments	42
4.1 Chemical composition of single layer hardfacing analyzed by EDX	74
4.2 Chemical composition of three layers hardfacing analyzed by EDX	75
4.3 Chemical composition of three layers hardfacing analyzed by EDX	76
4.4 Percent dilution for all conditions	82
4.5 Abrasive wear test results of all experimental conditions	88

List of Figures

Figures	Pages
2.1 Flowchart for the types of wear	5
2.2 Four different kinds of abrasion (a) Low-stress abrasion, (b) High-stress abrasion, (c) Gouging abrasion, and (d) Polishing	6
2.3 Welding process for repair and hardfacing	8
2.4 Submerged arc welding process	9
2.5 Operation of Single-wire Submerged arc welding	10
2.6 Function of Flux during welding by Submerged arc welding	10
2.7 Effect of increased welding current	11
2.8 Effect of increased welding voltage	12
2.9 Effect of increased electrode stick-out	12
2.10 Effect of increased Travel speed	13
2.11 Effect of increased wire diameter	13
2.12 Scheme diagram of phase transformation of the workpiece during welding	14
2.13 Effects of preheating temperature on hardness	16
2.14 Schematic diagram for welding dilution	16
2.15 Different types of welding electrode for submerged arc welding	17
2.16 A section through different kinds of wire electrode	18
2.17 The relation of welding current and deposition rate using different type of wire	18
2.18 Typical microstructure of Martensitic type	19
2.19 Typical microstructure of Austenitic type	20
2.20 Principle of hardness testing	20
2.21 ASTM G65 standard abrasion test	21
2.22 Abrasion testing (a) Morphology of abrasive particle (dry sand) and (b) Principle of abrasion test	22
3.1 3.5% Cr steel plate	26
3.2 Welding Electrodes (a) Hardfacing electrode (b) Buffer electrode	27
3.3 Welding machine (a) ESAB A2 Multitrac with A2-A6 Process Controller (b) ESAB Aristo 1000 AC/DC SAW power source	28

List of Figures (Continued)

Figures	Pages
3.4 Thermocouple and data logger	29
3.5 Flexible ceramics heating pad	29
3.6 Band saw	30
3.7 Abrasive cut-off machine	30
3.8 Vertical Milling Machine	31
3.9 Pace Technologie Nano 1000T single Grinder/Polisher	32
3.10 Polishing equipment (a) Metallographic paper (b) 5 μm alumina powder	32
3.11 Etching reagents	33
3.12 Optical microscope for macrostructural analysis	33
3.13 Optical microscope for microstructural analysis	34
3.14 Scanning Electron Microscope	34
3.15 Micro Vickers hardness tester	35
3.16 Abrasion wear testing machine	35
3.17 Precision electric balance	36
3.18 Experimental flow system	37
3.19 Preheating process(a) preheating before welding (b) arc welding transformer for preheating	38
3.20 Setting before welding (a) showing the parameters (b) ready for welding	39
3.21 Conducting welding process (a) initiating the welding process (b) hardfacing applied on the buffer layer	39
3.22 The deposited sample	40
3.23 Schematic diagram of welding design (a) Single layer hardfacing (b) three layers hardfacing	41
3.24 Welded sample	42
3.25 Cutting area of the welded sample	43
3.26 Cold-molded specimen	43
3.27 Polishing a metallographic specimen	44
3.28 Selecting the 8-bit type image	45
3.29 The 8-bit type image revealed the greyscale colour	45

List of Figures (Continued)

Figures	Pages
3.30 Setting scales	46
3.31 Installing specific values and unit	46
3.32 Adjusting to threshold	47
3.33 Setting scale in threshold	47
3.34 Select the function of analyze particles	48
3.35 Analyzing particles	48
3.36 Final results	49
3.37 Hardness values and parameters of test appeared on the digital screen	49
3.38 The abrasion specimen (a) before testing (b) tested specimen	50
3.39 Measuring weight of wear specimen (a) Initial weight (b) testing the specimen (c) final weight	50
4.1 Microstructure of 3.5% Cr steel	52
4.2 The appearance of the sample after depositing	53
4.3 The macrostructure of single layer hardfacing (a) 1B 1H 500A AC (b) 1B 1H 600A AC (c) 1B 1H 700A AC (d) 1B 1H 500A DC+ (e) 1B 1H 600A DC+ (f) 1B 1H 700A DC+	54
4.4 The macrostructure of three layers hardfacing (a) 1B 3H 500A AC (b) 1B 3H 600A AC (c) 1B 3H 700A AC (d) 1B 3H 500A DC+ (e) 1B 3H 600A DC+ (f) 1B 3H 700A DC+	55
4.5 The heat affected zone microstructure of single layer hardfacing (a) 1B 1H 500A AC (b) 1B 1H 500A DC+ (c) 1B 1H 600A AC (d) 1B 1H 600A DC+ (e) 1B 1H 700A AC (f) 1B 1H 700A DC+	56
4.6 The heat affected zone microstructure of three layers hardfacing (a) 1B 3H 500A AC (b) 1B 3H 500A DC+ (c) 1B 3H 600A AC (d) 1B 3H 600A DC+ (e) 1B 3H 700A AC (f) 1B 3H 700A DC+	57
4.7 The microstructure of buffer layer for single layer hardfacing (a) 1B 1H 500A AC (b) 1B 1H 500A DC+ (c) 1B 1H 600A AC (d) 1B 1H 600A DC+ (e) 1B 1H 700A AC (f) 1B 1H 700A DC+	59

List of Figures (Continued)

Figures	Pages
4.8 The microstructure of buffer layer for three layers hardfacing (a) 1B 3H 500A AC (b) 1B 3H 500A DC+ (c) 1B 3H 600A AC (d) 1B 3H 600A DC+ (e) 1B 3H 700A AC (f) 1B 3H 700A DC+	60
4.9 The microstructure of single layer hardfacing (a) 1B 1H 500A AC (b) 1B 1H 500A DC+ (c) 1B 1H 600A AC (d) 1B 1H 600A DC+ (e) 1B 1H 700A AC (f) 1B 1H 700A DC+	61
4.10 The microstructure of first of three layers hardfacing (a) 1B 3H 500A AC (b) 1B 3H 500A DC+ (c) 1B 3H 600A AC (d) 1B 3H 600A DC+ (e) 1B 3H 700A AC (f) 1B 3H 700A DC+	62
4.11 The microstructure of second of three layers hardfacing (a) 1B 3H 500A AC (b) 1B 3H 500A DC+ (c) 1B 3H 600A AC (d) 1B 3H 600A DC+ (e) 1B 3H 700A AC (f) 1B 3H 700A DC+	64
4.12 The microstructure of third of three layers hardfacing (a) 1B 3H 500A AC (b) 1B 3H 500A DC+ (c) 1B 3H 600A AC (d) 1B 3H 600A DC+ (e) 1B 3H 700A AC (f) 1B 3H 700A DC+	65
4.13 The area identification for microstructural analysis of single layer top surface	66
4.14 The top surface microstructure of single layer hardfacing (a) 1B 1H 500A AC (b) 1B 1H 500A DC+ (c) 1B 1H 600A AC (d) 1B 1H 600A DC+ (e) 1B 1H 700A AC (f) 1B 1H 700A DC+	66
4.15 The area identification for microstructural analysis of three layers top surface	67
4.16 The microstructure of third of three layers hardfacing (a) 1B 3H 500A AC (b) 1B 3H 500A DC+ (c) 1B 3H 600A AC (d) 1B 3H 600A DC+ (e) 1B 3H 700A AC (f) 1B 3H 700A DC+	68
4.17 SEM image of single layer hardfacing compared with the best and worst condition (a) 1B 1H 500A AC and (b) 1B 1H 600A DC+	69
4.18 SEM image of single layer hardfacing compared with different polarities (a) 1B 1H 500A AC and (b) 1B 1H 500A DC+	70
4.19 SEM image of three layers hardfacing compared to the best and worst condition (a) 1B 3H 500A AC and (b) 1B 3H 600A DC+	71

List of Figures (Continued)

Figures	Pages
4.20 SEM image of three layers hardfacing compared to different polarities (a) 1B 3H 500A AC and (b) 1B 3H 500A DC+	72
4.21 The SEM image of worn surfaces (a) 1B 3H 500A AC (b) 1B 3H 500A DC+ (c) 1B 3H 600A AC (d) 1B 3H 600A DC+ (e) 1B 3H 700A AC (f) 1B 3H 700A DC+	73
4.22 EDX point scanned on the SEM image of single layers hardfacing	74
4.23 EDX point scanned on the SEM image of three layers hardfacing	75
4.24 EDX mapping analysis of the sample welded with 500A using AC polarity	77
4.25 EDX mapping analysis of the sample welded with 700A using AC polarity	78
4.26 The amount of martensite phase in the micrographs analyzed by ImageJ	79
4.27 XRD patterns of single layer hardfacing	80
4.28 XRD patterns of three layers hardfacing	80
4.29 Single pass macrographs for measuring percent dilution (a) 1B 3H 500A AC (b) 1B 3H 500A DC+ (c) 1B 3H 600A AC (d) 1B 3H 600A DC+ (e) 1B 3H 700A AC (f) 1B 3H 700A DC+	81
4.30 Welding dilution (%)	82
4.31 Cross-sectional hardness values across single layer hardfacing	83
4.32 Cross-sectional hardness values across three layers hardfacing	84
4.33 Top surface hardness of single layer hardfacing	85
4.34 Top surface hardness of three layers hardfacing	85
4.35 Average top surface hardness of single layer hardfacing	86
4.36 Average top surface hardness of three layers hardfacing	87
4.37 Abrasive mass loss result comparing different layers (single and three)	89
4.38 Abrasive mass loss result comparing different polarities (AC and DC+)	90

List of Abbreviations

A	Ampere
AC	Alternating Current
Al ₂ O ₃	Aluminum Oxide
ASTM	American Society for Testing and Materials
B	Buffer Layer
BM	Base Metal
C	Carbon
°C	Celsius
CaF ₂	Calcium Fluoride
CaO	Calcium Oxide
Cr	Chromium
DC+	Direct Current Electrode Positive
EN	European Standard
Fe	Ferrous
H	Hardfacing Layer
HAZ	Heat Affected Zone
HV	Vickers Hardness
MgO	Magnesium Oxide
Mn	Manganese
MnO	Manganese Oxide
Mo	Molybdenum
Ni	Nickel
P	Phosphorus
SAW	Submerged Arc Welding
Si	Silicon
SiO ₂	Silicon Dioxide
TiO ₂	Titanium Dioxide
V	Voltage

Chapter-1

Introduction

1.1 Background and motivation

In the mining industry, the major component of the processing equipment, such as the crusher suffer severe wear problems. Different kinds of wear mechanism such as abrasion, impact and gouging etc. can occur on the surfaces of the crusher. When a part of crusher fails due to wear, the processing plant encounters many economic difficulties. Replacing a new crusher to continue plant operations is expensive. Therefore, the worn parts of the crusher and similar engineering components are usually repaired to extend the duration of their service lives.

At Mae Moh Mine, the electrical generating authority of Thailand (EGAT) is running a single roll coal crusher to generate electricity from coal. This power plant can generate about 2,100 MW of electricity using 50,000 tons of crushed coal per year. Crushing operation is one of the most important processes in that electricity generating plant.

The 3.5% Cr steel single roll coal crusher currently used at the Electricity Generating Authority of Thailand (EGAT) Mae Moh Lignite Coal Mine suffers from considerable abrasive and impact wear problems. The coal particles to be crushed from the mine are dropped from a high conveyor belt to the rotating roller surface causing impact wear. Further downstream the hard coal particles on the moving roller surface caused abrasive wear. That is, the machine surface components are damaged by heavy impacts and abrasive wear due to relative movements of hard abrasive trapped between the contacting surfaces moving under load.

In the current study, the effects of heat inputs (determined by the combination of welding current, weld voltage and weld travel speed used) and welding polarity (AC and DC+) of submerged arc welding on the wear resistance of a hardfaced 3.5% Cr steel single roll coal crusher from Mae Moh lignite mine was investigated by correlating the metallurgical structures and mechanical properties of the hardfaced deposits with wear rates obtained. The wear resistance of hardfaced samples obtained using

submerged arc welding process were tested using a dry sand rubber wheel abrasive wear testing machine according to ASTM G65 Standard procedure A.

1.2 Objectives

The objectives of this study are -

1.2.1 To study wear behaviour of the coal crusher and to investigate suitable hardfacing material to increase the abrasive wear resistance of 3.5% Cr steel.

1.2.2 To study hardfacing techniques for repairing single roll coal crusher.

1.2.3 To study metallurgical properties (Micro and Macro structure) and the associated mechanical properties-particularly the hardnesses and abrasive wear resistances of hardfaced layers.

1.3 Benefits of research

The following benefits are expected from this study.

1.3.1 Increase the knowledge to analyze the abrasive wear resistance of coal crusher.

1.3.2 Selecting a suitable hardfacing process for coal crusher.

1.3.3 Controlling the wear problem of coal crusher.

1.3.4 Saving time and money and by improving the service life of the coal crusher.

1.4 Research Scope

This research was to compare welding parameters of hardfacing of 3.5% Cr steel for a coal crusher. A submerged arc welding (SAW) process was used to apply surface layers onto 3.5% Cr steel plates. Two different types of wire electrodes were applied. Martensitic steel type electrode was deposited for hardfacing layers and austenitic stainless-steel electrode was welded for the buffer layer. The microstructures and wear resistance obtained were compared after using different welding currents (500 A, 600 A and 700 A), welding polarities (AC and DC+) and a number of hardfacing layers (Single and Three Layers). The metallurgical structures of welded samples were analyzed using an optical microscope and a scanning electron microscope. Energy-dispersive X-ray spectroscopy (EDX) analysis was also done. The hardness values of both cross-section and the top surface of hardfaced deposits were evaluated using a

micro Vickers hardness tester and a dry sand-rubber wheel machine according to procedure A of the ASTM G65 standard was carried out to check the abrasive wear resistance based on the mass loss of specimens.

1.5 Research Plans

This study followed procedures outlined below.

1.5.1 Reviewing published literature from related topics

1.5.2 Collecting raw materials, necessary equipment and performing a preliminary experiment

1.5.3 Conducting research

1.5.4 Characterizing metallurgical testing (Macro/micro)

1.5.5 Running hardness and abrasive wear test

1.5.6 Analyzing and discussing results obtained

1.5.7 Writing research papers, conference proceedings and thesis.

Chapter-2

Theories and Literature Reviews

Application of crusher is the reduction of the original materials size to suitable pieces. Various types of crusher for mineral processing are jaw crusher, gyratory crusher, cone crusher, single roll crusher, double roll crusher, pulverizers, ring granulators etc. [1]. Type of wear affecting the components mainly depends on the application of components.

Wearing on coal crushers surfaces is a common problem for coal-fired power plants to generate electricity. Hundreds of tons of coal from mine must be crushed and then pulverized into powder every hour to keep combustion furnaces running. Crushers reduce coal chunks of up to 4 in. (101 mm) diameter into pieces of 1 in. (25mm) the diameter or smaller. [2]

2.1 Theory of Wear

Generally, the definition of wear is the gradual deterioration to a surface damaged by the removing materials and the mechanical reaction of a sliding solid, liquid, or gas [3]. The quality of most metal products is up to their surfaces condition. The deterioration of components surface is an important factor in engineering industries; it is also the main factor to determine the limit of life and performance of engineering components [4].

There are various kinds of wear mechanism. For example, different types of wear in machine components may involve at the same time. Therefore, the analysis of wear is not simple in most conditions. Friction mechanism and wearing happen where different surfaces are contacting or moving under applied loading. The single type wear is very rare to find. There are many kinds of wear type (Fig 2.1) occurring under a variety of conditions, including wearing environment, loading type, speeds of moving parts, temperature, the chemical composition of the surface, surface finishing, lubricant, the content of impurities, hardness and density of the machine parts [5].

The different types of wear are;

- 1) Abrasive Wear
- 2) Adhesion Wear
- 3) Erosion Wear
- 4) Surface fatigue

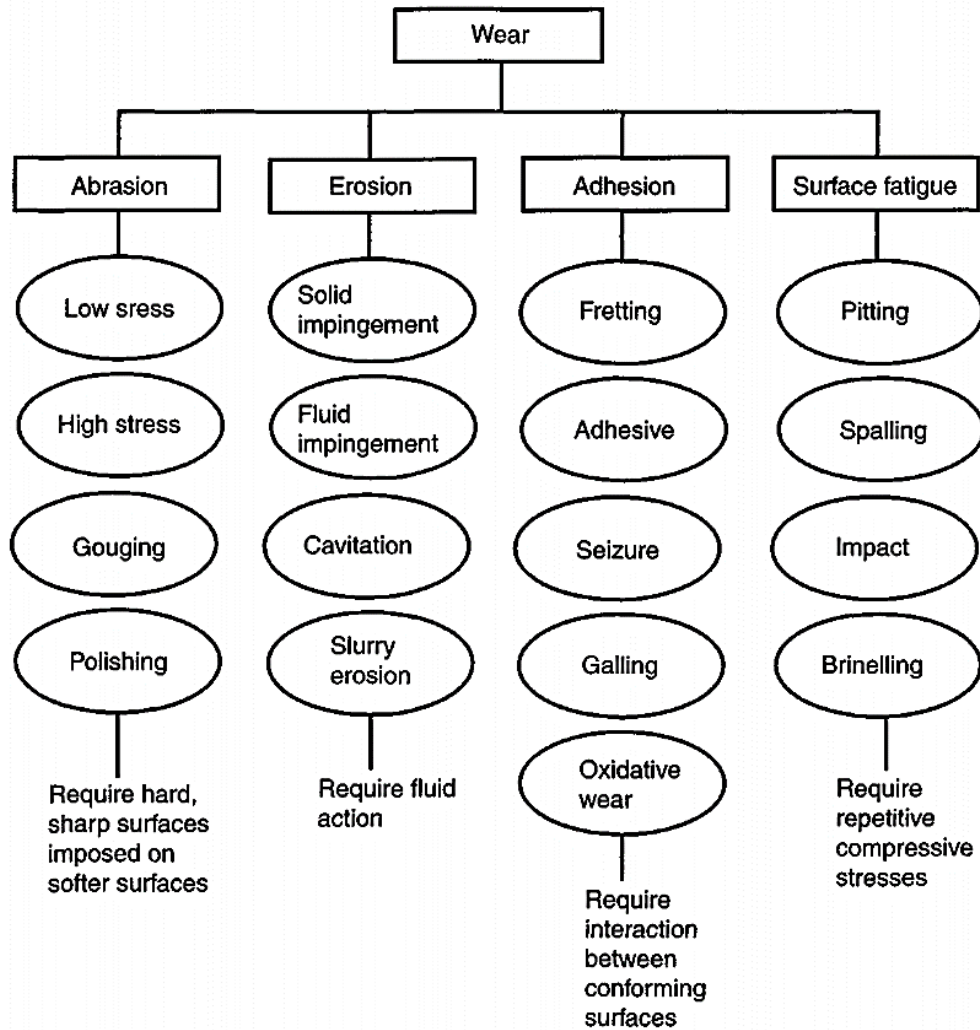


Fig 2.1 Flowchart for the types of wear [3]

2.1.1 Abrasive wear

Abrasive wear is the wear mechanism occurring surfaces or components because of hard particles sliding along a solid surface. Abrasion is typically classified in accordance with kinds of contact and environment of contact. Two-body abrasion

and three-body abrasion are studied by types of contact [3]. Abrasive wear is classified under two different abrasion:

(1.) Two body abrasion occurs when a surface is stronger than another contacting surface as can be seen in the figure. For instants: mechanical practices such as polishing, grinding, cutting, and machining.

(2.) Three body abrasion generally occurs when a small abrasive particle lodges in between the two softer surfaces and then it abrades one or both surfaces.

Abrasion wear can be often further categorized as low-stress abrasion, high-stress abrasion, gouging abrasion, and polishing, as shown in Fig 2.2. [3]

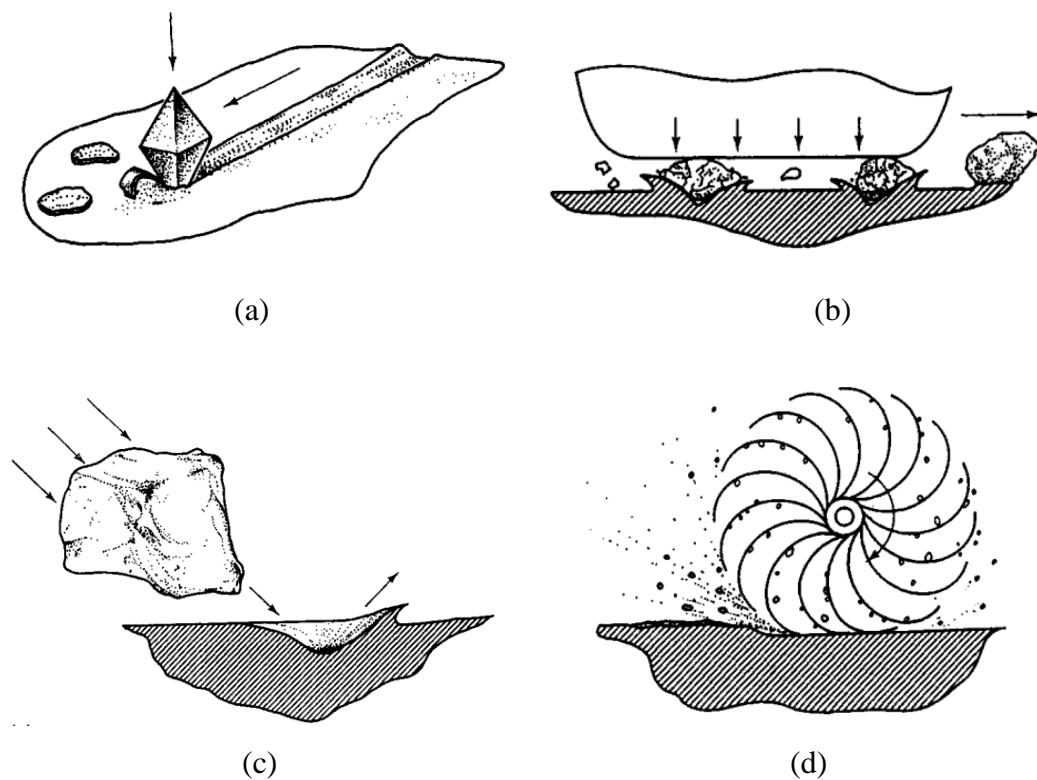


Fig 2.2 Four different kinds of abrasion (a) Low-stress abrasion, (b) High-stress abrasion, (c) Gouging abrasion, and (d) Polishing. [3]

2.2 Protection against Wear

Many materials and methods can be used to defence or mitigate wear. The selection of a suitable material and process depends on the actual service conditions, a knowledge of applicability and limitations of the materials and process, and their cost as well. The

sufficient knowledge needs to find a right decision on selecting the engineer or technician who can choose suitable materials to withstand wear [6].

Different methods for protecting the surface against wear are as follows:

1. Thermal treatments (e.g.: induction hardening, flame hardening)
2. Thermochemical diffusion treatments (e.g.: carburizing, nitriding)
3. Mechanical treatments (e.g.: shot-peening, grinding)
4. Plating (e.g.: electroplating, mechanical plating)
5. Thermal spraying (e.g.: flame, plasma)
6. Weld hardfacing (e.g.: Shielded Metal Arc Welding (SMAW), Submerged Arc Welding (SAW), Flux-Cored Arc Welding (FCAW)) [7]

2.2.1 Welding Hardfacing

Hardfacing is the deposition of a surface layer by welding or spraying, which is harder than the base material and to give wear resistance [8]. Hardfacing is used to maintain or mitigate machine components by mending the worn surfaces in actual practice, as well as to provide the hard or good wear-resistant surfaces of machinery parts. [4]

The advantages of hardfacing are

- (1) It can be used to repair the localized areas,
- (2) Strong and wear-resistant materials are accessible, and
- (3) It is effective to prevent or save high-cost alloys against wear problems extensively. [6]

Many kinds of welding techniques can be applied to deposit hardfaced materials as shown in Fig 2.3.

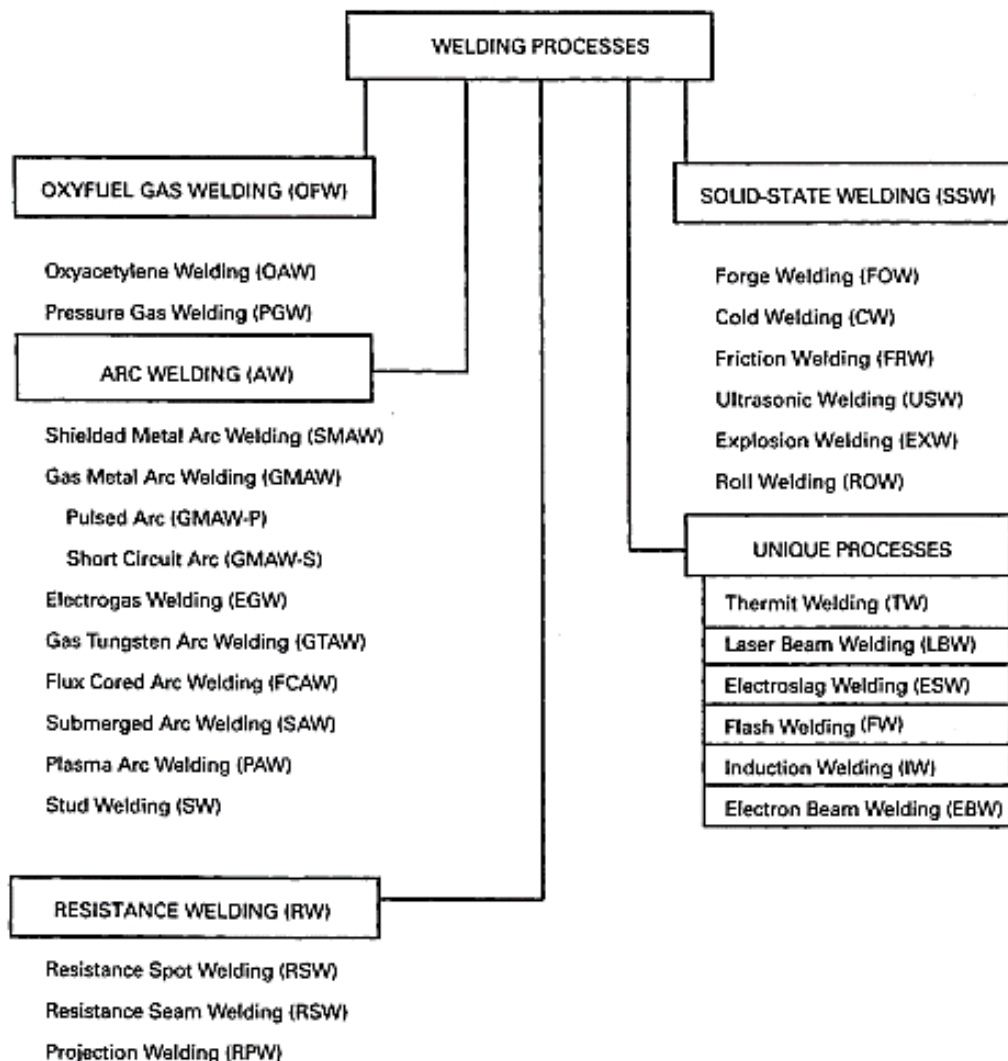


Fig 2.3 Welding process for repair and hardfacing [2]

2.3 Submerged arc welding

Submerged arc welding is one of the arc welding processes that the welding arc is covered by the granular flux as a blanket. The heat source of submerged arc welding is initiated by an arc between a wire electrode and the base plate. The arc is maintained in a blanket of fusion flux, that improves the deposited metal and prevents from the atmosphere. Metal powder addition can be also done by submerged arc welding. Fig 2.4 displays the schematic diagram of submerged arc welding operation.

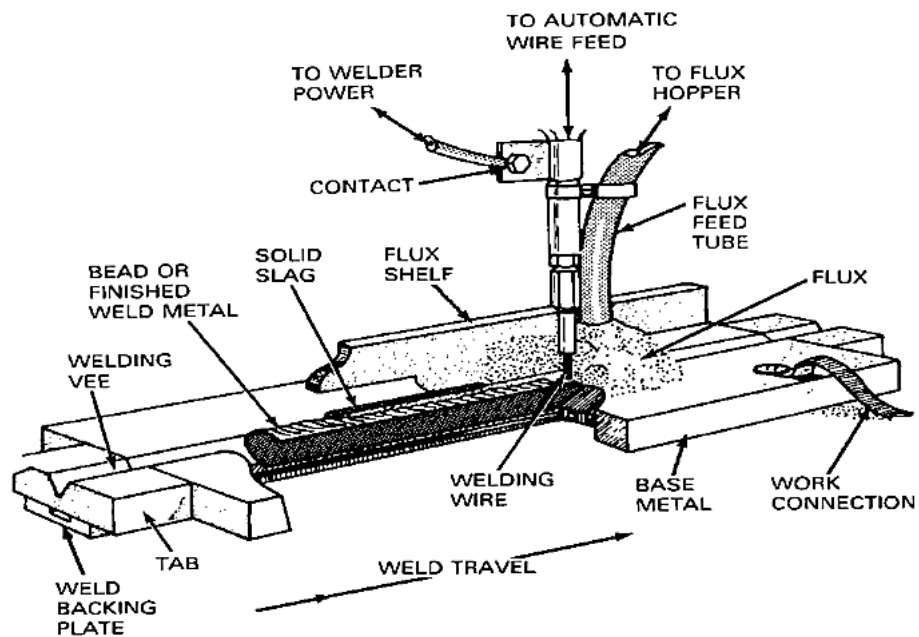


Fig 2.4 Submerged arc welding process [9]

Flux is an important ingredient for submerged arc welding. The stability of the arc depends and maintain the heat of weld. The flux can control mechanical, thermal, chemical properties, resistance to crack and other characteristics of the weld metal. Alloying elements in the flux improve the mechanical properties of the weld deposit and cracking resistance. Submerged arc welding can commonly be performed fully automatic. Currents ranging between 300 A and 1000 A are mostly applied. In multiple arc welding operation, currents up to 500 A can also be used. Either DC or AC is commonly chosen for power sources of single or multiple electrode systems in submerged arc welding. AC power source is most commonly used power sources for higher current applications.

2.3.1 Principle of operation

A wire electrode is mechanically fed onto the base metal by powered drive rolls. A granular welding flux layer is being covered along the Arc travel. Welding current which creates the Arc is supplied to the electrode through the contact tube. The terms and conditions of submerged arc welding process are illustrated in Fig 2.5.

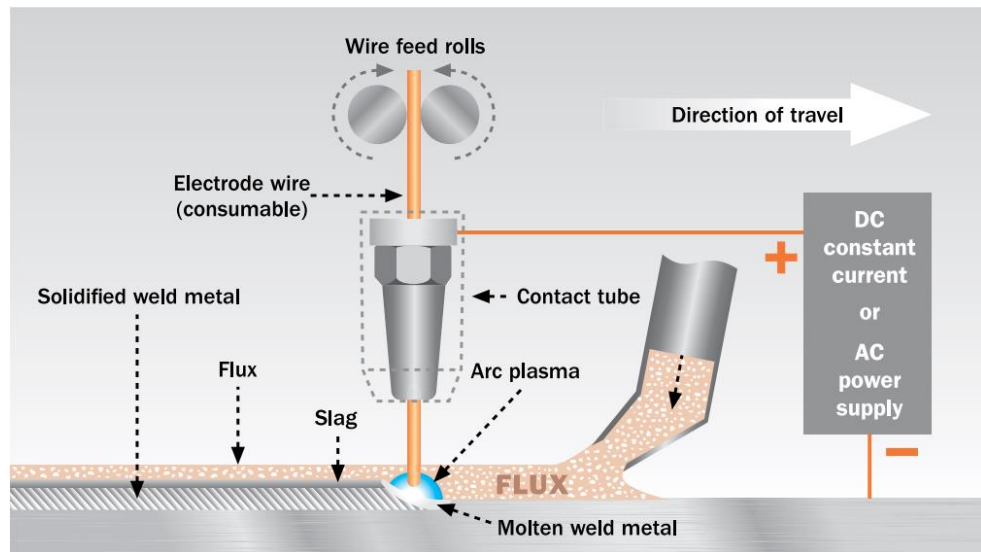


Fig 2.5 Operation of Single-wire Submerged arc welding [10]

The un-fused flux and slag (Fig 2.6) must be removed from weld metal after solidification. The solidified slag should be kept, crushed, refined, and blended back into the new flux. It can be re-used. Submerged arc welding can operate both semi-automatic and fully automatic process. Most popular type is fully automatic operation. In the operation of automatic submerged arc welding, travel speed during welding and direction of welding are being maintained mechanically, and flux is continuously supplied from a hopper in front of the welding arc along the weld travel, and then the un-fused flux is recovered to re-use after welding.

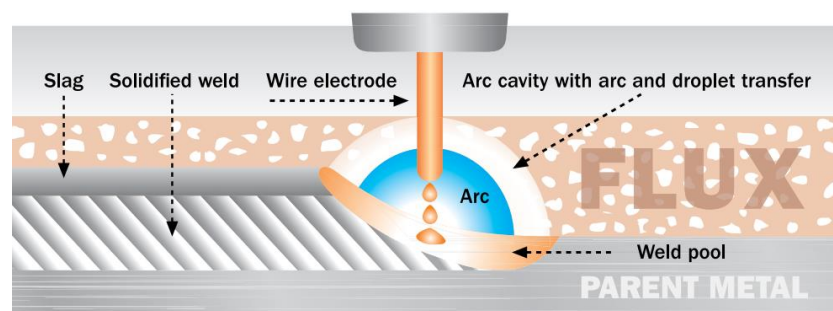


Fig 2.6 Function of Flux during welding by Submerged arc welding [10]

Submerged arc welding process is a high-quality arc welding process and it gives a higher deposition. This process is commonly used to weld or join thick sections

and it is limited to weld in the flat position. The qualities of weld deposits using submerged arc welding process are judged by the following parameters.

- a. Welding Current
- b. Welding voltage
- c. Electrode stick out
- d. Travel speed
- e. Heat Input

The effect of the above welding parameters are most important factors to control on weld bead geometry to get optimum results and it is also important the selecting these variables and adjust the effects of selected parameters on the shape of the weld bead. To obtain a sound qualified weld, the setting of several variables must be correct before operating submerged arc welding.

2.3.2 Welding Current

The welding current influences penetration and deposition rate. A bigger and narrower weld bead size with a deeper penetration produces when a higher welding current is used, as shown in Fig 2.7. However, using an extremely high welding current can result in various defects, such as undercutting, an irregular weld convexity, burn-through, heat cracks, an unsuitable merging angle with the base metal [11].

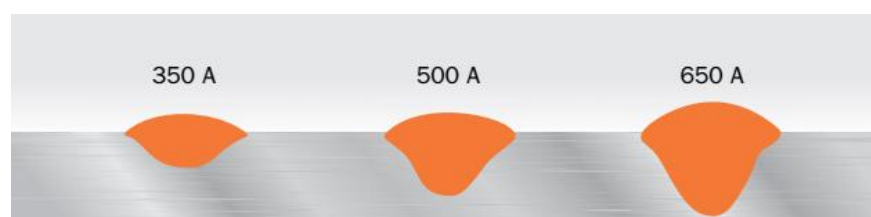


Fig 2.7 Effect of increased welding current [10]

2.3.3 Welding arc voltage

A higher welding voltage creates a wider weld bead with shallow penetration. It means that a high voltage is applicable for wide gaps welding. Then, flux consumption is high and the solidified slag is more difficult to remove. High welding voltage also leads to increase welding defects, especially in fillet welds. Furthermore,

a low arc voltage makes weld convexity high and produces a difficult contact angle with the workpiece material. [11] Fig 2.8 shows the effect of welding voltage.

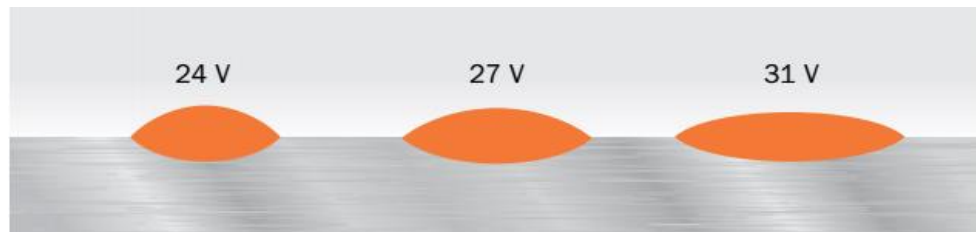


Fig 2.8 Effect of increased welding voltage [10]

2.3.4 Electrode stick-out

The amount of melting rate is higher when the longer electrode stick-out is applied. Longer wire stick-out consumes the energy from the arc more. The weld bead width and dilution decrease with the lower arc voltage. The bead width cannot be same with a normal electrode extension, see in Fig 2.9 because lower arc voltage tends to be higher convexity of the bead. Therefore, the setting of arc voltage on the machine should be increased to control the suitable arc length when the longer electrode extension is used to increase the melting rate. A long extension of wire electrode with constant current can increase the deposition rates from 25 per cent to 50 per cent. [9]

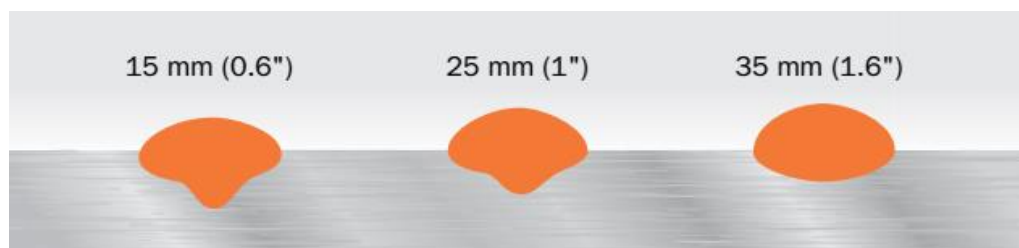


Fig 2.9 Effect of increased electrode stick-out [10]

2.3.5 Travel speed during welding

The travel speed during welding affects the dilution and the cross-sectional area of the weld. A narrow weld bead with shallow penetration is produced when a high welding speed is applied, as can be seen in Fig 2.10. An extremely high speed creates the various welding defect. A very low speed produces an irregular weld surface, and a mushroom-shaped penetration, that causes thermal cracking. Moreover, it also creates

a board weld cavity, which flows around the arc and presents an irregular surface and slag inclusions. [11]

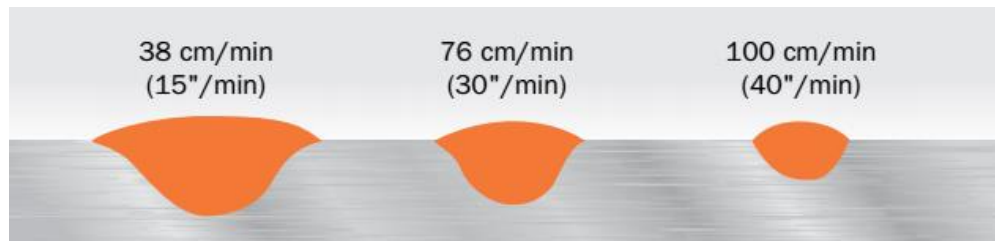


Fig 2.10 Effect of increased Travel speed [10]

2.3.6 Wire diameter

A small diameter of wire electrode produces deeper penetration. Effect of the diameter of wire electrode is illustrated in Fig 2.11. The stability of arc for constant welding current is better using a thinner wire because of higher current density. On one hand, a thicker diameter of filler wire with a low welding current can bridge a wide joint more easily. [11]

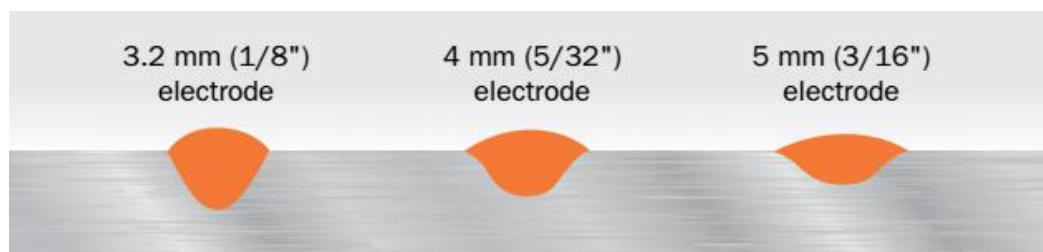


Fig 2.11 Effect of increased wire diameter [10]

2.3.7 Heat input

The heat source for the welding process controls the cooling rate of the weld metal as a considerable factor. The source of energy input for welding is commonly described in terms of the heat input per unit length of weld pass, as described in Eq. (1). It mostly describes in units of kJ/mm if the travel speed is controlled in mm/min. Yet, if travel speed is in cm/min or in/min, it will also use in kJ/cm or kJ/in. [12]

$$Q = \frac{V \times I \times 60}{S \times 1000} \cdot \text{Efficiency} \quad (1)$$

Where Q = Heat input (KJ/cm)

V = Welding voltage (V)

I = Welding current (A)

S = Travel Speed (cm/min)

Efficiency* MMA: 0.8

MIG/MAG: 0.8

SAW: 1.0

TIG: 0.6 [11]

2.4 Metallurgy of Welding

2.4.1 Heat-affected Zone (HAZ)

The various phase transformations at HAZ of base metal occur during welding. The HAZ has several sub-zones. These are shown in Fig 2.12 and as follows:

1. Grain growth zone
2. Grain refined zone
3. Partially transformed zone
4. Zone of spheroidized zone
5. Zone of unchanged base material [13]

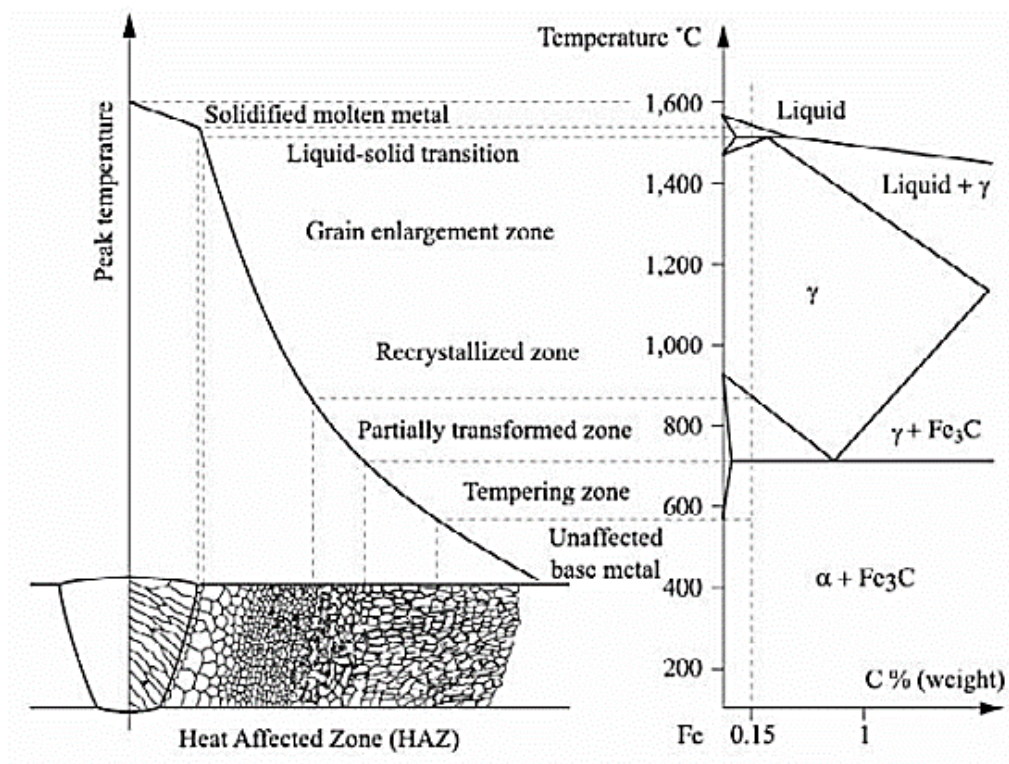


Fig 2.12 Scheme of phase transformation of the workpiece during welding [13]

2.4.2 Preheating

The preheating temperature before welding is one of the crucial parameters to obtain a sound weld metal. Preheating decreases

- (1.) the hydrogen-induced cracking
- (2.) the contraction stresses
- (3.) the cold cracking
- (4.) the heat affected zone (HAZ) hardness

To choose the suitable preheating temperature, the base metal composition must be known because it is maintained by two major factors.

1. including carbon per cent in the chemical composition of the base material
2. including alloying content in the chemical composition of the base material

The base material containing higher carbon content fundamentally needs to preheat at a higher temperature. This is also related to alloy content of the workpiece. The preheating temperature can be calculated by the carbon equivalent (CE) equation (Eq. 2) based on the base material's chemical composition. [14,15]

$$CE = \%C + \%Mn/6 + (\%Cr + \%Mo + \%V)/5 + (\%Ni + \%Cu)/15 \quad (2)$$

Preheating temperature of base metal can be considered by following carbon equivalent (CE) values;

1. CE < 0.45 preheat 100 °C
2. CE < 0.45-0.60 preheat 100 - 250 °C
3. CE < 0.6-0.8 preheat 250 - 300 °C
4. CE > 0.8 preheat 300 - 350 °C

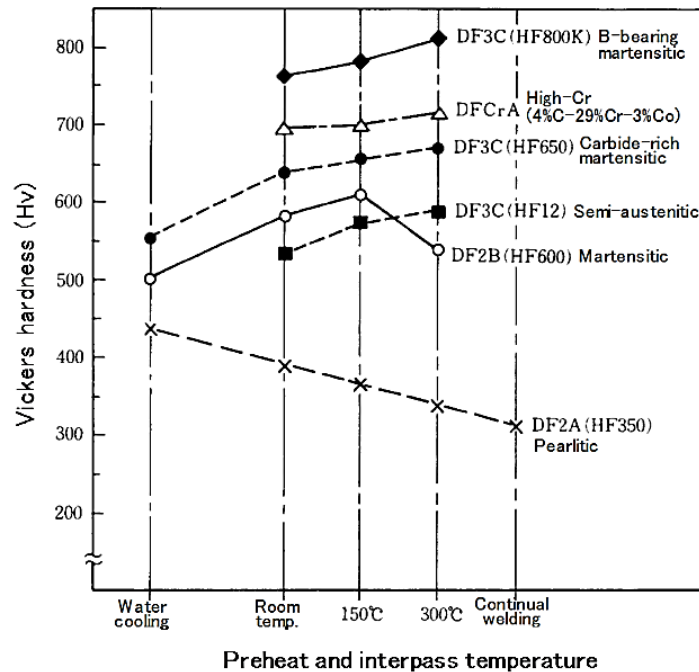


Fig 2.13 Effects of preheating temperature on hardness [4]

The thickness and dimension of the base metal should be considered as another main issue to determine the proper preheating temperature. It is very important that the correct preheating temperature maintains when the welding operation is carrying out. All welding operations applied to preheat should be slow-cooled.

2.4.3 Dilution

The welding dilution is expressed as the per cent ratio of the melted base metal area to the total weld metal area [16], as depicted in Fig 2.14. In hardfacing, lower dilution is better to obtain the optimum properties because weld metal's hardness and chemical composition vary due to the per cent dilution.

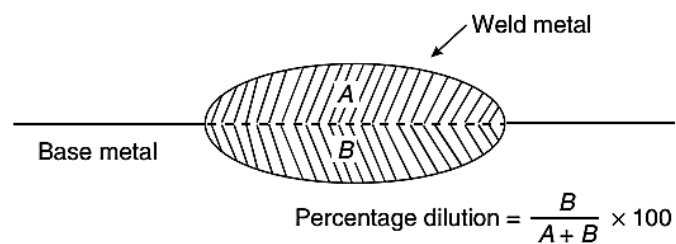


Fig 2.14 Schematic diagram for welding dilution [17]

Percentage of welding dilution can be controlled by the following factors:

1. Selection the right welding technique
2. Choosing the correct welding polarity
3. Welding position
4. The thickness of weld metal
5. The position of the weld bead
6. Welding current and heat input
7. Proper electrode stick-out and speed [8]

2.5 Hardfacing Materials

2.5.1 Type of Electrodes

There are various types of submerged arc welding electrodes according to the usage and function of electrodes, see in Fig 2.15 and Fig 2.16. The effect of welding current and deposition rate on different welding electrode type is graphed in Fig 2.17.

Consumable electrode for SAW can be divided into three group.

- (1) Solid Wires
- (2) Flux-cored or Tubular Wires
- (3) Strips [18]

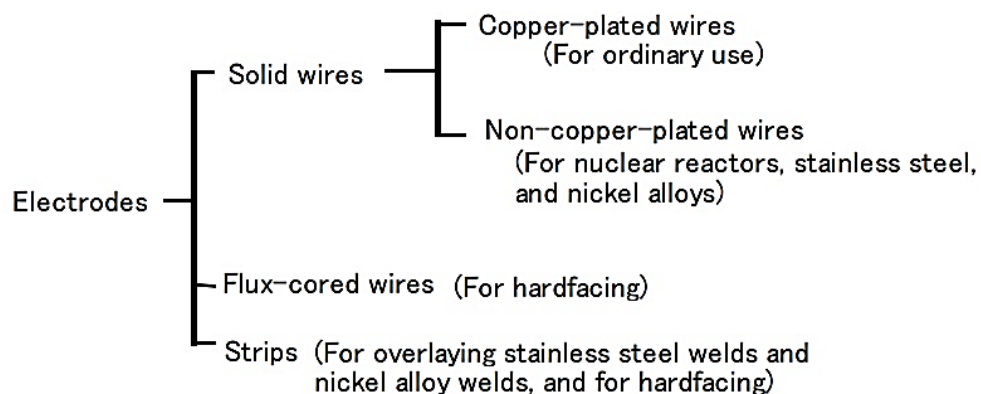


Fig 2.15 Different types of welding electrode for submerged arc welding [18]

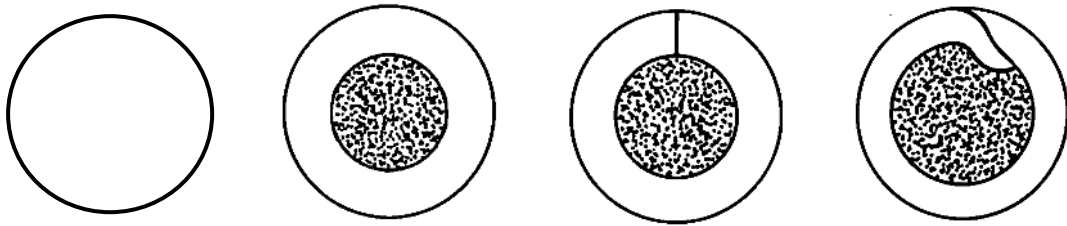


Fig 2.16 A section through different kinds of wire electrode [19]

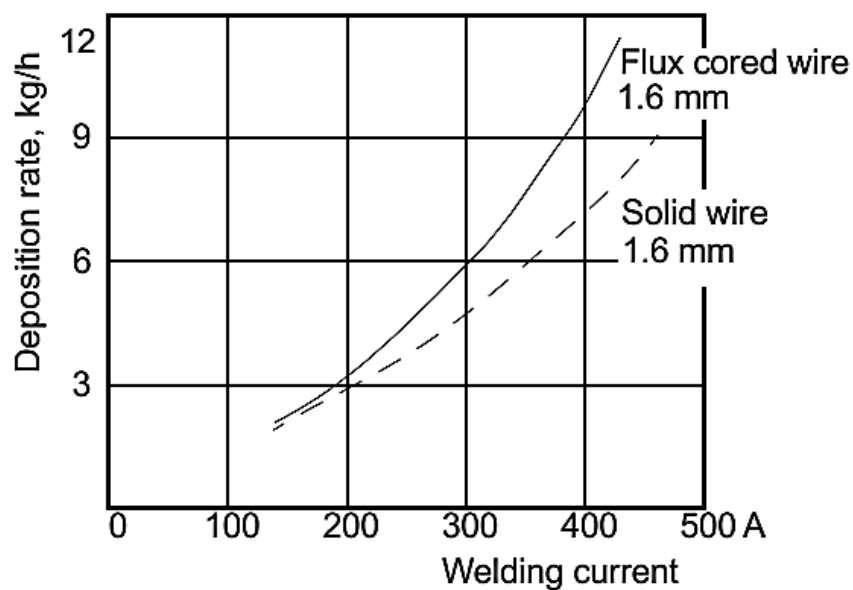


Fig 2.17 The relation of welding current and deposition rate using a different type of wire [19]

2.5.2 Hardfacing filler metal

Before the suitable filler materials for hardfacing have been selected, it is vital to approach the characteristics and properties of filler metal and application of hardfacing. [4] Materials for hardfacing can be classified into two main groups due to their properties, characteristics and wear resistance. They are:

Iron-based group

- Martensitic alloys
- Austenitic alloys
- Carbide-rich alloys

Non-iron based group

- Cobalt-based alloys
- Nickel-based alloys [14]

2.5.3 Martensitic alloys

Martensitic hardfacing filler contains amounts of carbon and alloying elements enough to appear martensite microstructure in the as-welded condition of hardfaced layers at room temperature after welding. The martensitic hardfacing weld has superior abrasive wear resistance because of its very high hardness, but it is not resistible to impact wear because of its lower ductility. [4] Martensitic steels have the advantage of low initial costs, good hardness, strength, abrasion resistance and toughness. They have been mainly used as buildup layers under other alloy compositions. [6] Fig 2.18 presents the typical microstructure of martensite.

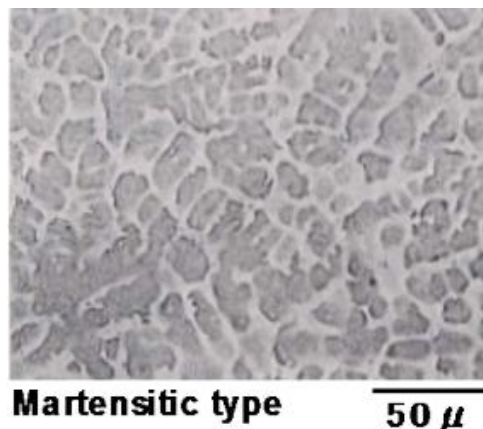


Fig 2.18 Typical microstructure of martensitic type [4]

2.5.4 Austenitic alloys

Austenitic alloys contain 12–16% Mn and up to 1% C. Austenite phase in the steel microstructure is obtained at about 1000 °C. Fig 2.19 shows the particular microstructure of austenite structure. According to their chemical composition, the austenitic microstructure can be seen at room temperature [4]. This phase is metastable. Vickers hardness of this material is between 200 and 600 HV [17]. This material has a high resistance to impact loading associated with abrasion [4,20].

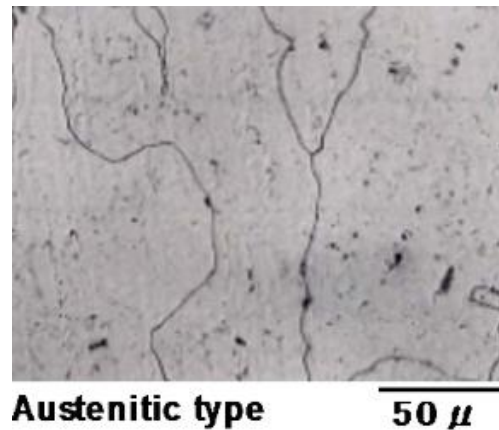


Fig 2.19 Typical microstructure of Austenitic type [4]

2.6 Hardness Testing

ASTM E92 standard is used to test the Vickers hardness of metallic materials [21]. The general principle of Vickers' hardness test is same as that of the Brinell test. An equipment of micro-Vickers' hardness testing is necessary a pyramid-shaped diamond indenter with an included angle of 136 Degree. To perform the test, the indenter is pressed on to the intended area of sample surface for testing to appear a square-based pyramid indentation as shown in figure [22].

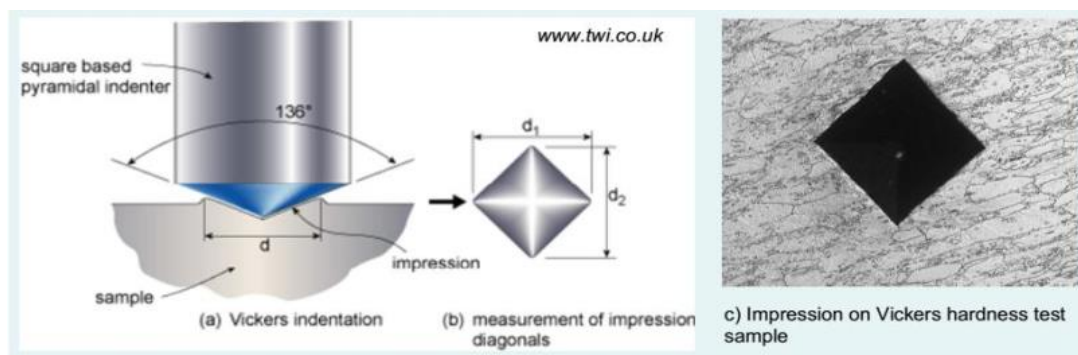


Fig 2.20 Principle of hardness testing [22]

The value of Vickers' hardness (VHN) can be calculated by the following equation (Eq. 3). The applied load is divided by total areas of indentation, at which the latter is derived from the diagonals of the pyramid as expressed in the equation below [22] Fig 2.20 illustrates the fundamental principle of Vickers' hardness testing.

$$\text{VHN} = \frac{2P \sin(\theta/2)}{d^2} = \frac{1.854P}{d^2} \quad (3)$$

Where P is the applied load, kg

d is the average length of the diagonals = $(d1+d2)/2$ mm

θ is the angle between the opposite faces of the diamond) = 136 Degree [22]

2.7 Abrasion Wear Test

ASTM G65 standard test (Fig 2.21) is one of the most widely used three-body abrasion testing methods [23]. This method determines the resistance of metallic materials to scratching abrasion. The size of standard specimens is 14 mm × 25.4 mm × 74.6 mm. Round quartz sand size with the range from 212 to 300 μm was used as abrasive particles in this test. The applied load and flow rate of sand are 130N and 300 g/min. Rubber wheel rotation speed during running the machine, the diameter of the wheel and a total distance of wheel rotation were 200 rpm, 228.6 mm and 4309 m respectively. After running the experiments, the mass losses of specimens were measured and recorded on an electric balance, and weight losses were determined and recorded [24]. Fig 2.22 shows the principle of abrasion testing and abrasive particles.

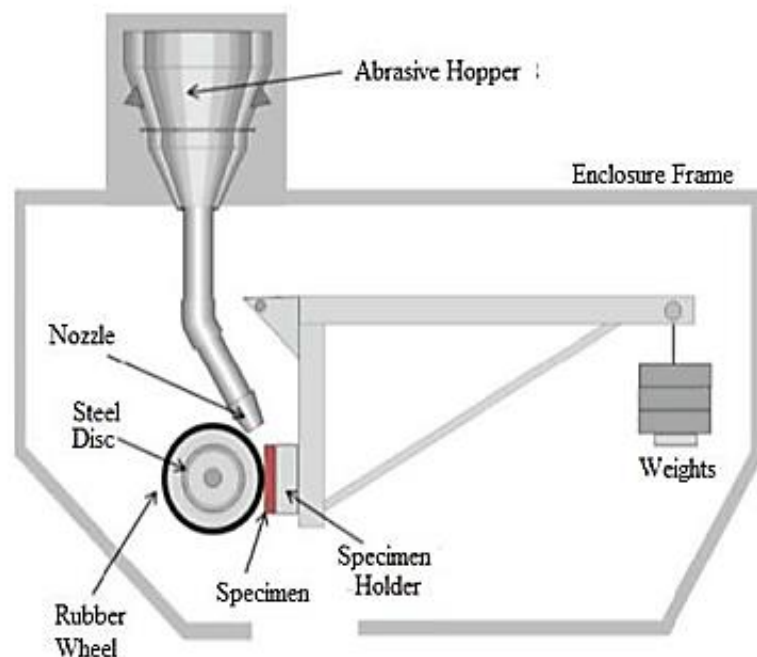


Fig 2.21 ASTM G65 standard abrasion test [23]

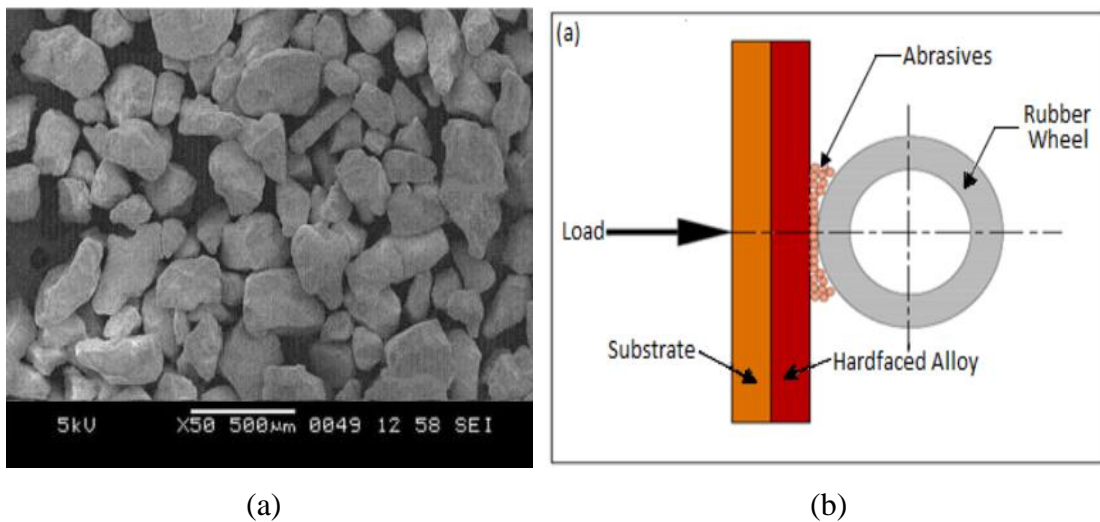


Fig 2.22 Abrasion testing (a) Morphology of abrasive particle (dry sand) and (b) Principle of abrasion test [23]

2.8 Literature Reviews

Chia-Ming Chang et al. [25] studied the microstructure and abrasive wear behaviors of high carbon Fe–Cr–C hardfacing alloy. ASTM A36 steel base metal was hardfaced with chromium and graphite alloy fillers by gas tungsten arc welding (GTAW). ASTM G65 standard (dry sand rubber wheel machine) was performed to measure the abrasive wear resistance. The hardness of hardfacing and amount and size of primary carbide varied with the carbon content.

M.F. Buchely et al. [26] investigated the effect of microstructure on abrasive wear of hardfacing alloys. ASTM A36 carbon steel substrates were deposited by a shielded metal arc welding (SMAW). Three kinds of commercial electrodes were used. According to the experimental results, the wear resistance of hardfacing depends on the size, shape, distribution and chemical composition of the carbides and the matrix microstructure as well. The SEM images of worn surfaces showed micro-cutting of the matrix and brittle fracture of the carbides.

Ramin Zahiri et al. [27] studied the microstructure and properties of hardfaced coatings welded using Submerged Arc Welding (SAW) process. Ferro-alloy powder mixtures were used to produce Fe–Cr–C hardfacing. The additional boron powder replaced carbon in the carbide-based coatings partially or fully and produced the

modified alloy. The abrasive wear resistance of hypereutectic microstructure was higher than that of the hypoeutectic microstructure.

Karsten Günther et al. [28] conducted the microstructural evolution and wear properties of hypereutectic FeCrC deposits using gas metal arc welding with additional hot wires. Hot wires addition can independently adjust the deposition and dilution rates. HW-GMAW was able to apply hypereutectic solidification at very high deposition rates of 9 kg/h. The wear properties of HW-GMAW overlays were higher than those of GMAW overlays.

J. Tus̃ek et al. [29] carried out the research on multiple wires submerged arc welding with metal powder addition. The metal powder inputs were controlled in three different ways. Submerged arc welding process is the most suitable welding process for using multiple wires and additional metal powder. Metal powder addition increases the deposition rate and arc efficiency and reduces the consumption of flux.

Gopa Chakraborty et al. [30] studied the Dashpot piston of a nuclear reactor was deposited using nickel base hardfacing alloy and Inconel 625 was used to reduce crack formation. Then, the effect of the buffer layer on the microstructure of hardfacing was also investigated. Using buffer layer with post welded heat treatment can reduce the hardness of HAZ and cracking of hard layer. The thickness of hardfacing affects the crack formation.

Morsy M. et al. [31] compared two covered electrodes to two tubular electrodes. The chemical composition of weld metal, the coating flux of covered electrodes and flux inside tubular electrodes were characterized by XRD. The most important factor to determine the wear resistance is the microstructure of the hardfaced layers. The two tubular electrodes are better than two covered electrodes because of the large area of iron-chromium carbide friction. A tubular electrode using MMA process is the best condition for the wear resistant of hardfacing among the others in this paper.

V. T. Bhanu Kiran et al. [32] studied the development of multilayer hardfacing welded using a cobalt-free electrode onto low carbon steel base metal for slurry pump components. Chromium carbide based tubular hardfacing electrode and manganese-based austenitic buffer electrode were used to substitute cobalt-based hardfacing electrodes. The hardness of three layers hardfacing showed about 60 HRC and wear resistance compared with original components made of high chromium steel material.

Thicker base metal ($< 15\text{mm}$) should not be welded three or more layers hardfacing without preheating because it can cause cracking because of contraction strain. The base metal $\geq 15\text{mm}$ thickness can be deposited in multiple layers hardfacing. Before welding, the base steel plate was preheated at 200°C to prevent cracking.

John J. Coronado et al. [33] studied four different welding deposits welded using flux cored arc welding (FCAW) and shielded metal arc welding (SMAW). One and three layers of hardfacing were studied. FCAW deposits resulted in better abrasive wear resistance than SMAW welds. Generally, higher abrasive wear resistance was presented in three layers hardfacing. In this paper, there is no direct correlation hardness with the abrasive wear resistance of hardfacing. The authors claimed that the most important factor to determine abrasion resistance is the microstructure of hardfacing deposits, where the carbides act as barriers to abrasive particle cutting.

Keshav Prasad et al [34] studied the effect of welding current and travel speed on the microstructure, hardness, and toughness of HSLA steel weld joints. The variable welding current between 500 and 700A and different travel speed from 200 to 300 mm/min were used to join the workpieces. Varying the current and speed, heat inputs for submerged arc welding were also increased (3.0 to 6.3 KJ/mm). Using welding current from 500 A to 600 A with welding speed (200 mm/min or 300 mm/min) gave higher toughness but welding current up to 700 A made the toughness minimized. SEM images revealed that the high heat input gave the ductile fracture while low heat input fracture mode was largely brittle.

Chatterjee et al. [35] investigated the weld procedure effects i.e. preheating or without preheating, one layer or two layers hardfacing and with buffer or without a buffer layer. Two commercial and four iron based high Cr high C type hardfacing electrodes were used to deposit onto the grey cast iron plate in flat position using MMAW. Buffer layers were welded between the base metal and the hardfacing layer to maintain dilution and solidification strain. The highest strength of bonding was resulted in the sample with high nickel buffer layer, whereas the sample without buffer layers showed the lowest bonding strength.

Choteborsky et al. [36] reported that Fe-Cr-C hardfacing alloys containing high Cr content can be used in harsh abrasive conditions. Inexpensive Cr rich hardfacing electrodes are broadly employed. Four different hard facing alloys contained primary

Cr carbides and complex carbides were used. The low carbon steel was hardfaced using GMAW process. Pin on disc machine was carried out for wear resistant testing. The primary carbides significantly affect the abrasive wear resistance of hardfacing. The results showed that the double layer complex carbide deposits resulted in the best abrasive wear resistance.

Chapter-3

Experimental Procedures

3.1 Materials and Equipment

3.1.1 Base Metal (3.5% Cr steel)

In this project, the 3.5% Cr steel was used as the base metal. The 3.5% Cr steel is an alloy steel with no specific standard steel grade. A mixture of ferrite, pearlite and bainite microstructures can be seen in the 3.5% Cr steel base metal. The hardness value of this material is about 200 HV. The chemical composition of the 3.5% Cr steel examined by the Optical Emission Spectroscopy (OES) shows in Table 3.1.



Fig 3.1 3.5% Cr steel plate

Table 3.1 Chemical composition of the base metal (wt.%)

C	Si	Mn	Ni	Cr	Mo	Cu	Fe
0.38	0.40	0.52	0.17	3.42	0.30	0.04	Balance

3.1.2 Electrodes

There are two types of wire electrode used for hardfacing and buffer layer.

(1) Martensitic steel type wire electrodes (EN 14700: T Fe8) was used to deposit for hardfacing layers. Single and three layers hardfacing were performed.

Table 3.2 Chemical composition of the wire electrode for Hardfacing (wt.%)

Electrodes	C	Si	Mn	Cr	Ni	Fe
Hardfacing	0.5	2.5	1.5	8.5	-	Balance

(2) In all experiments of this project, the single buffer layer was used. Austenitic stainless-steel type wire electrodes (EN 14700: T Fe10) was applied to weld for the buffer layer.

Table 3.3 Chemical composition of the wire electrode for Buffer (wt.%)

Electrodes	C	Si	Mn	Cr	Ni	Fe
Buffer	0.1	0.5	6	19	9	Balance



(a)

(b)

Fig 3.2 (a) Hardfacing electrode (b) Buffer electrode

3.1.3 Flux

An agglomerated basic flux (EN 760: S A FB 2 65 DC H5) having basicity index of 2.3 made by welding alloys company was used for covering the welding arc during using the submerged arc welding. The chemical composition of welding flux used for submerged arc welding is given in Table 3.4.

Table 3.4 Chemical composition of flux for Submerged Arc Welding (wt.%)

SiO ₂ + TiO ₂	CaO + MgO	Al ₂ O ₃ + MnO	CaF ₂
18	35	23	22

3.1.4 Power source

The twin-wire submerged arc welding is controlled by Aristo 1000 AC/DC SAW power source and controller, see in Fig 3.3. The controller contained the digital screen can adjust and monitor all welding parameters. The power source can generate maximum 1000 A current and use either AC or DC+ polarity.

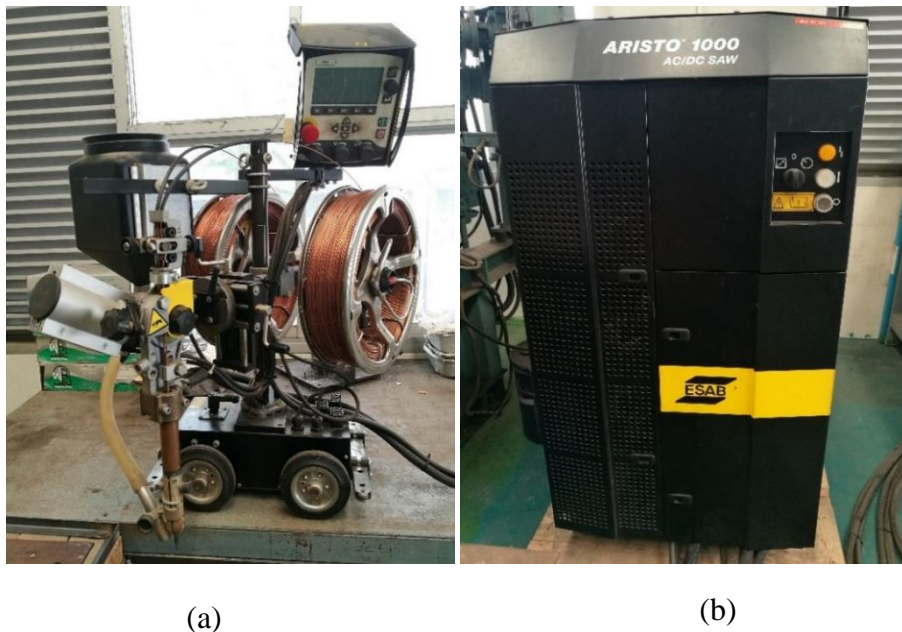


Fig 3.3 Welding machine (a) ESAB A2 Multitrac with A2-A6 Process Controller (b) ESAB Aristo 1000 AC/DC SAW power source

3.1.5 Thermocouple and Data Logger

The thermocouple used to measure temperature before and during welding is shown in Fig 3.4. A Picolog USB TC-08 model thermocouple data logger consisting of 8 channel thermocouple data logger and K type thermocouple was applied to measure temperature by plugging into a computer.



Fig 3.4 Thermocouple and data logger

3.1.6 Flexible ceramics pad heaters

Fig 3.5 shows the flexible ceramics pad heaters to preheat the base metal before depositing.



Fig 3.5 Flexible ceramics heating pad

3.1.7 Band saw

The manual type UE-712A band saw is shown in Fig 3.6. It was used for cutting from the original size from company to the welding condition size.



Fig 3.6 Band saw

3.1.8 Abrasive cut-off machine

The abrasive cut-off machine (HITACHI CC 14ST) was used for cutting from the original size of the as-welded sample to the size of metallurgical testing and abrasion specimens. Fig 3.7 presents this machine.



Fig 3.7 Abrasive cut-off machine

3.1.9 Vertical Milling Machine

The vertical milling machine HELLER Model 2S was operated to shape the dimension of abrasion testing specimens and to prepare the surface of the specimens for abrasion test and the surface of cold moulded metallurgical characterization specimens. Fig 3.8 depicts the vertical milling machine used for the project.



Fig 3.8 Vertical Milling Machine

3.1.10 Metallographic Polishing

The Pace Technologie Nano 1000T single Grinder/Polisher was applied to get the optimum surface finished for carrying out macro/microstructural characterization. Fig 3.9 shows the polisher. The series of metallographic polishing papers from 80 grits to 800 grits and the solution mixed with 5 μm alumina powder and water using the soft pad for final polishing was used with this polisher. Fig 3.10 shows the metallographic polishing papers and 5 μm alumina powder.



Fig 3.9 Pace Technologie Nano 1000T single Grinder/Polisher

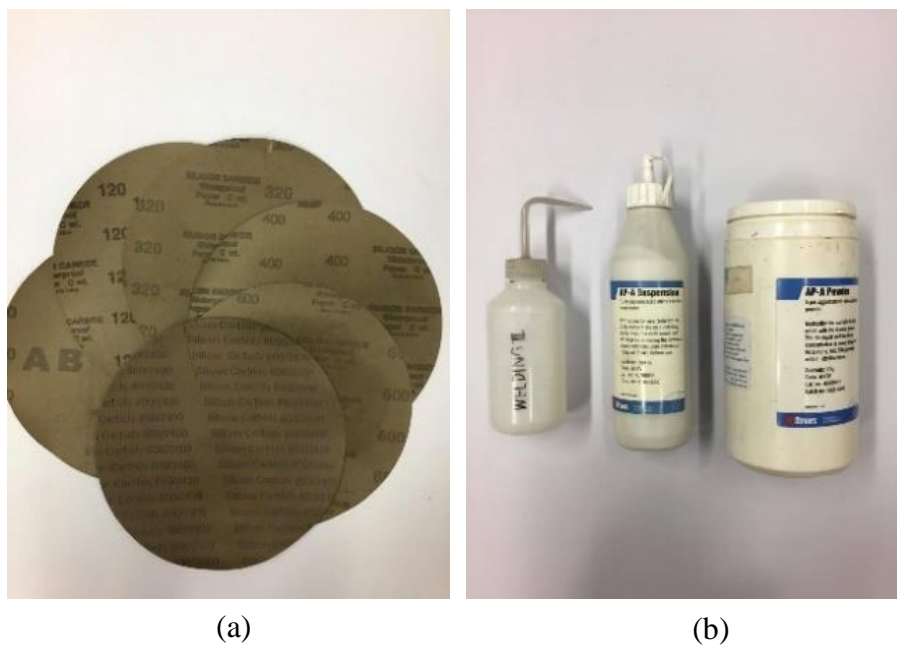


Fig 3.10 Polishing equipment (a) Metallographic paper (b) 5 μ m alumina powder

3.1.11 Etching reagents

In Fig 3.11, etching reagents for metallurgical characterization are shown. Before checking the macro/microstructural examination, the surface of the specimen must be etched by the suitable chemical reagents. In this project, two kinds of etching reagents were used. They are-

- (1) 2% Nital (2 cc HNO₃ + 98 cc Ethyl alcohol)
- (2) Viella's (5 cc HCl + 2 gr Picric acid + 100 cc Ethyl alcohol)



Fig 3.11 Etching reagents

3.1.12 Microscopes

Three types of microscope were used to characterize.

- (1) An optical microscope: Olympus SZ2-ET has been used to check the macrostructure of specimens, see Fig 3.12. It can only magnify to 4-28 times.

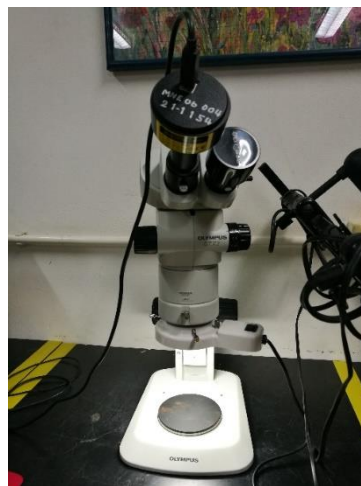


Fig 3.12 Optical microscope for macrostructural analysis

- (2) Fig 3.13 shows a Zeiss Axio Scope.A1 model optical microscope that was used to analyze the microstructure of specimens. It can magnify to 25-500 times.



Fig 3.13 Optical microscope for microstructural analysis

(3) The FEQ Quanta 400 model scanning electron microscope (SEM-Quanta) is shown in Figure 3.14. This microscope was used to check EDX results, SEM image of phase morphology and SEM image of worn surfaces. This microscope was equipped with backscattered electron detector (BSE) to take SEM image of metallurgical phase analysis. To capture SEM image of worn surfaces, secondary electron detector was installed in this microscope.



Fig 3.14 Scanning Electron Microscope

3.1.13 Micro Vickers hardness tester

A micro Vickers hardness tester (MATSUZAWA MMT-X78) is shown in Fig 3.15. The cross-sectional and top surface hardness values were measured using this device.



Fig 3.15 Micro Vickers hardness tester

3.1.14 Abrasive wear testing instrument (ASTM G65)

The dry sand rubber wheel abrasion machine according to ASTM G65 (Fig 3.16) was used to measure the abrasive wear resistance of hardfacing based on the abrasive mass loss of the specimens. The parameters of this test are shown in Table 3.5.



Fig 3.16 Abrasion wear testing machine

Table 3.5 Standard parameters of ASTM G65

ASTM G65 Parameters	Values
Procedure	A
Round quartz sand size (μm)	212-300
Applied load (N)	130
Sand flow rate (g/min)	300
Rubber wheel rotation speed (rpm)	200
Wheel diameter (mm)	228.6
Wheel rotation distance (m)	4309

3.1.15 Precision balance

Fig 3.17 shows the Denver Instrument TB-214 precision balance with an accuracy of ± 0.1 mg. After running ASTM G65 machine, the mass losses of wear specimens were measured and recorded on the balance, and weight losses were determined and recorded.

**Fig 3.17** Precision electric balance

3.1.16 Other Equipment

- (1) Driller
- (2) Vernier calliper
- (3) Hand grinder
- (4) Slag hammer
- (5) Brass brush
- (6) SiC paper
- (7) Polishing Pad
- (8) Alumina powder
- (9) Blower
- (10) Desiccator
- (11) Screw tap
- (12) Screwdrivers
- (13) Gloves refractory

3.2 Research procedures

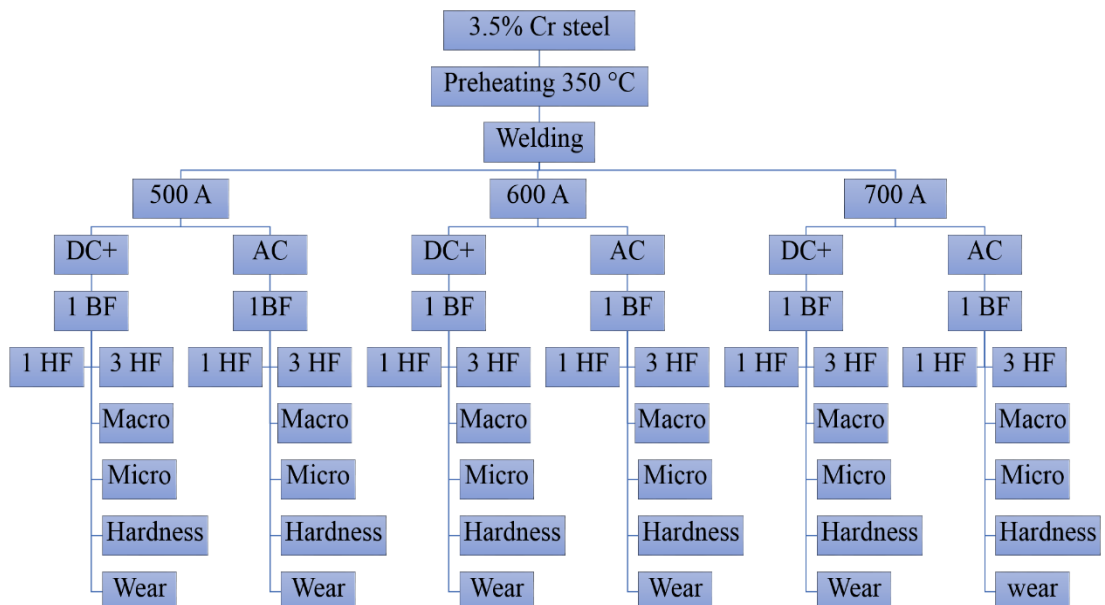


Fig 3.18 Experimental flow system

3.3 Samples preparation for welding

The base metal plate samples (3.5% Cr steel) were cut the original size (250 mm × 150 mm × 20 mm) to 250 mm × 75 mm × 20 mm dimension using band saw. After cutting the suitable size, four holes with 12 mm depth and 6.5 mm diameter were drilled and M8 x 1.5 threads were made for each hole. The reason why these holes were made is to avoid the distortion problem during welding. Then, two holes having 3 mm diameter and 12 mm depth were also created in both top and bottom of the cut samples for installing the thermocouples.

3.4 Preheating

When the sample preparation was finished, the base 3.5% Cr steel plate was preheated at 350°C for all experimental conditions. Preheating of the base metal before welding was done by Tokai 500A arc welding transformer with flexible ceramics pad. An asbestos blanket was covered during preheating. Fig 3.19 shows preheating of the base metal before deposition.

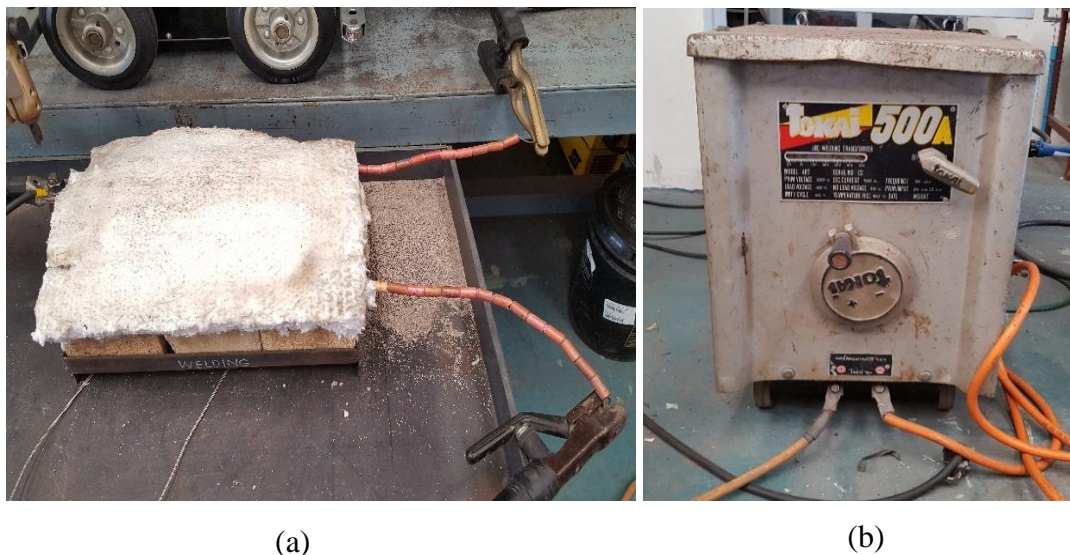


Fig 3.19 Preheating process (a) preheating before welding (b) arc welding transformer for preheating

3.5 Deposition using submerged arc welding

No sooner had preheating at 350°C done than the deposition of the single buffer layer was started. Welding voltage and travel speed during operating the process were

kept constant. There are 12 experimental conditions varied with different currents (500A, 600A and 700A) and polarities (AC and DC+). Fig 3.20 shows the fixed parameters of submerged arc welding on the digital screen.

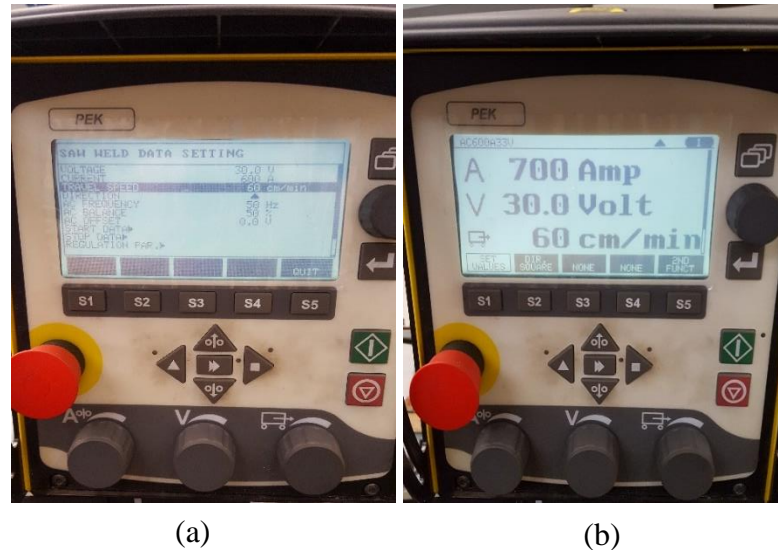


Fig 3.20 Setting before welding (a) showing the parameters (b) ready for welding

In Fig 3.21, the initiated welding process and a single pass of hardfacing on buffer surface were demonstrated.



Fig 3.21 Conducting welding process (a) initiating the welding process (b) hardfacing applied to the buffer layer

The final welded sample with single and three layers hardfacing presents in Fig 3.22.



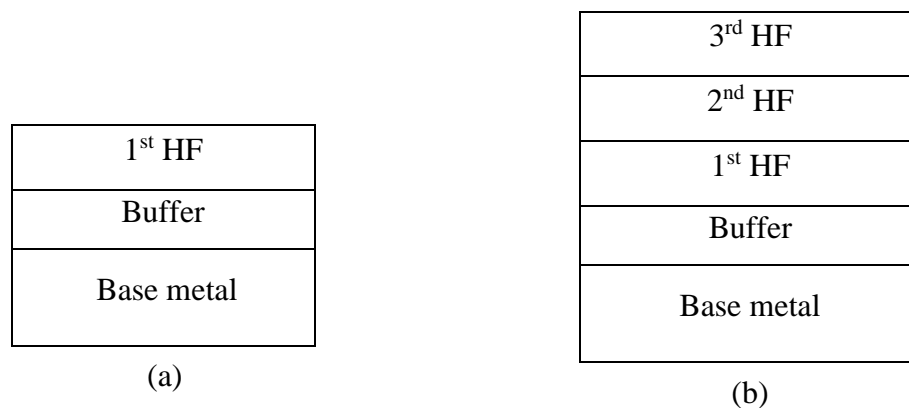
Fig 3.22 The deposited sample

Table 3.6 Fixed welding conditions

Parameters	Electrodes	
	Buffer layer	Hardfacing layer
Welding Process	SAW (Twin wires)	SAW (Twin wires)
Wire diameter (mm)	2.4	2.4
Wire extension (mm)	25.4	25.4
Voltage (V)	27-32	27-32
Travel speed (cm/min)	55-63	55-63

Table 3.7 Variable parameters of the experiment

Conditions	Buffer layer	Hardfacing layer	Current (A)	Type of polarity
1B 1H 500A AC	1	1	500	AC
1B 3H 500A AC	1	3	500	AC
1B 1H 500A DC+	1	1	500	DC+
1B 3H 500A DC+	1	3	500	DC+
1B 1H 600A AC	1	1	600	AC
1B 3H 600A AC	1	3	600	AC
1B 1H 600A DC+	1	1	600	DC+
1B 3H 600A DC+	1	3	600	DC+
1B 1H 700A AC	1	1	700	AC
1B 3H 700A AC	1	3	700	AC
1B 1H 700A DC+	1	1	700	DC+
1B 3H 700A DC+	1	3	700	DC+

**Fig 3.23** Schematic diagram of welding design (a) Single layer hardfacing (b) three layers hardfacing

(1) Initially, the buffer layer was deposited on the 350°C preheated base metal (3.5% Cr steel) using austenitic steel type wire electrode (EN 14700: T Fe10). Single layer buttering was applied for all experimental conditions. Table 3.6 shows the fixed parameters of the project and the variable parameters of the project are showing in Table 3.7.

(2) All hardfacing layers were welded using martensitic steel type hardfacing wire electrode (EN 14700: T Fe8). Single and three hardfacing layers were laid over the austenitic buffer layer, as illustrated in Fig 3.23.

(3) Six or five beads were deposited to form each layer (buffer and hardfacing) and the overlap between the beads was approximately 30%. The welded samples were all air cooled to room temperature. Fig 3.24 shows a welded sample.

(4) Twin-wire submerged arc welding process was carried out in a flat position for all layers and conditions.



Fig 3.24 Welded sample

3.6 Macro/microstructural characterization

3.6.1 There are 12 samples varied with different currents and polarities to check macro/microstructure. Fig 3.25 shows where the macro/microstructural specimens were cut from the welded sample.

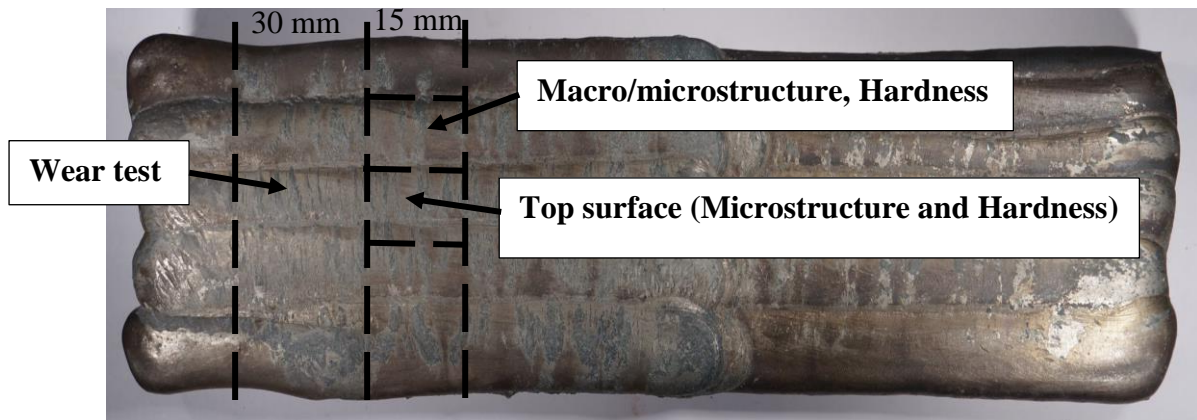


Fig 3.25 Cutting area of the welded sample

3.6.2 Fig 3.26 shows a cold-moulded specimen to check metallography. The cold mould was made from a suitable amount of epoxy resin mixed with hardener. 14 ml epoxy resin mixed with 1 drop of hardener.



Fig 3.26 Cold-molded specimen

3.6.3 After solidified the epoxy resin, the specimen was removed from pipe and surface of the cold-molded specimen was machined by milling to get a smooth surface.

3.6.4 The surface preparation of the specimen was finished. The specimen was polished using the polisher and the following order of metallographic sandpaper: 80 girts, 120 girts, 180 girts, 240 girts, 360 girts, 400 girts, 600 girts, 800 girts. Fig 3.27 demonstrates the metallographic polishing a specimen using a polisher.



Fig 3.27 Polishing a metallographic specimen

3.6.5 Alumina powder (5 μm) mixed with water and the smooth pad was used for a final stage of polishing. The polished specimen was cleaned with tap water and dried using a blower when every stage of polishing was carried out.

3.6.6 When final polishing was done, the specimen was etched by the suitable chemical reagents.

(1) To appear microstructure of the base metal (3.5% Cr steel) and Heat affected zone (HAZ), the specimen surface was etched with 2% Nital solution for 6 seconds.

(2) Viella's reagent was used to etch the surface of the specimen to reveal martensitic hardfacing microstructure and austenitic buffer microstructure for 15 seconds and 30 seconds respectively.

(3) Before changing the etchant, the specimen surface needs to re-polish and clean.

3.6.7 After metallurgical examination, all specimens are kept in a desiccator.

3.7 Phase analysis on microstructure by ImageJ

Generally, there are two phases in a micrograph. The dark phase represents martensite and the white phase represents austenite phase. Therefore, the amount of martensite phase contained in micrographs was analyzed using ImageJ software.

(1) First, the micrograph that wanted to analyze was chosen and opened it. Fig 3.28 shows selecting 8-bit type image. After selecting the 8-bit type, the micrograph changed from original colour to greyscale, see in Fig 3.29.

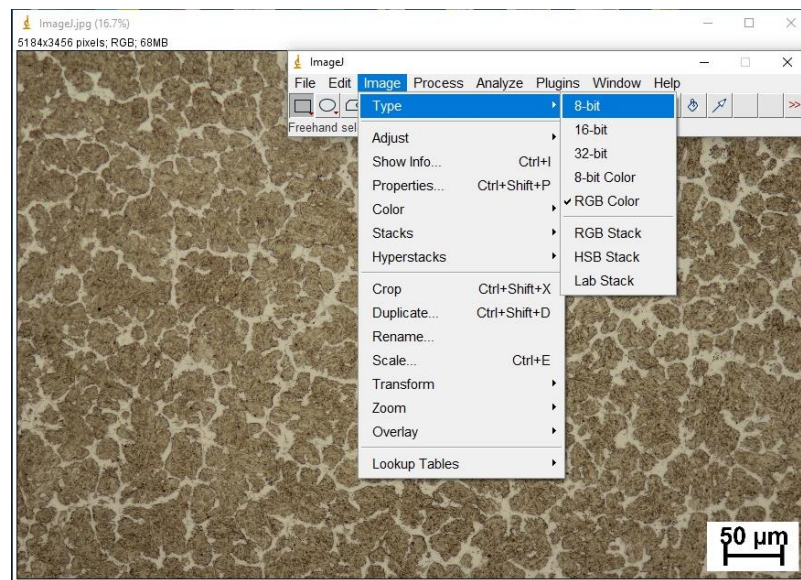


Fig 3.28 Selecting 8-bit type image

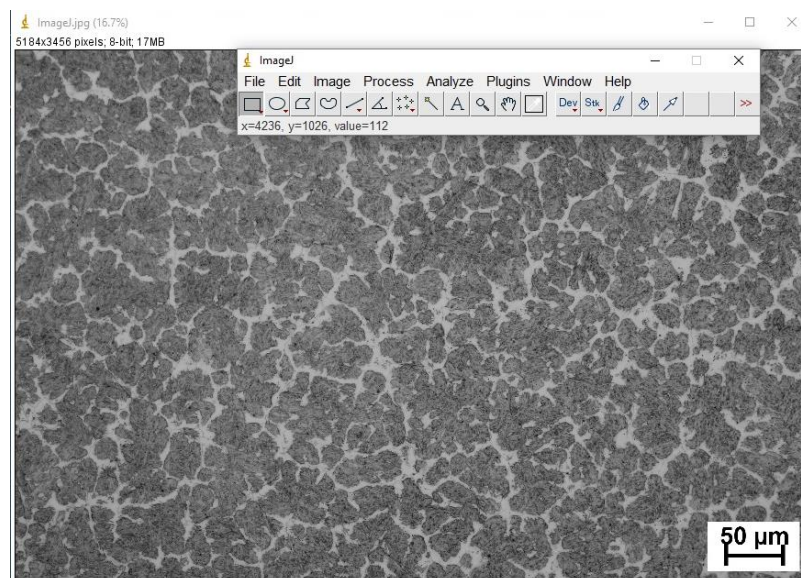


Fig 3.29 the 8-bit type image revealed the greyscale colour

(2) Setting the scale on micrograph shows in Fig 3.30 and Fig 3.31.

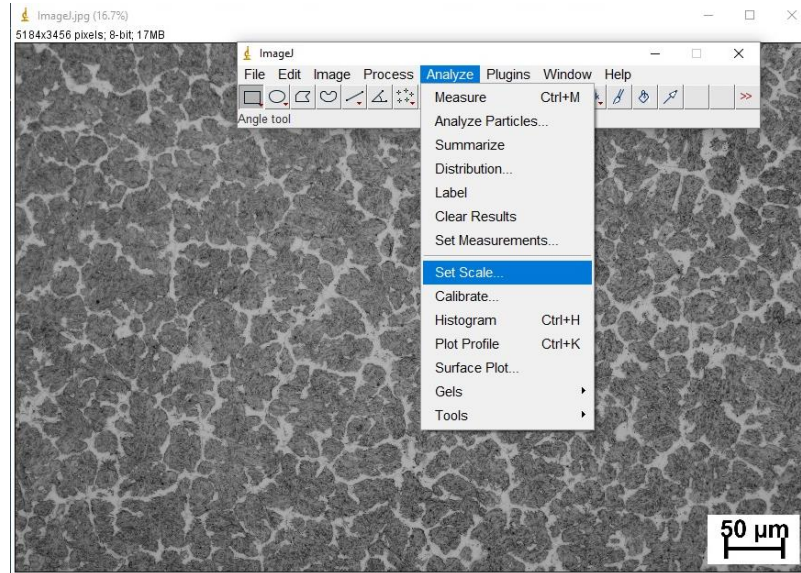


Fig 3.30 Setting scales

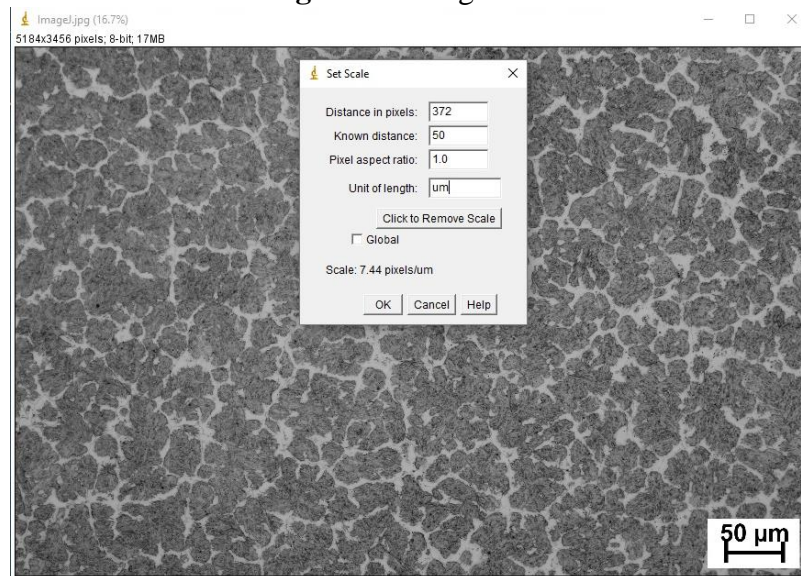


Fig 3.31 Installing specific values and unit

(3) Then, Fig 3.32 depicts adjusting the image to a threshold and it changed the black and white image. The setting of threshold changed means and B&W. It can see in Fig 3.33.

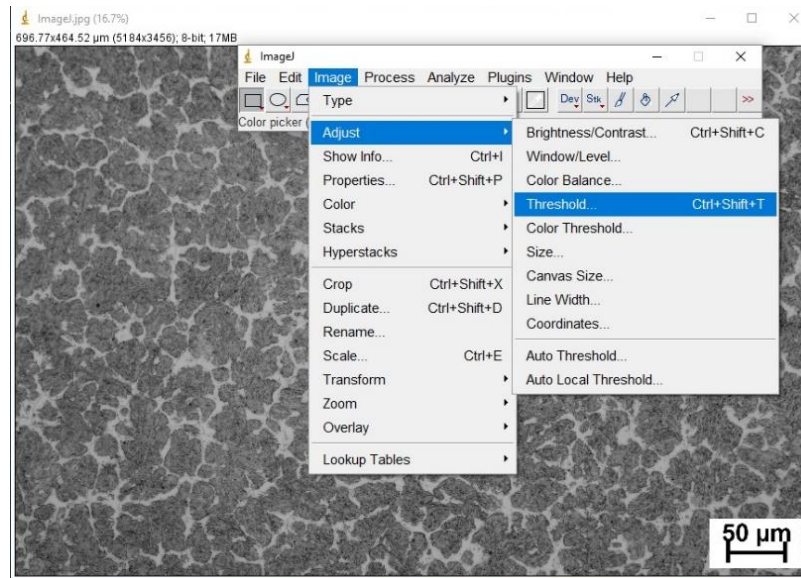


Fig 3.32 Adjusting to the threshold

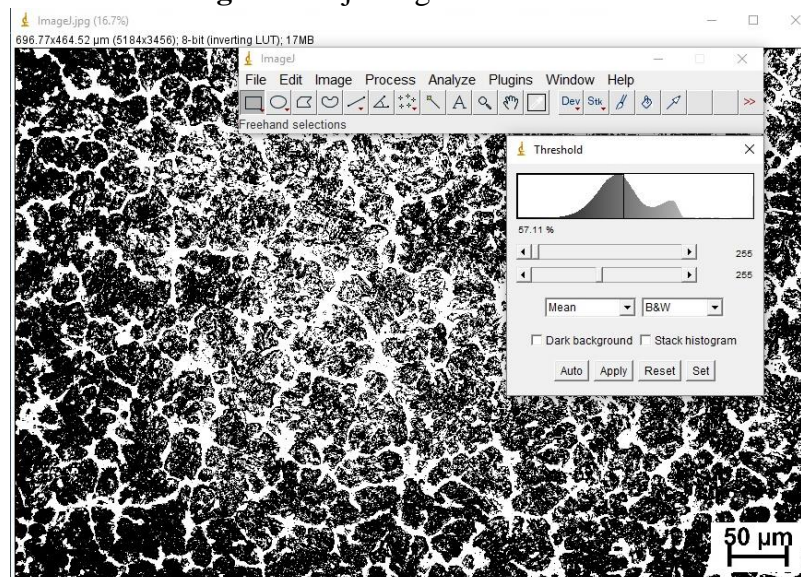


Fig 3.33 Setting scale in threshold

(4) Next, clicking the function of analyzing particles and setting the value to analyze the particles in micrograph are shown in Fig 3.34 and Fig 3.35.

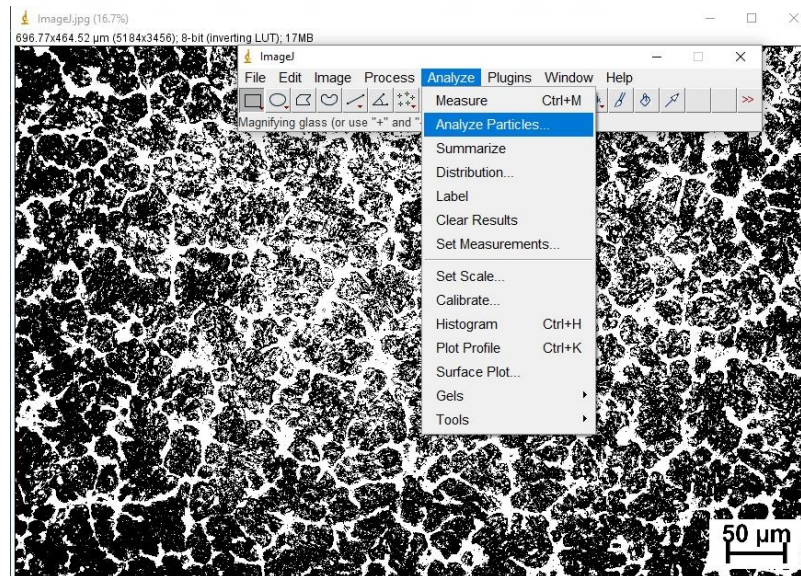


Fig 3.34 Selecting the function of analyzing particles

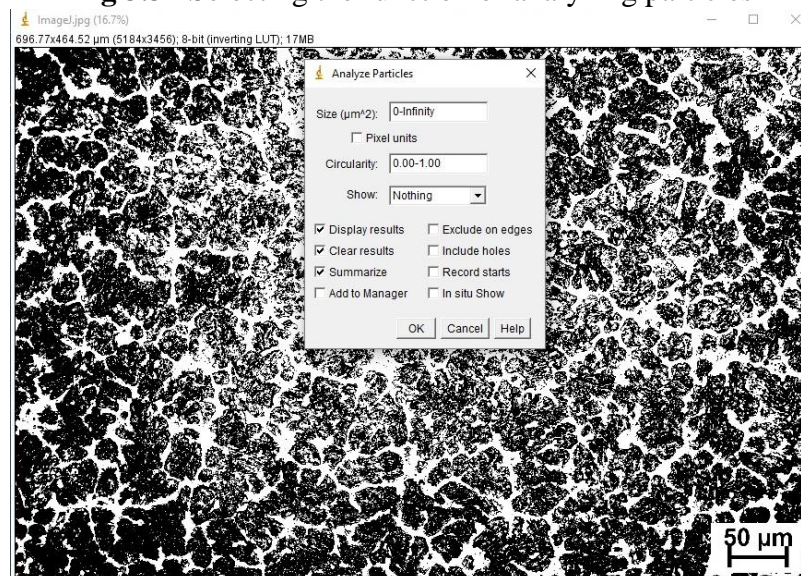


Fig 3.35 Analyzing particles

(5) Finally, Fig 3.36 shows the results of analyzing the area of martensite covered in micrograph using ImageJ software.

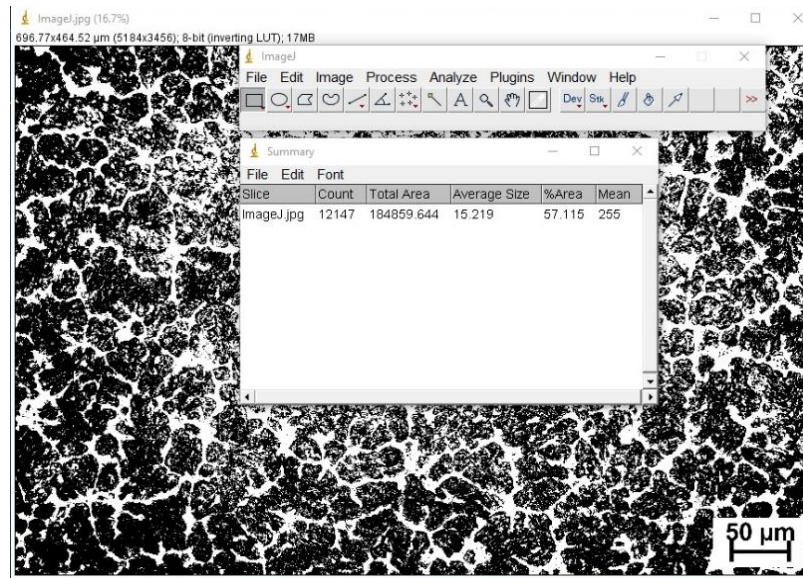


Fig 3.36 Final results

3.8 Hardness testing

A Vickers hardness tester was used to determine the microhardness distribution across the cross-sections of the samples, i.e. the base metal, heat affected zone (HAZ), the buffer layer, and hardfacing layers and the top surface of the welded samples. A test load of 200g (1961 mN), dwell time of 10 seconds and the distance between each data point of 0.25 mm for the cross section was used. The microhardness data of top surface obtained under different currents and polarities were randomly analysed on each sample. Fig 3.37 shows the hardness values and testing parameters on the digital screen.

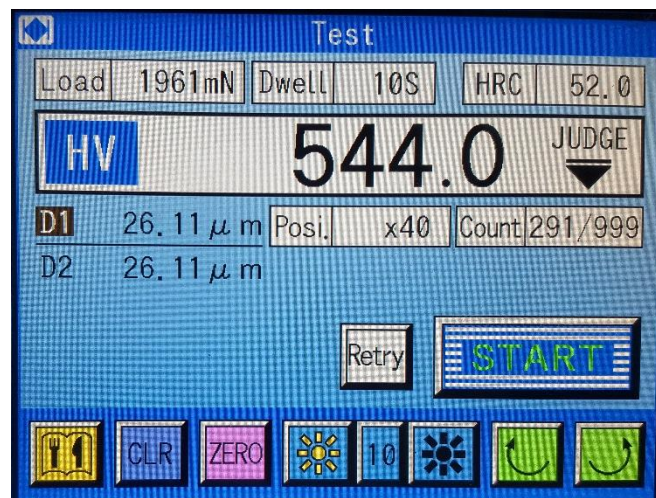


Fig 3.37 Hardness values and parameters of test appeared on the digital screen

3.9 Abrasive wear testing

Following ASTM G65 procedure A, a dry sand rubber wheel apparatus was used for testing and measuring the abrasive mass loss of the samples.

(1) The specimens cut to $14 \text{ mm} \times 25.4 \text{ mm} \times 74.6 \text{ mm}$ in accordance with ASTM G65 standard. Fig 3.37 shows the abrasion specimen before testing and the tested abrasion specimen.



Fig 3.38 The abrasion specimen (a) before testing (b) tested specimen

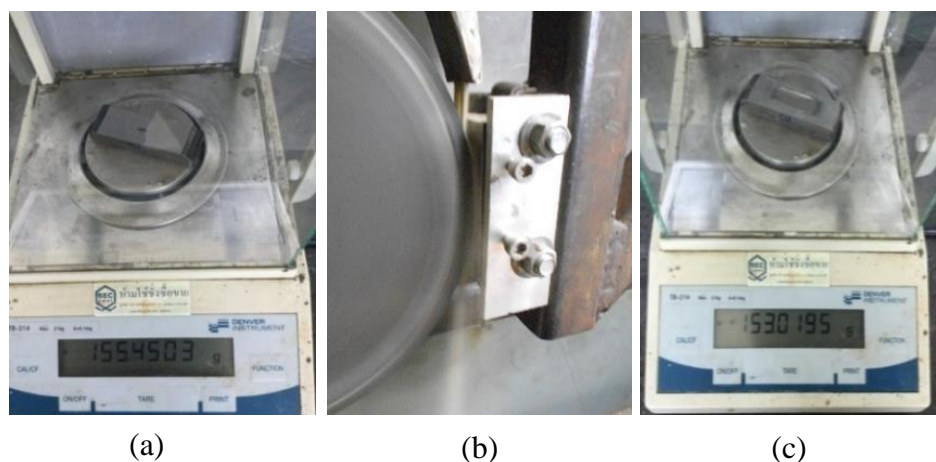


Fig 3.39 Measuring weight loss of abrasive wear tested specimen (a) Initial weight (b) testing the specimen (c) final weight

(2) Round quartz sand size with the range from 212 to 300 μm was used as abrasive particles in the wear tester. The applied load and flow rate of sand were fixed at 130N and 300 g/min. Rubber wheel rotation speed during running the machine, the diameter of the wheel and a total distance of wheel rotation were 200 rpm, 228.6 mm and 4309 m respectively.

(3) After running the experiments, the mass losses of specimens were measured and recorded on an electric balance, and weight losses were determined and recorded. Fig 3.38 shows weighting specimens before and after testing. Weighting before testing, running the test and after weighing the tested specimen are demonstrated in Fig 3.39.

Chapter 4

Results and Discussion

4.1 Base metal

4.1.1 The microstructure of Fe-3.5% Cr steel base metal at 200 magnifications by an optical microscope is shown in Fig 4.1. A mixture of ferrite, pearlite and bainite microstructures in the grain boundaries appears in the microstructure of the base metal. The white phase represents ferrite and the dark phase is the mixed structure of pearlite and fine bainite.

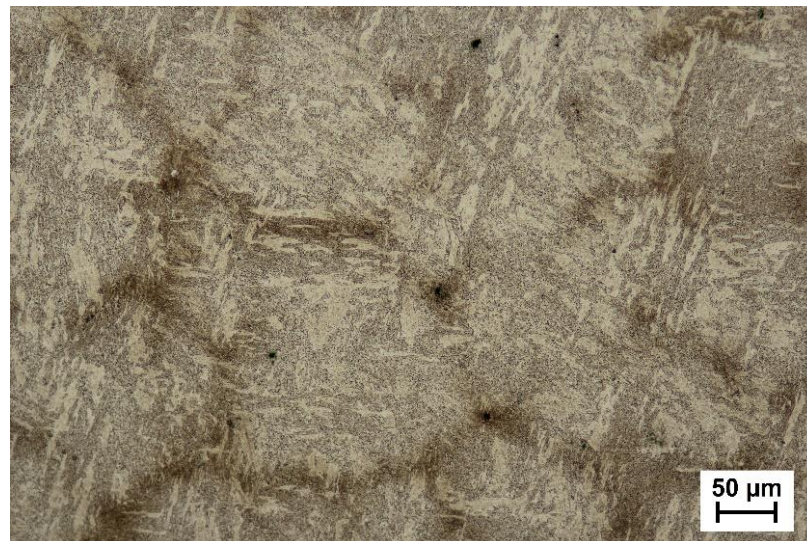


Fig 4.1 Microstructure of 3.5% Cr steel

4.1.2 The average hardness values of 3.5% Cr steel is about 190-210 HV.

4.1.3 The mass loss due to wear of 3.5% Cr steel is 2.7613 g and the wear resistance based on the mass loss is 1.56 m/mg.

4.2 Welded sample

Five weld beads were deposited to form layers and the overlap between the beads was approximately 30%. The welded samples were all air cooled to room temperature and were examined for presence weld defects. The complete absence of weld defect was observed, as shown in Fig.4.2.

Welded samples are shown divided into two parts; left side is the single layer hardfacing, and the right side is the three layers hardfacing. A single buffer layer was applied in all samples prior to hardfacing.



Fig 4.2 The appearance of the sample after depositing

4.3 Macrostructural Analysis

The initial macrostructural examinations of the samples magnified to 4 magnifications were done using an optical microscope. In the heat affected zone in the base metal and in the welded layers, no defect, flaw and crack were found. Also, good bonding between layers was evident. The average thicknesses of the base metal, the deposited layer and the heat affected zone are about 13-15 millimetres, 3-4 millimetres and 2-3 millimetres. In Fig 4.3, the macrostructures of the single layer hardfacing laid using different currents and polarities is shown. No defects and cracks can be seen in all of the macrographs. The thickness of the deposited layer varies with the different currents, as the layers laid using higher current gives thicker deposited layer.

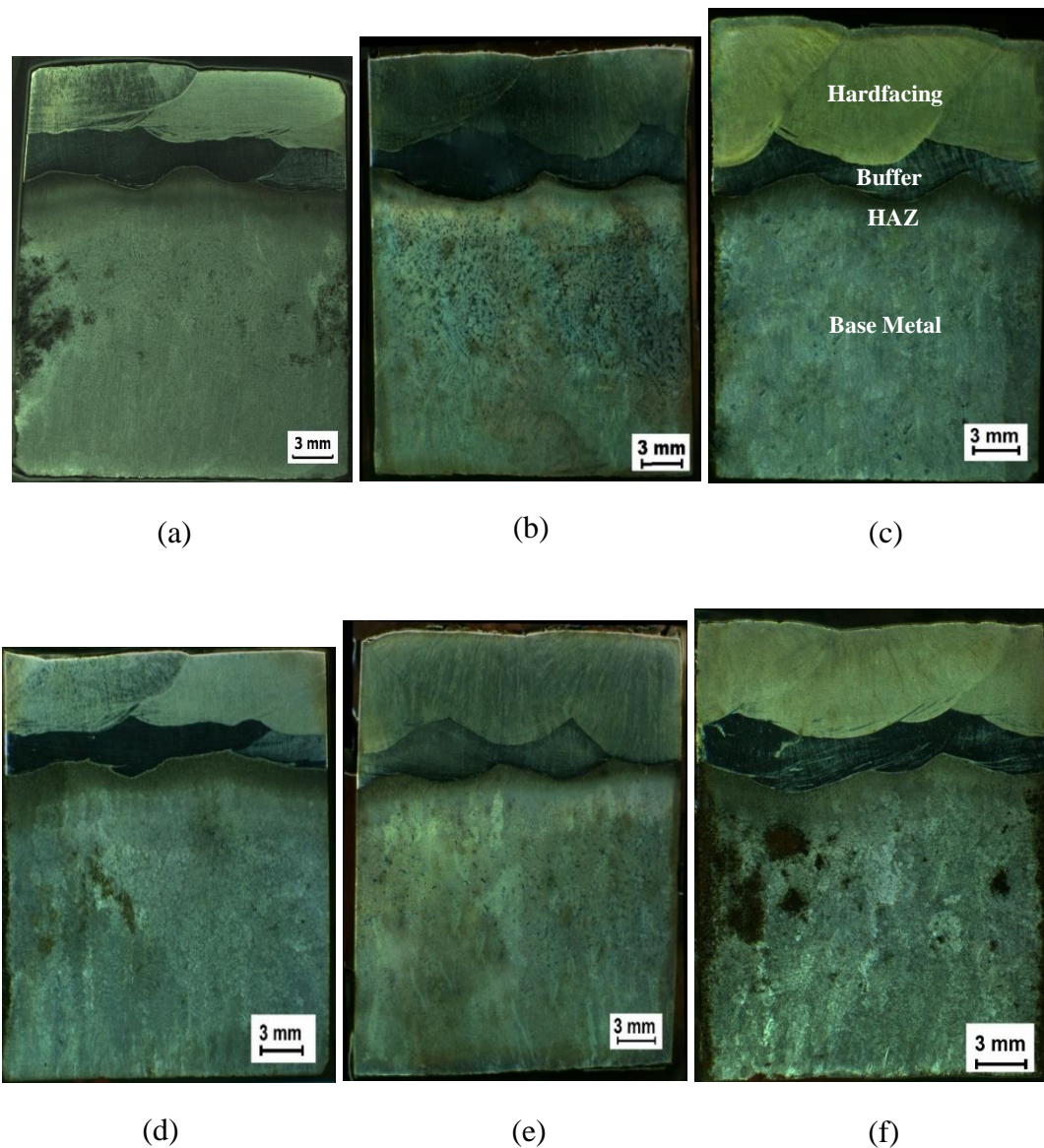


Fig 4.3 The macrostructure of single layer hardfacing (a) 1B 1H 500A AC (b) 1B 1H 600A AC (c) 1B 1H 700A AC (d) 1B 1H 500A DC+ (e) 1B 1H 600A DC+ (f) 1B 1H 700A DC+

The macrostructures of the three layers hardfaced samples welded using different currents and polarities are shown in Fig 4.4. Defects were not seen in the heat affected zone, buffer layer; and in the first, second, and third hardfaced layers. The interfaces between the base metal and the adjoining layer, as well as the interfaces between the different hardfaced layers are apparent.

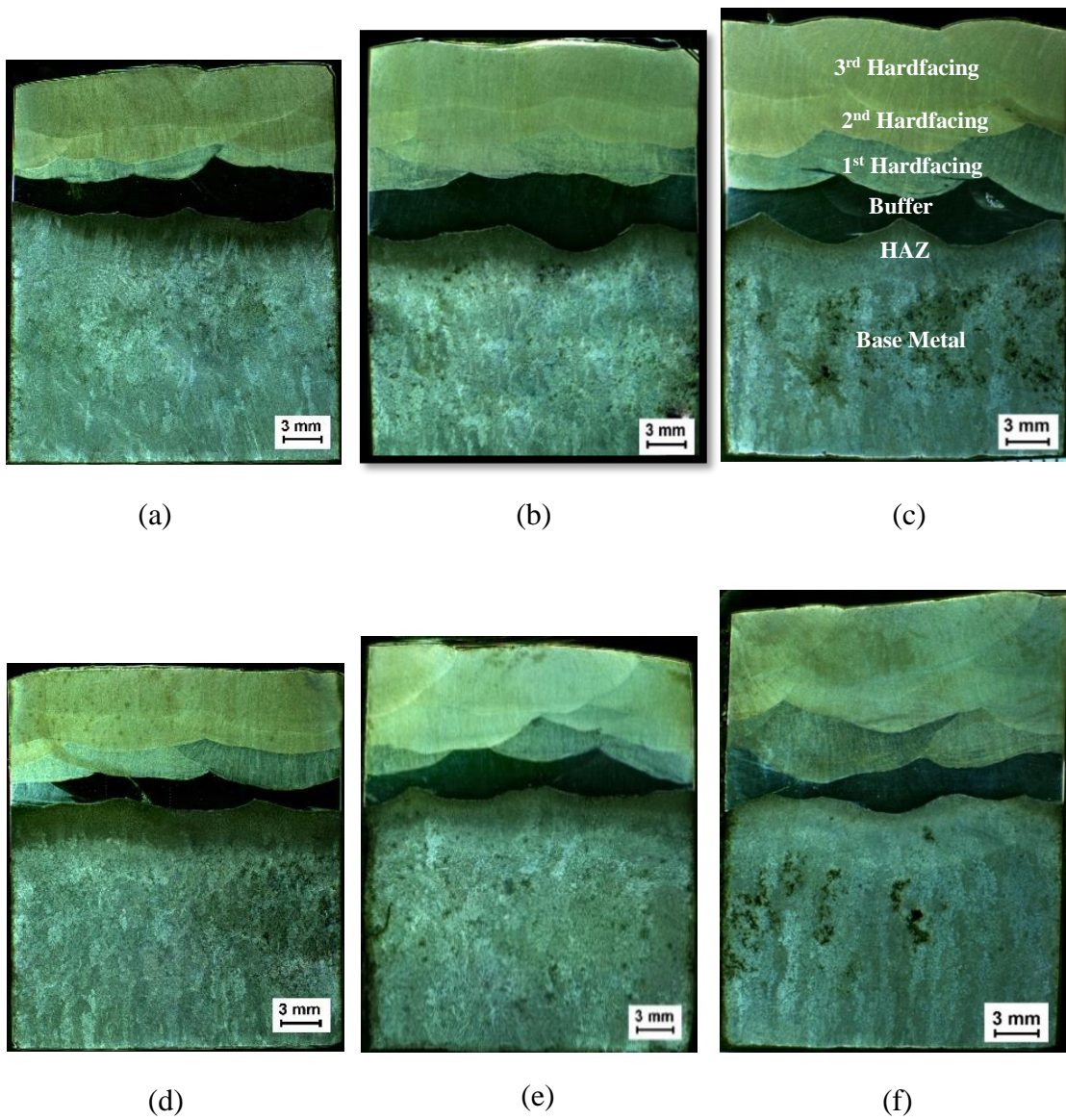


Fig 4.4 The macrostructure of three layers hardfacing (a) 1B 3H 500A AC (b) 1B 3H 600A AC (c) 1B 3H 700A AC (d) 1B 3H 500A DC+ (e) 1B 3H 600A DC+ (f) 1B 3H 700A DC+

4.4 Microstructural characterization

4.4.1 Heat affected zone

The microstructures of the heat affected zone of single layer hardfacing welded using 500A, 600A, 700A welding currents, and with either AC or DC+ polarity is shown in Fig 4.5. This area is in the base metal adjacent to the fusion line is heated to sufficiently high temperatures, to cause structural changes within the initial base metal structure. It should note the presence of needle-shaped martensite and retained austenite. This was seen in the heat affected zones of all samples. The needle-like dark area is martensite phase and white region in the micrograph is retained austenite phase that cannot transform to the martensite phase. This area was not melted during welding, but the high temperatures essentially caused heat treatment. Martensite was formed in the fast-cooled regions.

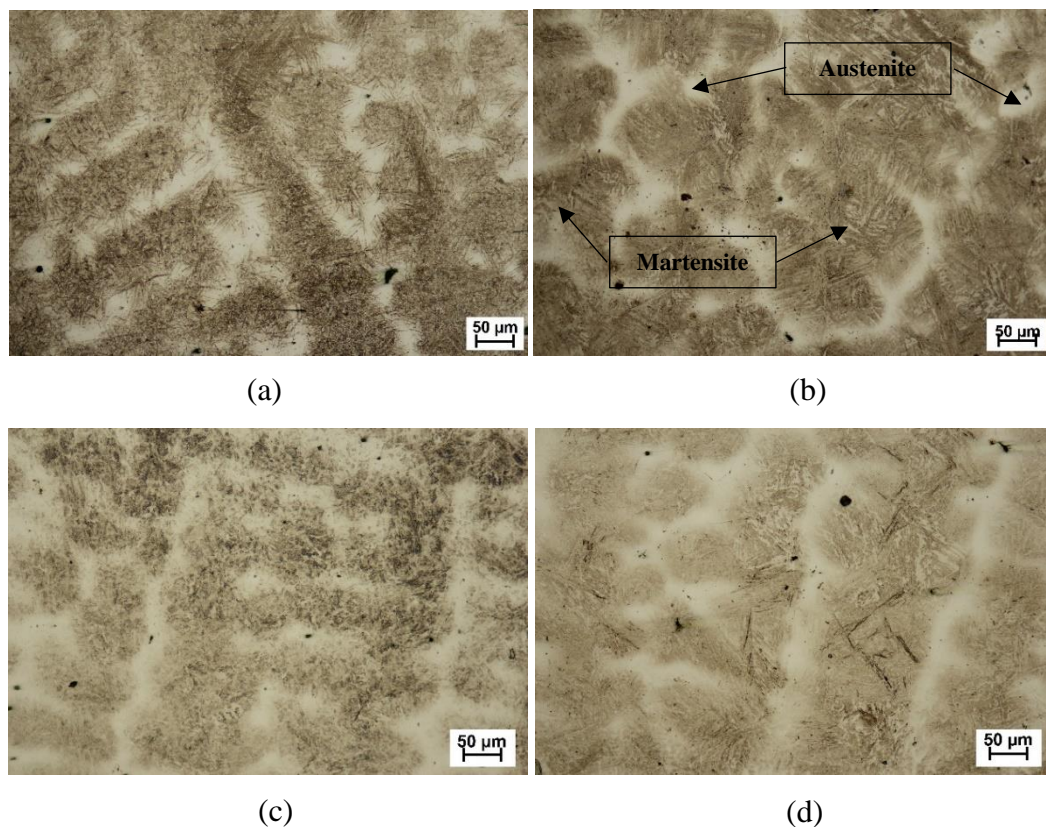


Fig 4.5 The heat affected zone microstructure of single layer hardfacing (a) 1B 1H 500A AC (b) 1B 1H 500A DC+ (c) 1B 1H 600A AC (d) 1B 1H 600A DC+ (e) 1B 1H 700A AC (f) 1B 1H 700A DC+

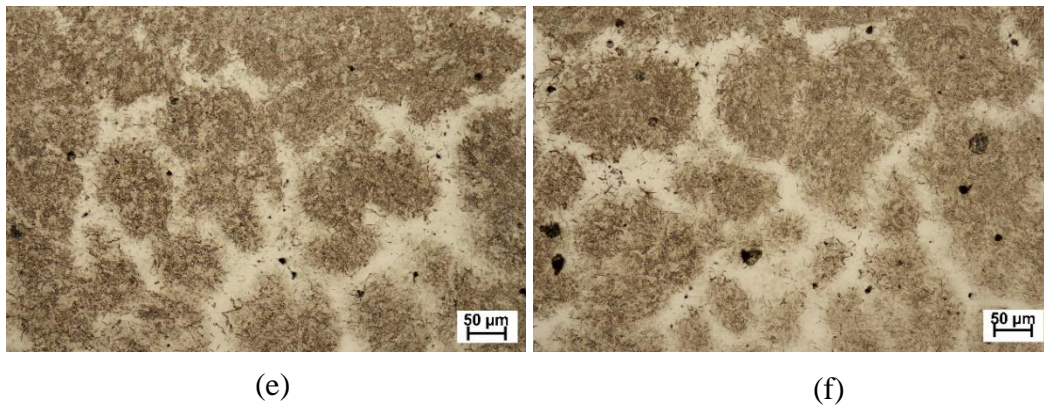


Fig 4.5 The heat affected zone microstructure of single layer hardfacing (a) 1B 1H 500A AC (b) 1B 1H 500A DC+ (c) 1B 1H 600A AC (d) 1B 1H 600A DC+ (e) 1B 1H 700A AC (f) 1B 1H 700A DC+ (continued)

The heat affected zone microstructure of three layers hardfacing deposited with 500A, 600A, 700A and using AC and DC+ polarity presents in Fig 4.6. The heat affected zone microstructural appearance of three layers hardfacing is same as that of single layer hardfacing. Comparing with the heat affected zone micrographs of three layers and single layer, the larger phase of martensite found in the micrographs of three layers because the base metal for three layers hardfacing was more affected by repeated heat treating of a second and third layer of three layers hardfacing.

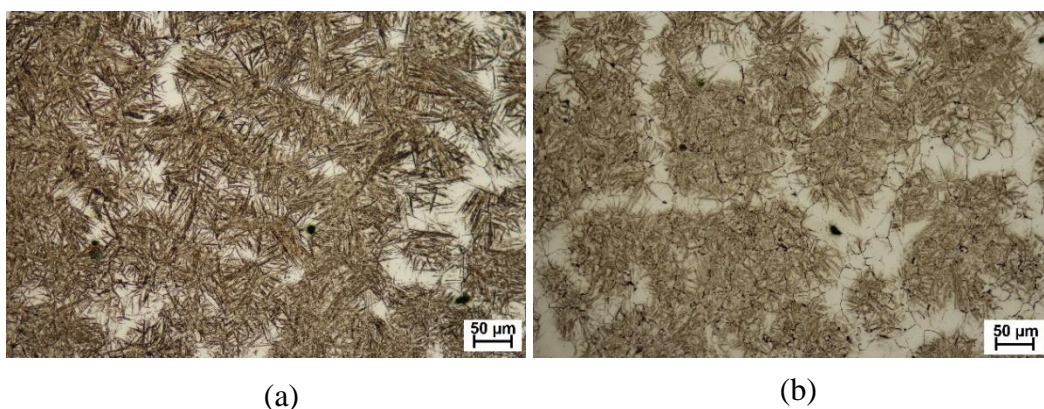


Fig 4.6 The heat affected zone microstructure of three layers hardfacing (a) 1B 3H 500A AC (b) 1B 3H 500A DC+ (c) 1B 3H 600A AC (d) 1B 3H 600A DC+ (e) 1B 3H 700A AC (f) 1B 3H 700A DC+

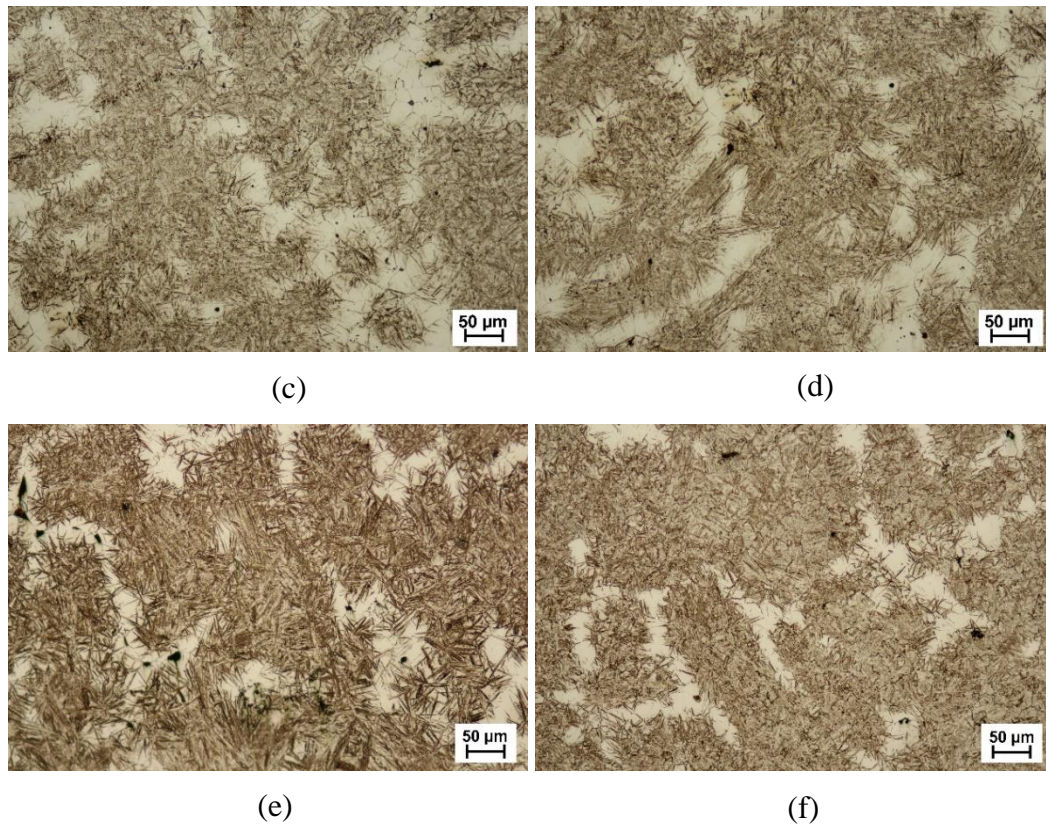


Fig 4.6 The heat affected zone microstructure of three layers hardfacing (a) 1B 3H 500A AC (b) 1B 3H 500A DC+ (c) 1B 3H 600A AC (d) 1B 3H 600A DC+ (e) 1B 3H 700A AC (f) 1B 3H 700A DC+ (Continued)

4.4.2 Buttering

In this project, the buffer layer was applied to the area between the base substrate and the hardfacing layer and prior to hardfacing layer. Austenitic stainless-steel type electrode was used to deposit for the buffer layer. This alloy has high ductility and impacts resistance but lower strength. Fig 4.7 and Fig 4.8 show the microstructure of buffer layer for single layer and three layers hardfacing. In the micrographs of the buffer layer for all experimental conditions, the austenitic microstructure in the grain boundaries appears.

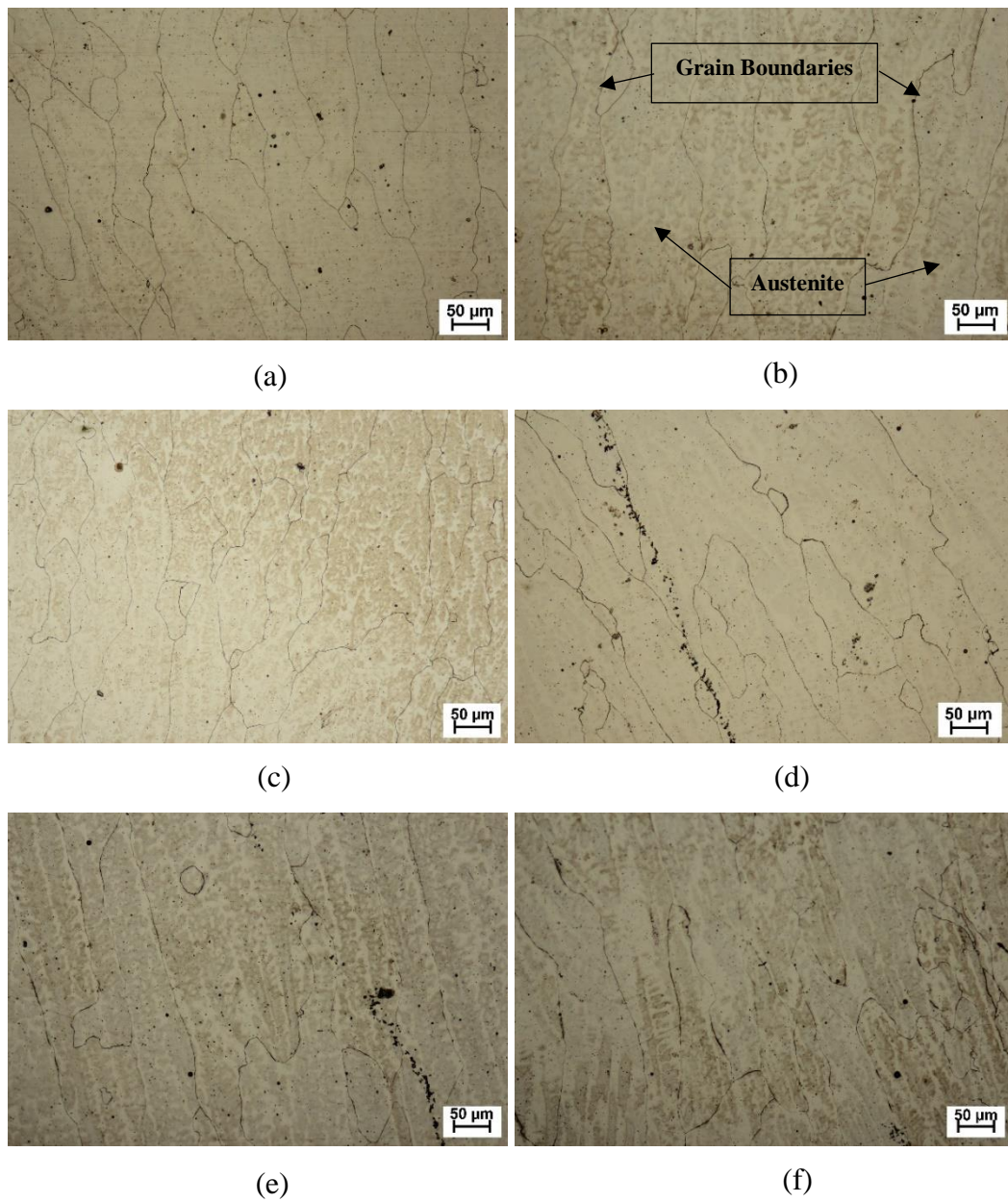


Fig 4.7 The microstructure of buffer layer for single layer hardfacing (a) 1B 1H 500A AC (b) 1B 1H 500A DC+ (c) 1B 1H 600A AC (d) 1B 1H 600A DC+ (e) 1B 1H 700A AC (f) 1B 1H 700A DC+

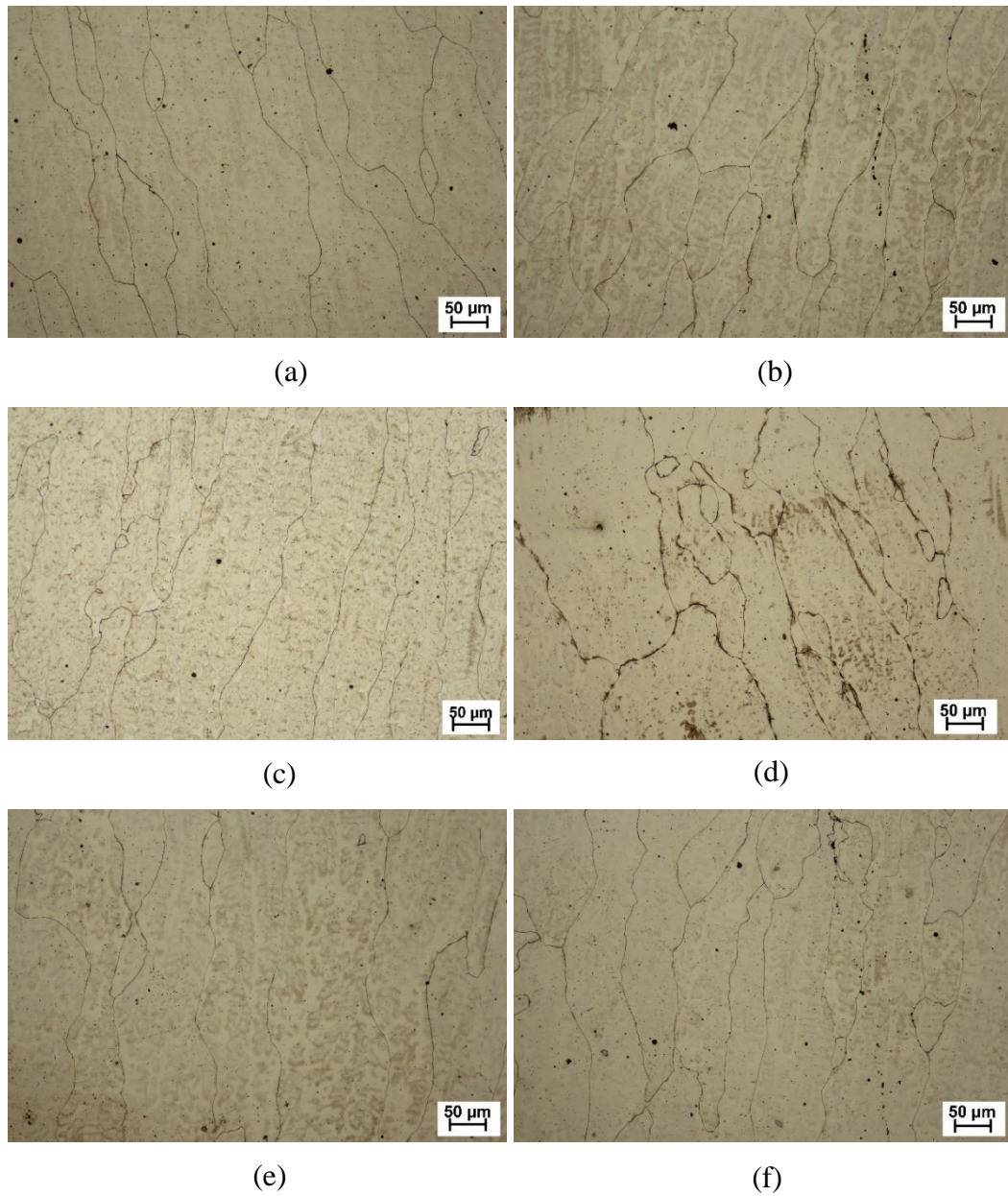


Fig 4.8 The microstructure of buffer layer for three layers hardfacing (a) 1B 3H 500A AC (b) 1B 3H 500A DC+ (c) 1B 3H 600A AC (d) 1B 3H 600A DC+ (e) 1B 3H 700A AC (f) 1B 3H 700A DC+

4.4.3 Single layer hardfacing

The microstructure of single layer hardfacing for all experiments shows in Fig 4.9. The micrographs reveal the martensite phase (dark phase) mixed with austenite phase (white phase) in the grain boundary. This layer was deposited after the buffer layer has been welded. Although the martensitic type wire electrode was applied for the hardfacing layer, the much amount of austenitic microstructure revealed in the micrographs. This was due to the fact that the higher dilution with the austenitic buffer layer occurred when the martensitic hardfacing was welding.

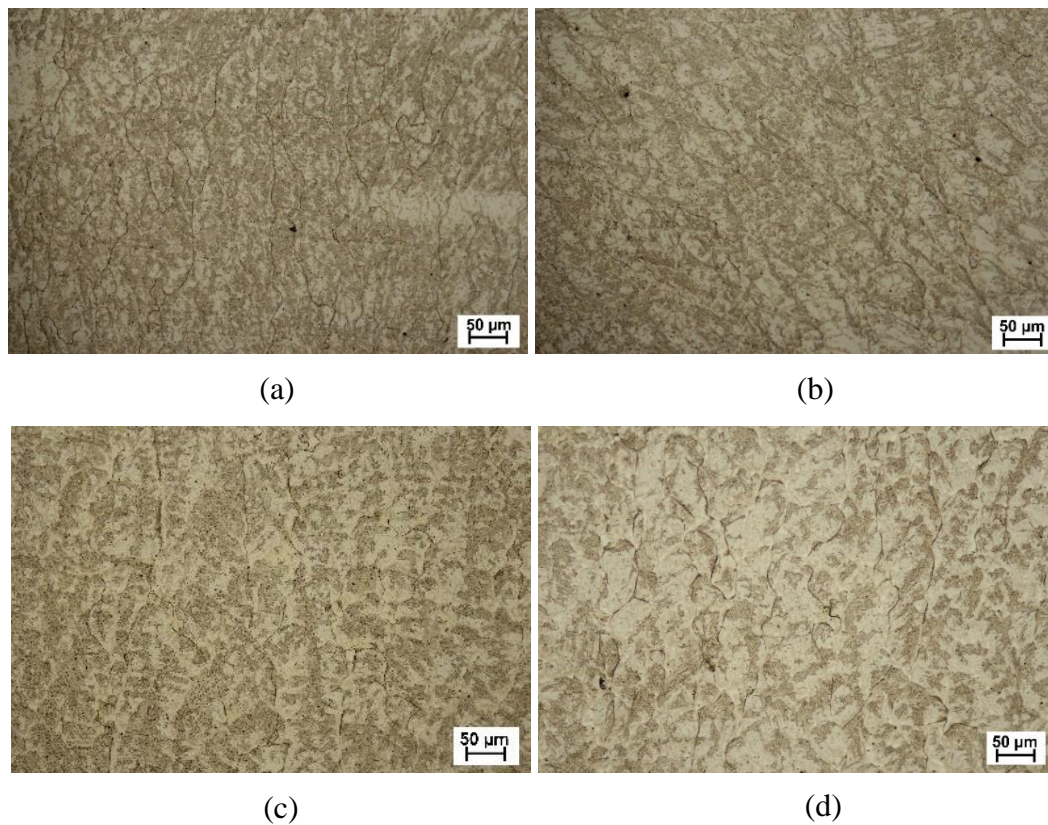
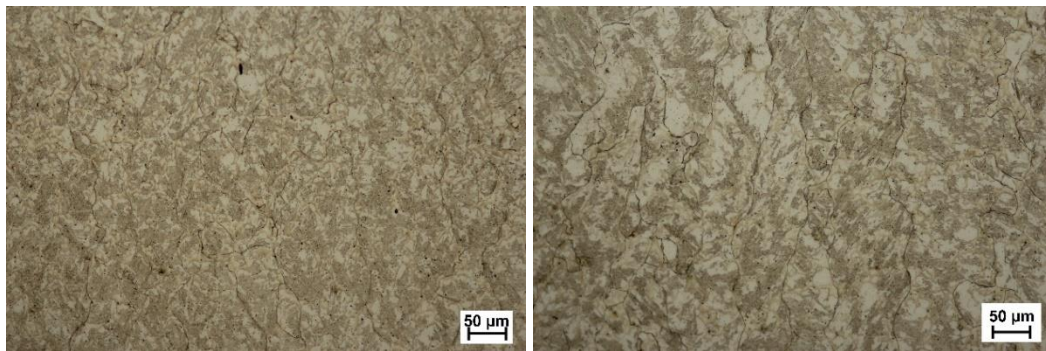


Fig 4.9 The microstructure of single layer hardfacing (a) 1B 1H 500A AC (b) 1B 1H 500A DC+ (c) 1B 1H 600A AC (d) 1B 1H 600A DC+ (e) 1B 1H 700A AC (f) 1B 1H 700A DC+



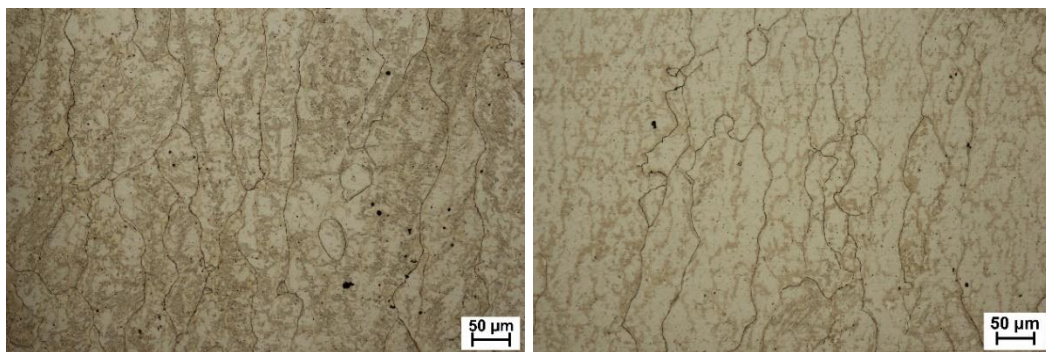
(e)

(f)

Fig 4.9 The microstructure of single layer hardfacing (a) 1B 1H 500A AC (b) 1B 1H 500A DC+ (c) 1B 1H 600A AC (d) 1B 1H 600A DC+ (e) 1B 1H 700A AC (f) 1B 1H 700A DC+ (Continued)

4.4.4 First of three layers hardfacing

A large amount of austenitic microstructure with martensitic microstructure in the grain boundaries can be seen in the microstructure of first of three layers hardfacing (Fig 4.10). Comparison between the microstructure of single hardfacing and a first hardfacing layer of three layers hardfacing, first of three layers hardfacing's microstructure gives more austenitic microstructure than that of a single layer.



(a)

(b)

Fig 4.10 The microstructure of first of three layers hardfacing (a) 1B 3H 500A AC (b) 1B 3H 500A DC+ (c) 1B 3H 600A AC (d) 1B 3H 600A DC+ (e) 1B 3H 700A AC (f) 1B 3H 700A DC+

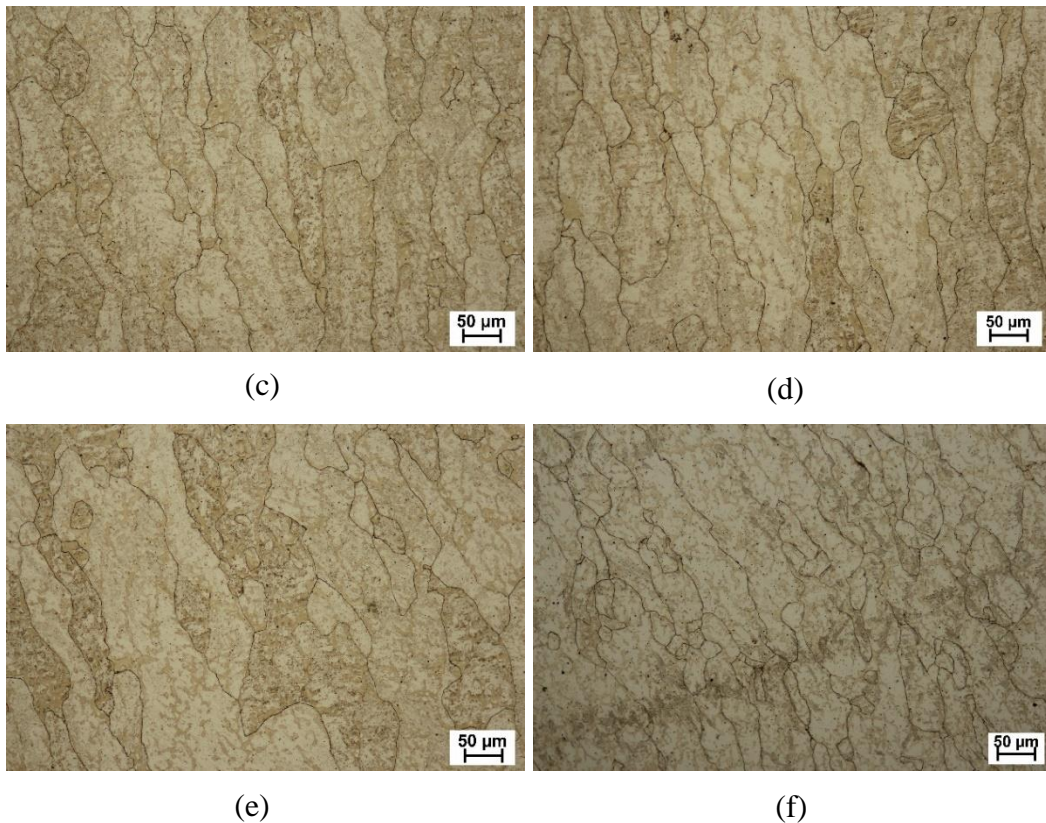


Fig 4.10 The microstructure of first of three layers hardfacing (a) 1B 3H 500A AC (b) 1B 3H 500A DC+ (c) 1B 3H 600A AC (d) 1B 3H 600A DC+ (e) 1B 3H 700A AC (f) 1B 3H 700A DC+ (Continued)

4.4.5 Second of three layers hardfacing

There was more martensite in the second layer as compared to that in the bottom layer. This layer also showed martensite and retained austenite in the grain boundaries. In this layer, the martensite phase generally shows a dendritic pattern. In addition, the amount of martensite found was more than that seen in the single layer hardfacing as more dilution with the buffer layer occurred in the latter case. Fig 4.11 shows the microstructures found in the second layer of three layers hardfacing tests for all samples.

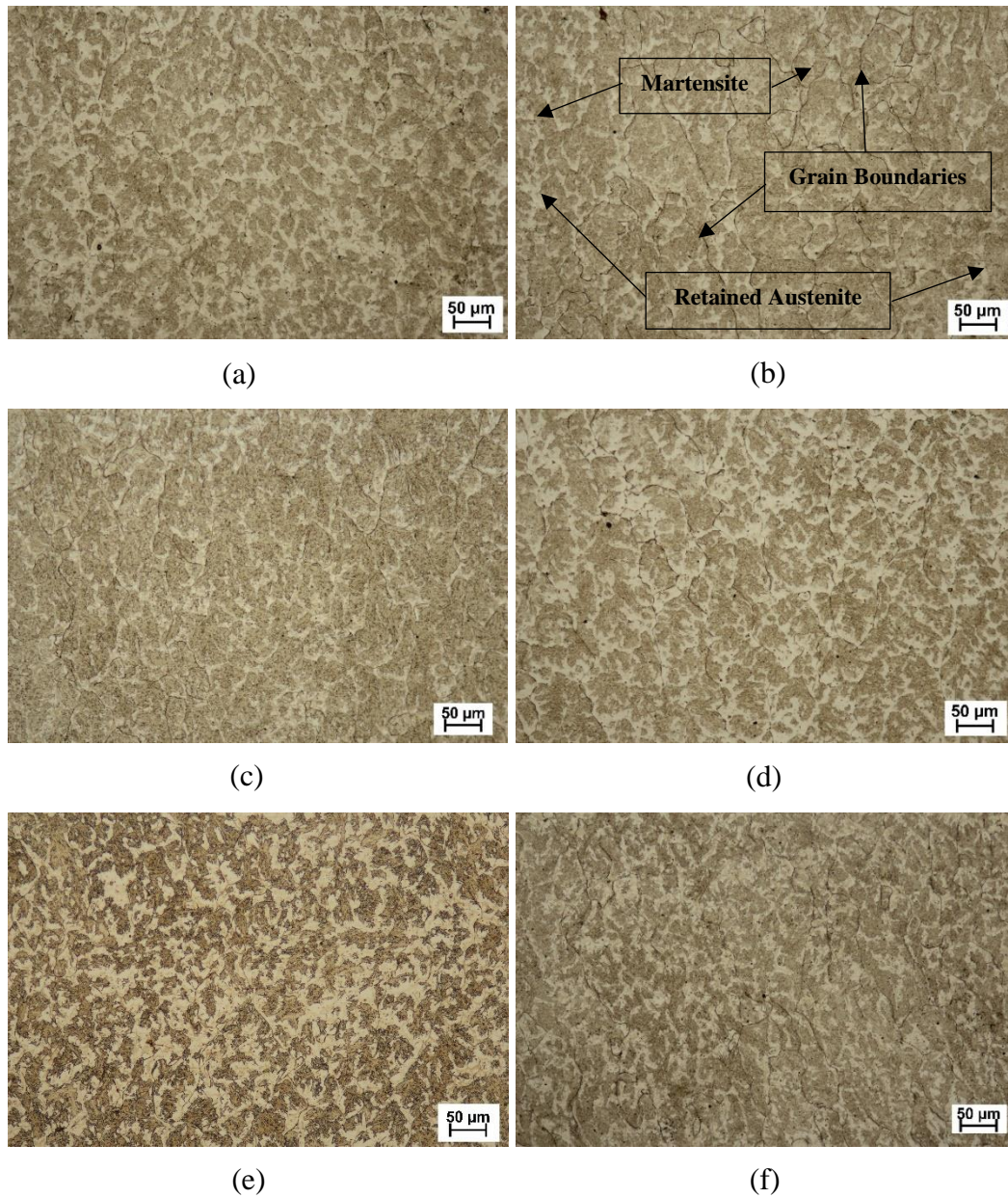


Fig 4.11 The microstructure of second of three layers hardfacing (a) 1B 3H 500A AC (b) 1B 3H 500A DC+ (c) 1B 3H 600A AC (d) 1B 3H 600A DC+ (e) 1B 3H 700A AC (f) 1B 3H 700A DC+

4.4.6 Third of three layers hardfacing

The microstructure of third hardfacing layer of three layers hardfacing welded with 500A, 600A and 700A using AC and DC+ polarity shows in Fig 4.12. The full martensite phase surrounded by a small amount of retained austenite phase can be seen in this condition. The retained austenite phase in this condition is not because of the

dilution with austenitic buffer layer but because of the very fast cooling rate. The microstructures of the third hardfacing welded with different currents and polarities are almost same as each other.

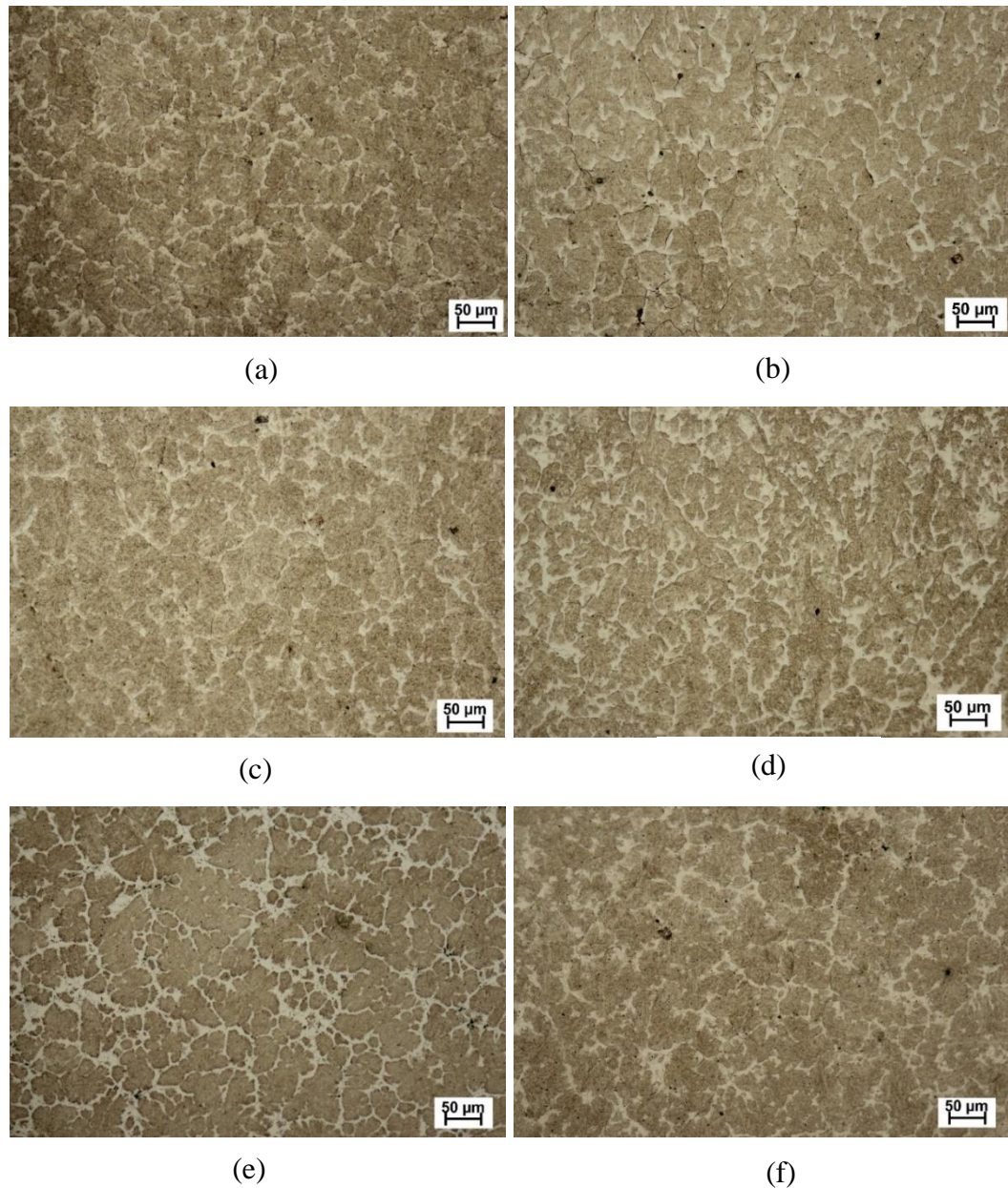


Fig 4.12 The microstructure of third of three layers hardfacing (a) 1B 3H 500A AC (b) 1B 3H 500A DC+ (c) 1B 3H 600A AC (d) 1B 3H 600A DC+ (e) 1B 3H 700A AC (f) 1B 3H 700A DC+

4.4.7 Top surface

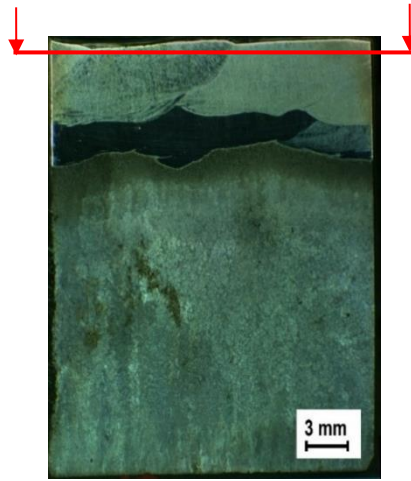


Fig 4.13 The area identification for microstructural analysis of single layer top surface

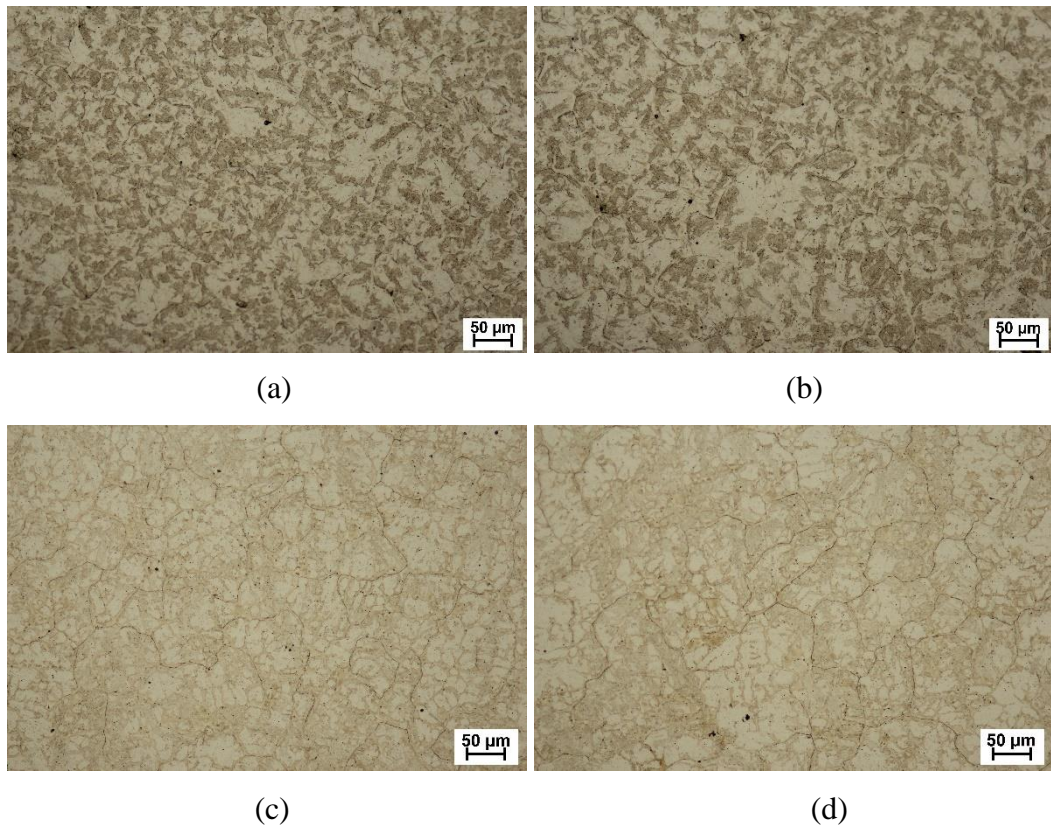
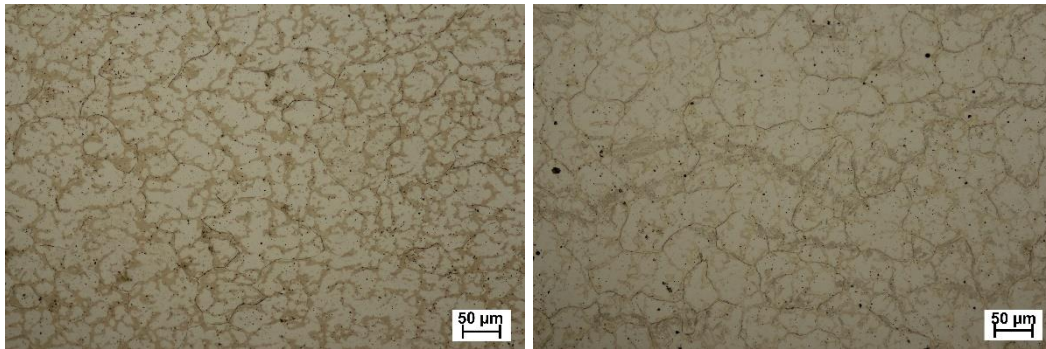


Fig 4.14 The top surface microstructure of single layer hardfacing (a) 1B 1H 500A AC (b) 1B 1H 500A DC+ (c) 1B 1H 600A AC (d) 1B 1H 600A DC+ (e) 1B 1H 700A AC (f) 1B 1H 700A DC+



(e)

(f)

Fig 4.14 The top surface microstructure of single layer hardfacing (a) 1B 1H 500A AC (b) 1B 1H 500A DC+ (c) 1B 1H 600A AC (d) 1B 1H 600A DC+ (e) 1B 1H 700A AC (f) 1B 1H 700A DC+ (Continued)

The top surface microstructure of single layer hardfacing shows in Fig 4.14. In comparison with the cross-sectional microstructure, the microstructure of top surface results in the small amount of martensite phase.

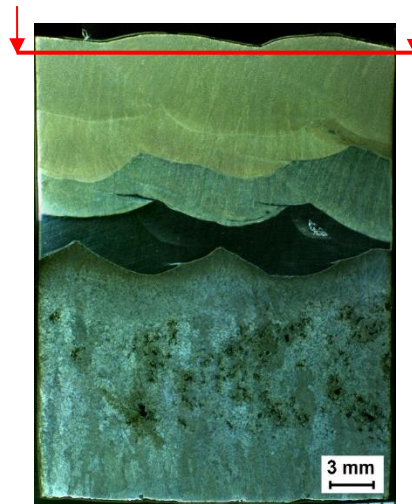


Fig 4.15 The area identification for microstructural analysis of three layers top surface

The top surface micrographs of three layers hardfacing can be seen in Fig 4.16. Fully martensite phase with retained austenite in the grain boundaries presents in these micrographs. It is not too different appearance compared with the cross-sectional microstructure.

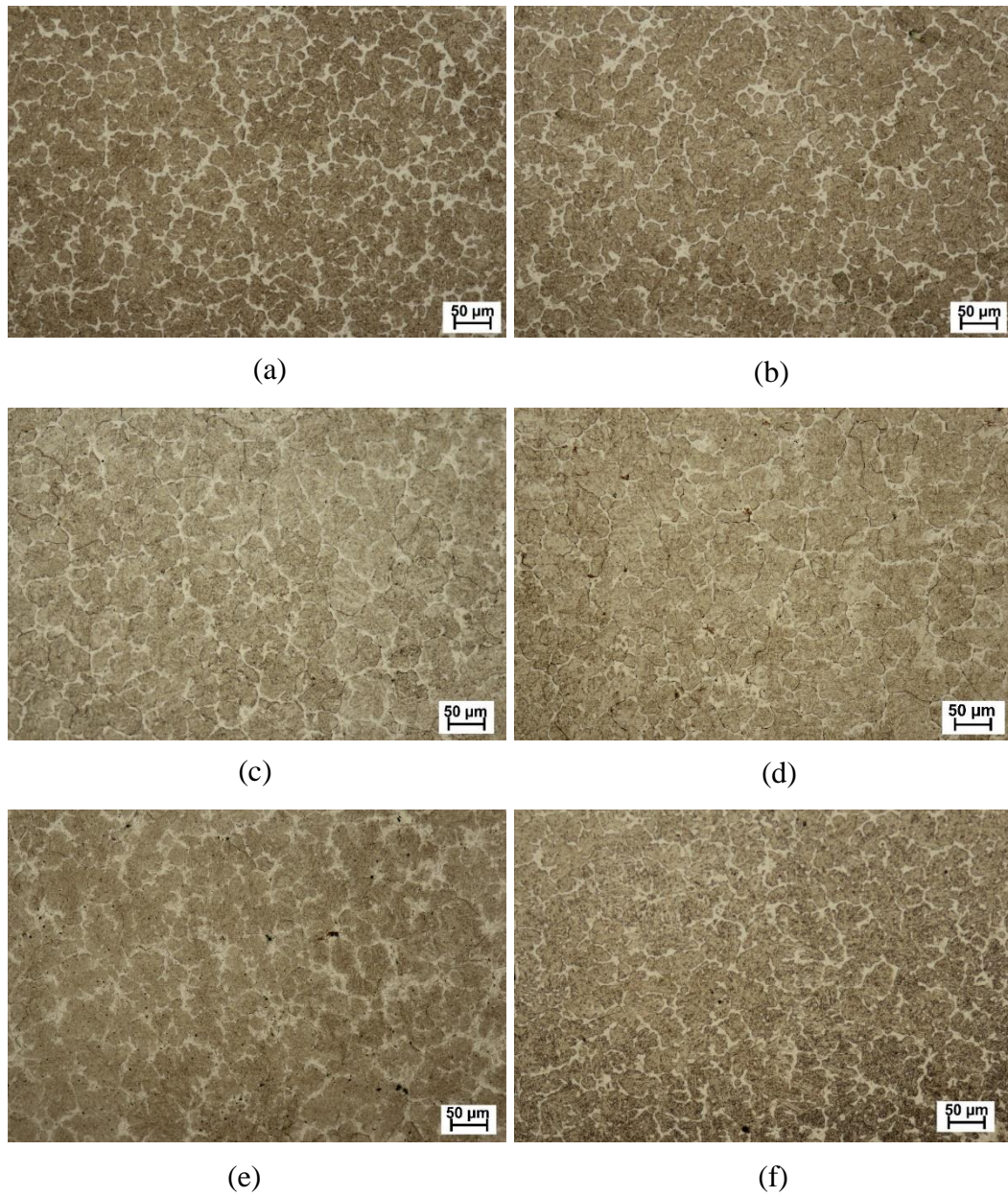


Fig 4.16 The microstructure of third of three layers hardfacing (a) 1B 3H 500A AC (b) 1B 3H 500A DC+ (c) 1B 3H 600A AC (d) 1B 3H 600A DC+ (e) 1B 3H 700A AC (f) 1B 3H 700A DC+

4.4.8 SEM images

The SEM images of samples deposited with a single layer hardfacing of highest abrasive wear resistance sample (a) and lowest abrasive wear resistance (b) are shown in Fig 4.17. SEM image of the sample welded using 500A with AC polarity shows a mixture of martensite and retained austenite phase. The SEM result of 1B1H 600A DC+ condition shows martensite island surrounded by austenite phase. The images clearly indicate that the sample (b) contains a higher amount of austenite phase compared with the sample welded using 600A with DC+ polarity. Therefore, it can be expected that the sample contained a higher amount of austenite phase results in lower hardness and higher abrasive mass losses.

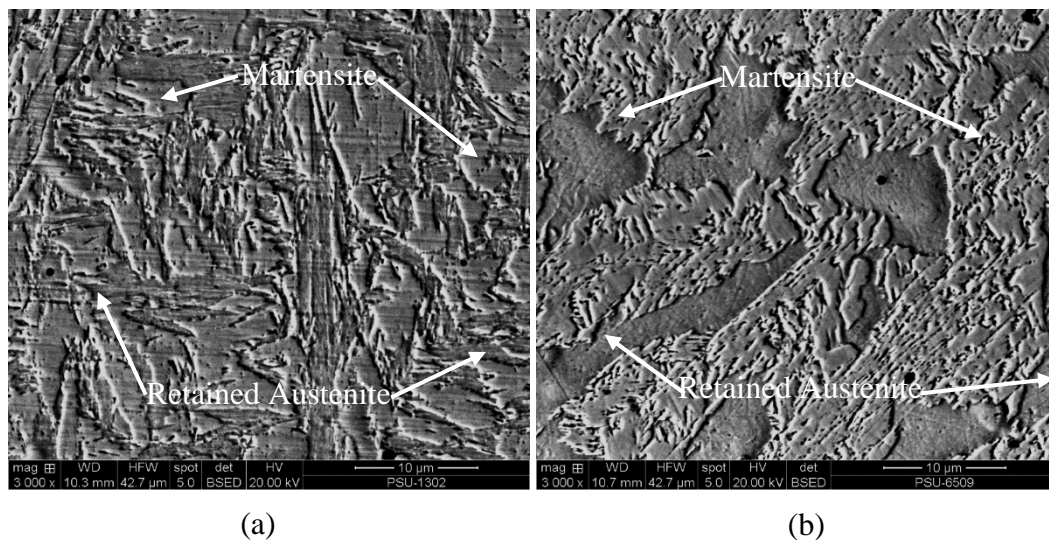


Fig 4.17 SEM image of single layer hardfacing compared with the best and worst condition (a) 1B 1H 500A AC and (b) 1B 1H 600A DC+

In comparing the effects of using two different polarities in applying single layer hardfacing, the result showed that DC+ polarity caused more austenite phase to form than AC polarity, see Fig 4.18. In the samples given a single layer hardfacing, austenite phase formation is mainly due to the dilution with the underlying austenitic buffer layer. Samples harefaaced using alternating current (AC) polarity showed shallower dilution than the direct current electrode positive (DC+) polarity. The submerged arc welding process using DC+ usually cause high weld penetration; when DC - polarity is used, high penetration and a high deposition are seen. The characteristic

of the AC electrical output, with the 2 parts of the wave acting alternatively, can explain the difference between DC+ and AC dilution results [37].

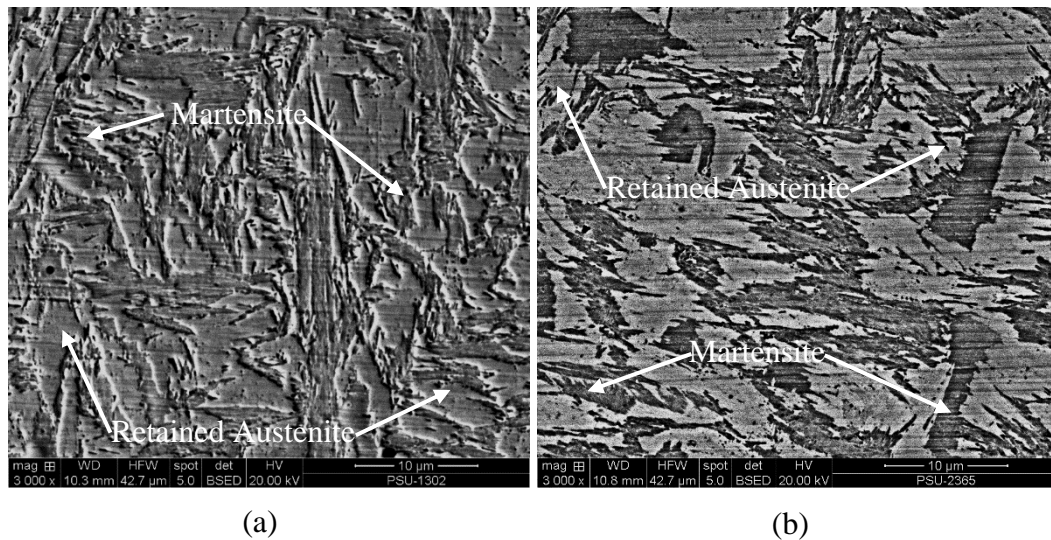


Fig 4.18 SEM image of single layer hardfacing compared with different polarities

(a) 1B 1H 500A AC and (b) 1B 1H 500A DC+

The cross-sections of the third hardfacing layers were examined using an SEM equipped with backscattered electron detector, and the images obtained from the samples showing the best and worst results are compared in Fig 4.19. SEM images of the samples welded using 500A with AC polarity contained martensite islands surrounded by retained austenite, and the sample welded using 600A with DC + polarity also showed the mixture of martensite and retained austenite phases. The sample with the lowest mass loss, (1B 3H 500A AC) clearly showed higher amounts of martensite in islands surrounded by retained austenite phase; whereas the sample with the highest mass loss, (1B 3H 600A DC+) showed more retained austenite phase mixed with martensite phase. Usually the amount of martensite and retained austenite phase that form depend mainly on the cooling rate of the welded metal. The minimum cooling rate necessary to get a suitable microstructure and properties can also vary with the composition, and type of welded steel. The effects of welding heat input and preheating temperature on martensite formation are similar. Higher heat input leads to the slower cooling rate [38]. The slower cooling rate allows more retained austenite formation because the fine austenitic structures tend to lower the temperature where martensite

form, i.e. the martensite start, M_s temperature. Subsequent cooling to room temperature cannot cause completion of austenite to martensite transformation [39-41]. Hence, it can be expected that the high heat input associated with 600 A welded samples will show more retained austenite and less martensite, since higher heat input increases cooling time, i.e. reduced cooling rate, which leads to retaining more austenite formation, because not all the austenite initially present in the alloy at high temperature can transform to martensite.

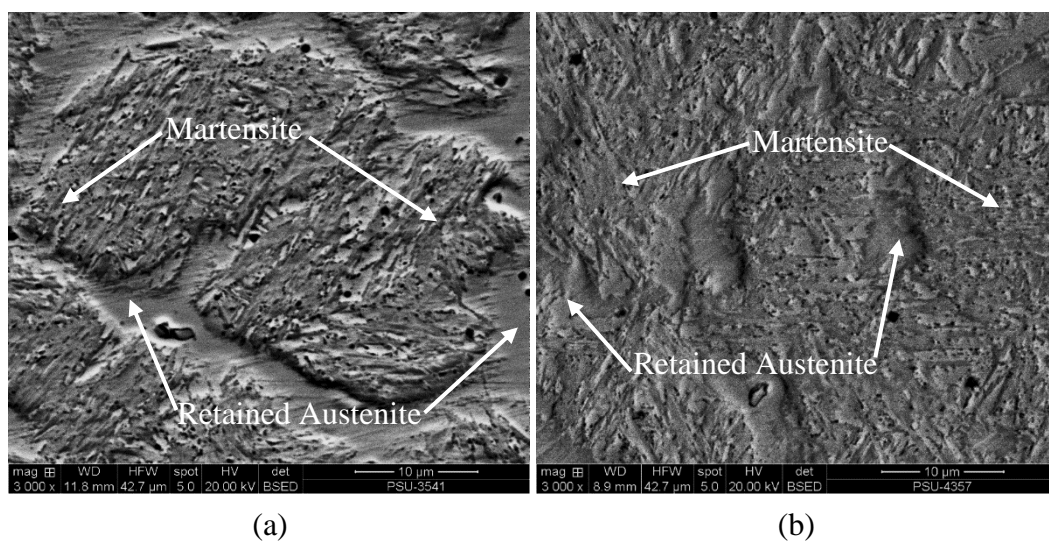


Fig 4.19 SEM image of three layers hardfacing compared to the best and the worst condition (a) 1B 3H 500A AC and (b) 1B 3H 600A DC+

Fig 4.20 shows the SEM images of three hardfacing layers welded with same welding current (500A) but using different welding polarities. These images show that the amount and size of the martensite islands surrounded by retained austenite are determined by the type of welding polarity used. These SEM results showed that the sample welded with AC polarity showed a large areas of martensite phase and small amount of retained austenite, whereas, the opposite result: small area of martensite phase with large area of retained austenite was seen in the sample welded with DC+ polarity. The austenite region leads to lower hardness that give higher mass losses: In the area where the large of austenite phase are located, deep ploughing and holes or voids due to abrasion in the softer austenite are seen.

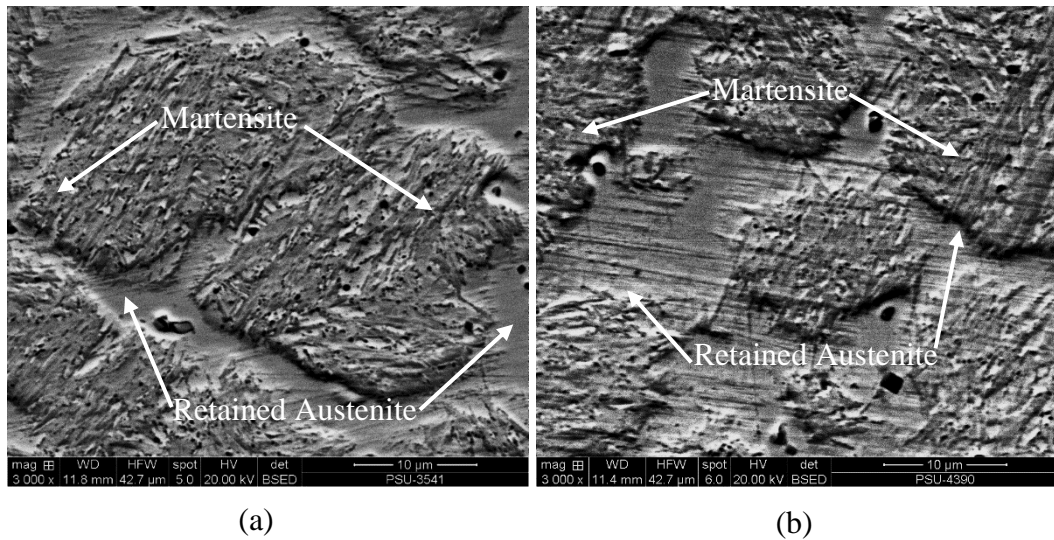
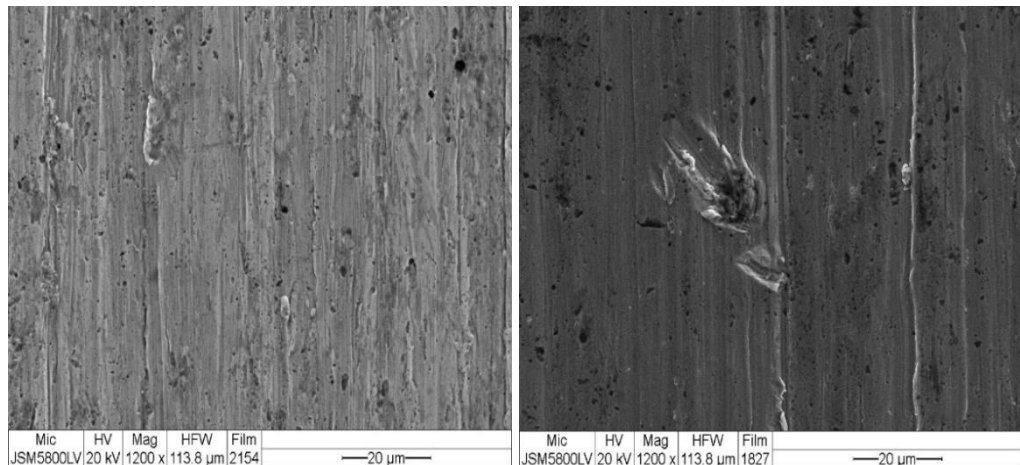


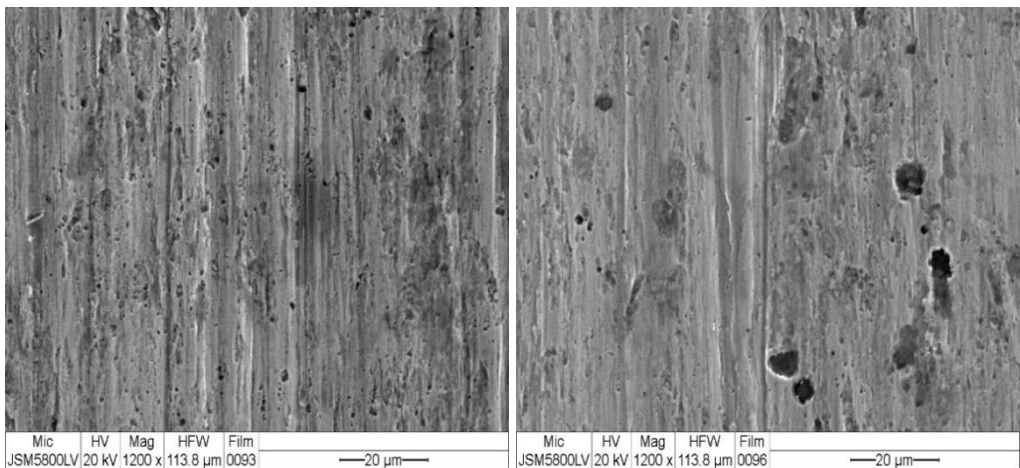
Fig 4.20 SEM image of three layers hardfacing compared to different polarities (a) 1B 3H 500A AC and (b) 1B 3H 500A DC+

Types of wear mechanisms acting on samples tested for their abrasion resistances were determined using SEM equipped with secondary electron detector examination of the worn surfaces. SEM images of three layers hardfacing worn surfaces are shown in Fig 4.21. The main wear mechanism seen was micro-ploughing. The images of the worn surface are similar, but the sample, B, welded using 600A with DC+, showed abrasive voids across the image, Fig 4.19 (d). These led to the higher mass loss of the sample. This sample also showed the highest amount of austenite phase and the lowest top surface hardness. Comparing higher to lower current, more abrasive cutting voids can be seen in both samples welded using 600A. These samples also contained a lower amount of martensite, and lower top surface hardness. The regions containing the softer austenite phase areas were worn easily by the hard-abrasive particles. All samples welded using differing currents, but with DC+ polarity, exhibited abrasive cutting voids due to the larger amount of retained austenite clearly seen in SEM image when compared to what the sample welded with AC polarity showed. The retained austenite areas have a much lower resistance against wear by abrasive particles used in the test runs. The area located retained austenite cannot withstand the wearing of abrasive particles during running the test and these areas might occur and leave the abrasive cutting holes on the tested worn surfaces.



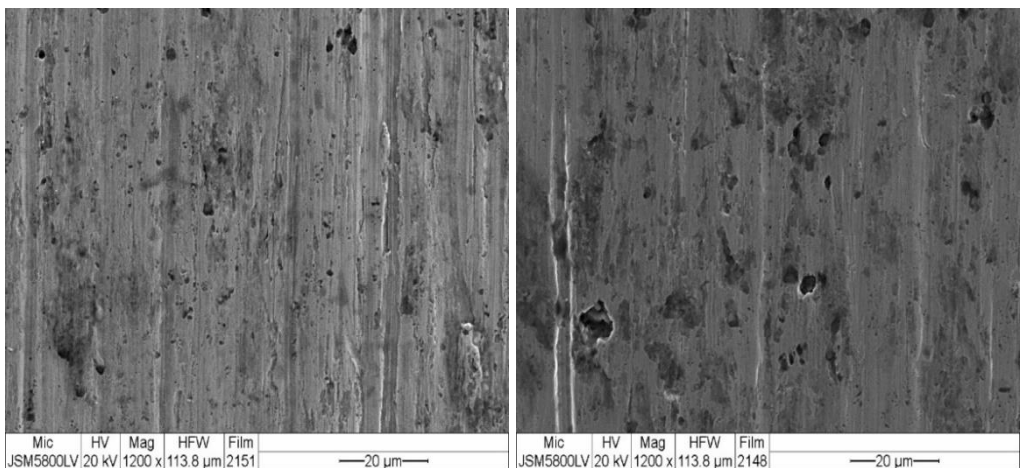
(a)

(b)



(c)

(d)



(e)

(f)

Fig 4.21 The SEM image of worn surfaces (a) 1B 3H 500A AC (b) 1B 3H 500A DC+ (c) 1B 3H 600A AC (d) 1B 3H 600A DC+ (e) 1B 3H 700A AC (f) 1B 3H 700A DC+

4.4.9 Emission-dispersive x ray result (Point Scan)

The SEM image of single layer hardfacing to characterize EDX analysis is shown in Fig 4.22. In Table 4.1, the chemical composition of single layer hardfacing characterized by EDX presents. There are three specific areas analyzed using EDX. The result of spectrum 3 in single layer hardfacing represents the austenitic microstructure and the chemical composition of martensitic microstructure results in the rest of spectrums.

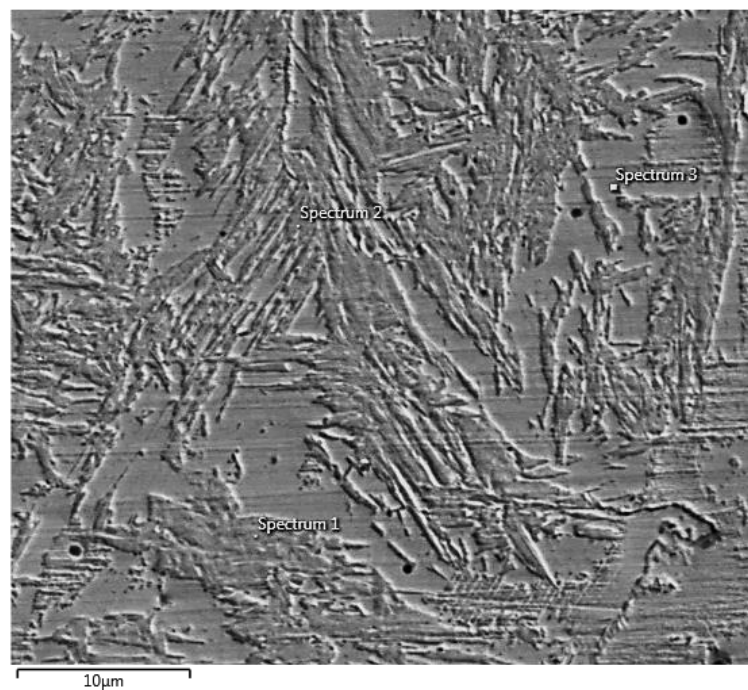


Fig 4.22 EDX point scanned on the SEM image of single layers hardfacing

Table 4.1 Chemical composition of single layers hardfacing analyzed by EDX

Spectrum	%Fe	%C	%Cr	%Mn	%Ni	%Si
1	80.4	8.6	6	1.2	1.0	0.7
2	80.3	8.6	6.1	1.3	1.1	0.7
3	80.6	7.4	6.7	1.5	1.1	0.8

Fig 4.23 shows SEM microstructure of three layers hardfacing for EDX analysis. The EDX result of three layers hardfacing can be seen in Table 4.2. The chemical composition of austenitic microstructure shows in spectrum 1 and the chemical composition of martensitic microstructure results in the spectrum 2 and 3.

Comparison between the EDX results of single layer hardfacing and three layers hardfacing, three layers hardfacing shows a higher amount of carbon, chromium and manganese.

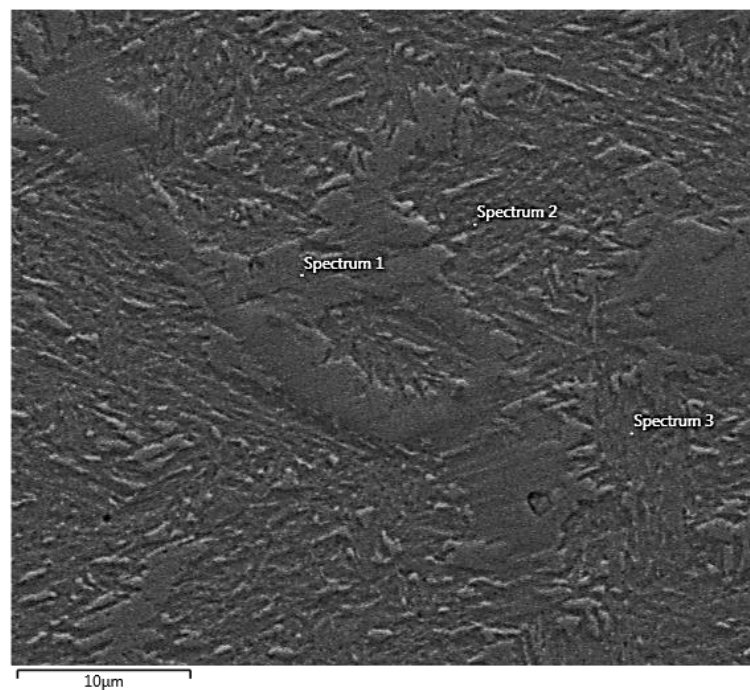


Fig 4.23 EDX point scanned on the SEM image of three layers hardfacing

Table 4.2 Chemical composition of three layers hardfacing analyzed by EDX

Spectrum	%Fe	%C	%Cr	%Mn	%Si	%Ni	%Mo
1	69.7	13.1	8.4	2.1	1.5	0.7	0.7
2	69.1	16	7.1	1.4	1.3	0.9	-
3	68.8	16	7.3	1.6	1.6	-	-

4.4.10 Emission-dispersive x ray result (Mapping)

The area analysis of cross-sectional microstructure of the three-layered samples welded with 500A and 700A using AC polarity by EDX compositional mapping method have been also done. Fig 4.24 shows the EDX result of sample welded with 500A using AC polarity and Fig 4.25 depicts the EDX result of sample welded with 700A using AC polarity as shown in Table 4.3. The reason why the couple of samples have been compared is that both showed the similar results of the amount of martensite, hardness and wear resistance but the overall results of 500A AC sample was superior than those of 700A AC sample.

According to the results, there are four chemical elements (C, Cr, Mn and Ni) combined mainly in those samples. The result of both samples is very similar, but the composition of manganese (Mn). The weight percent of chromium, nickel and molybdenum are almost uniform. The sample welded with 700A contains more weight percent of manganese than the 500A sample. Manganese is a critical element of austenitic stainless steel and is an austenite former as well. Normally, the austenitic stainless steel contains the amount of 1 to 2 wt% of manganese and then the martensitic stainless steel presents the range of manganese less than 1 wt% [42]. It can be proved as one factor why the sample welded with 700A showed more amount of austenite than the sample welded with 500A. As discussed above, higher amount of martensite phase decreases with hardness and wear resistance of the hardfaced samples.

Table 4.3 Chemical composition of three layers hardfacing analyzed by EDX

Condition	%Fe	%C	%Cr	%Mn	%Ni	%Mo
3H 500A AC	80.6	6.3	10.0	1.9	0.8	0.4
3H 700A AC	80.9	5.4	10.4	2.2	0.6	0.4

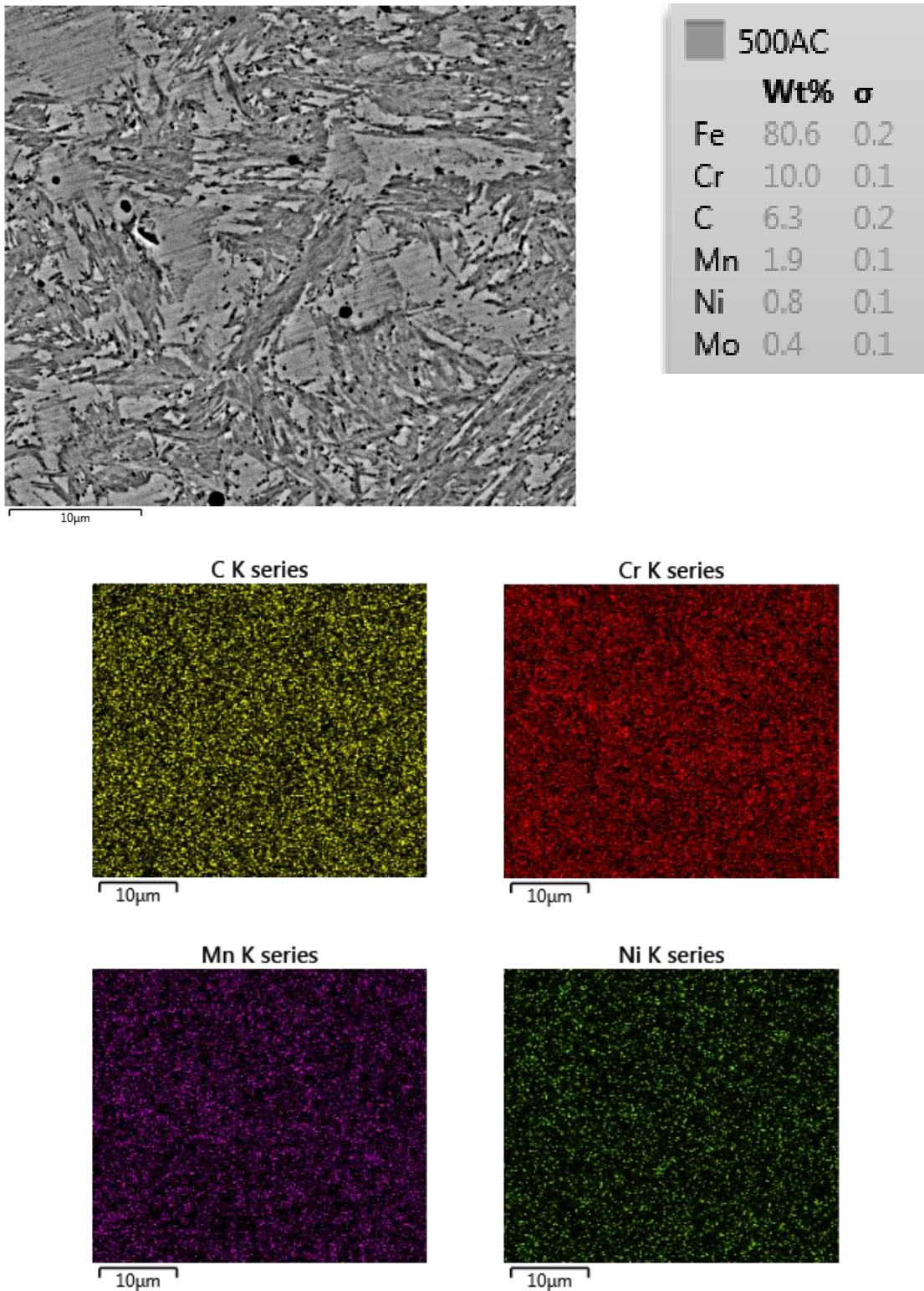


Fig 4.24 EDX mapping analysis of the sample welded with 500A using AC polarity

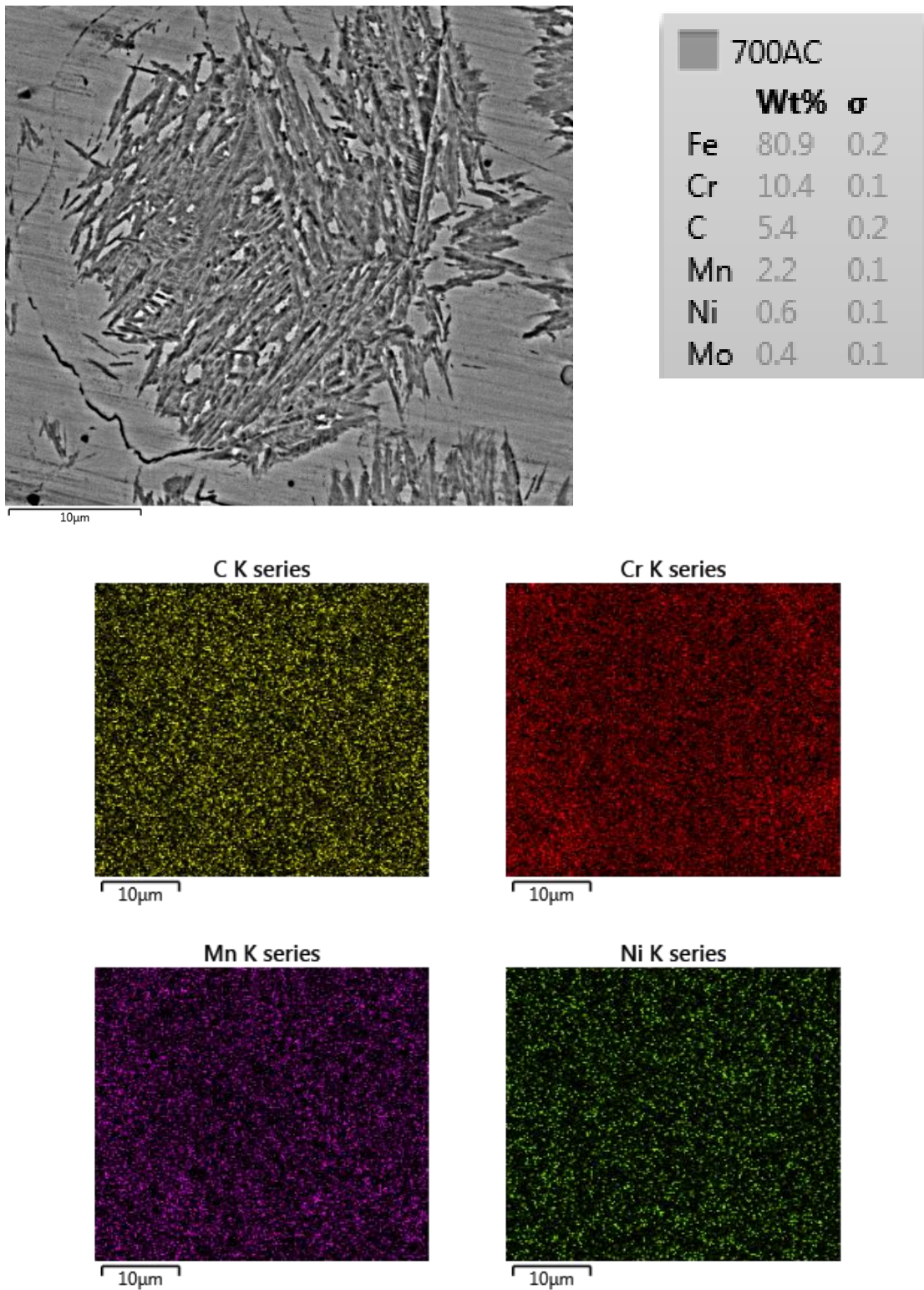


Fig 4.25 EDX mapping analysis of the sample welded with 700A using AC polarity

4.5 Amount of martensite phase in the micrographs

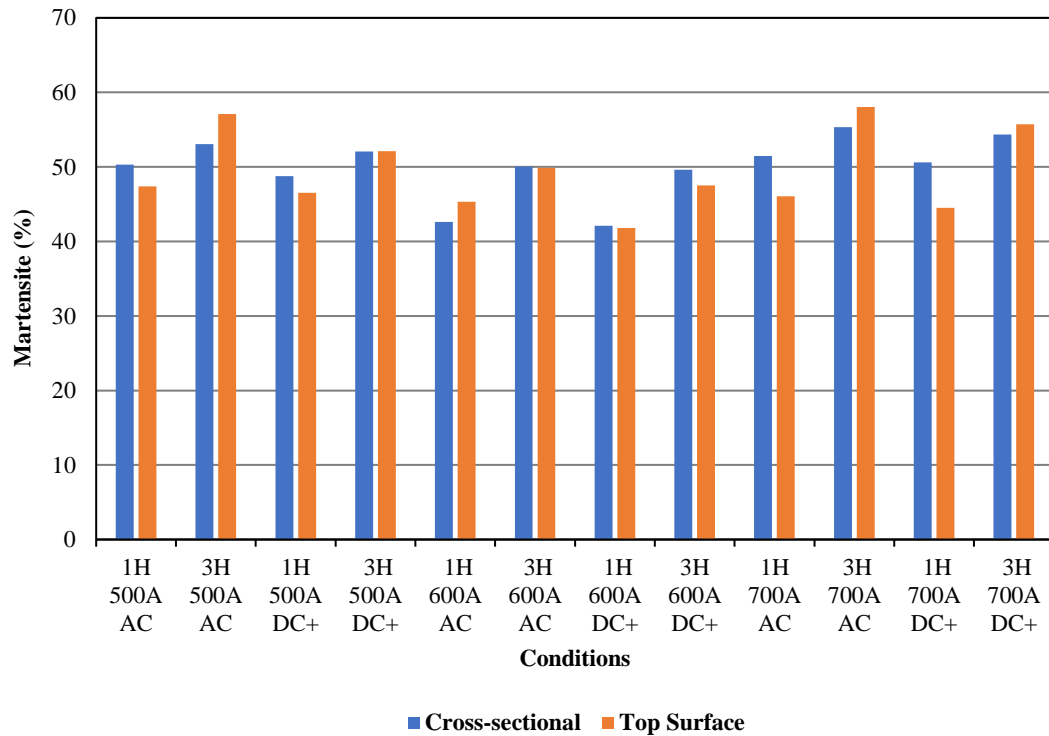


Fig 4.26 The amount of martensite phase in the micrographs analyzed by ImageJ

Fig 4.26 shows the martensitic area covered in the top and cross-sectional microstructure of single layer hardfacing and three layers hardfacing welded with 500A, 600A and 700A and using AC and DC+ polarity. According to the ImageJ results, the amount of martensite obtained the sample welded with 500A using AC polarity is highest and the sample welded 600A using DC+ shows the lowest amount of martensite observed on its microstructure by ImageJ software.

4.6 Phases identified by X-ray Diffraction (XRD)

The martensite and retained austenite microstructures seen in a single layer and three layers hardfacing are confirmed using X-ray diffraction, as shown in Fig 4.27 and Fig 4.28. In the XRD spectra, the peaks of single layers hardfacing and three layers hardfacing confirmed the presence of martensite and retained austenite.

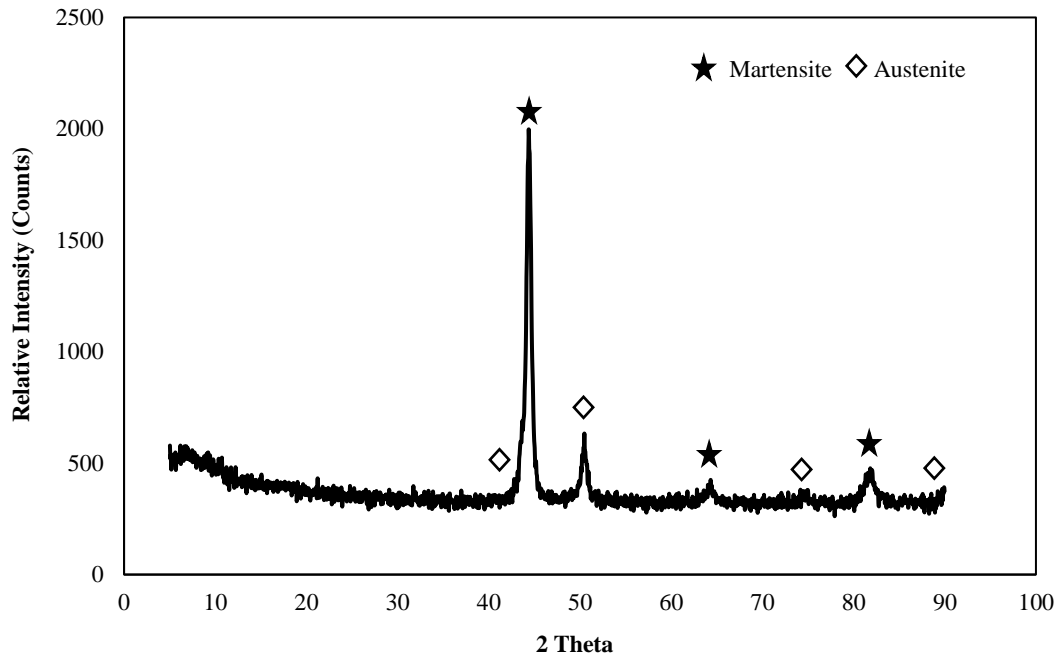


Fig 4.27 XRD patterns of single layer hardfacing

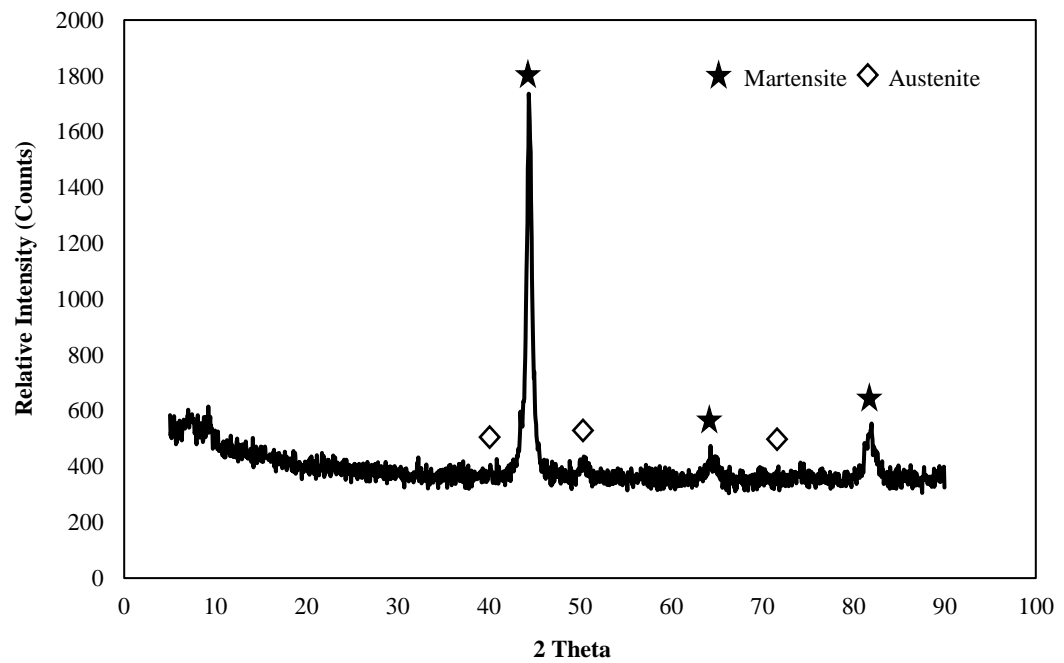


Fig 4.28 XRD patterns of three layers hardfacing

4.7 Dilution

To calculate welding dilution, single pass welds were done on 3.5% Cr steel coupons for all conditions. After welding, macrographs of samples were all captured. Each macrograph of welding dilution was analyzed using ImageJ software. Fig 4.29 depicts single pass macrographs for all samples.

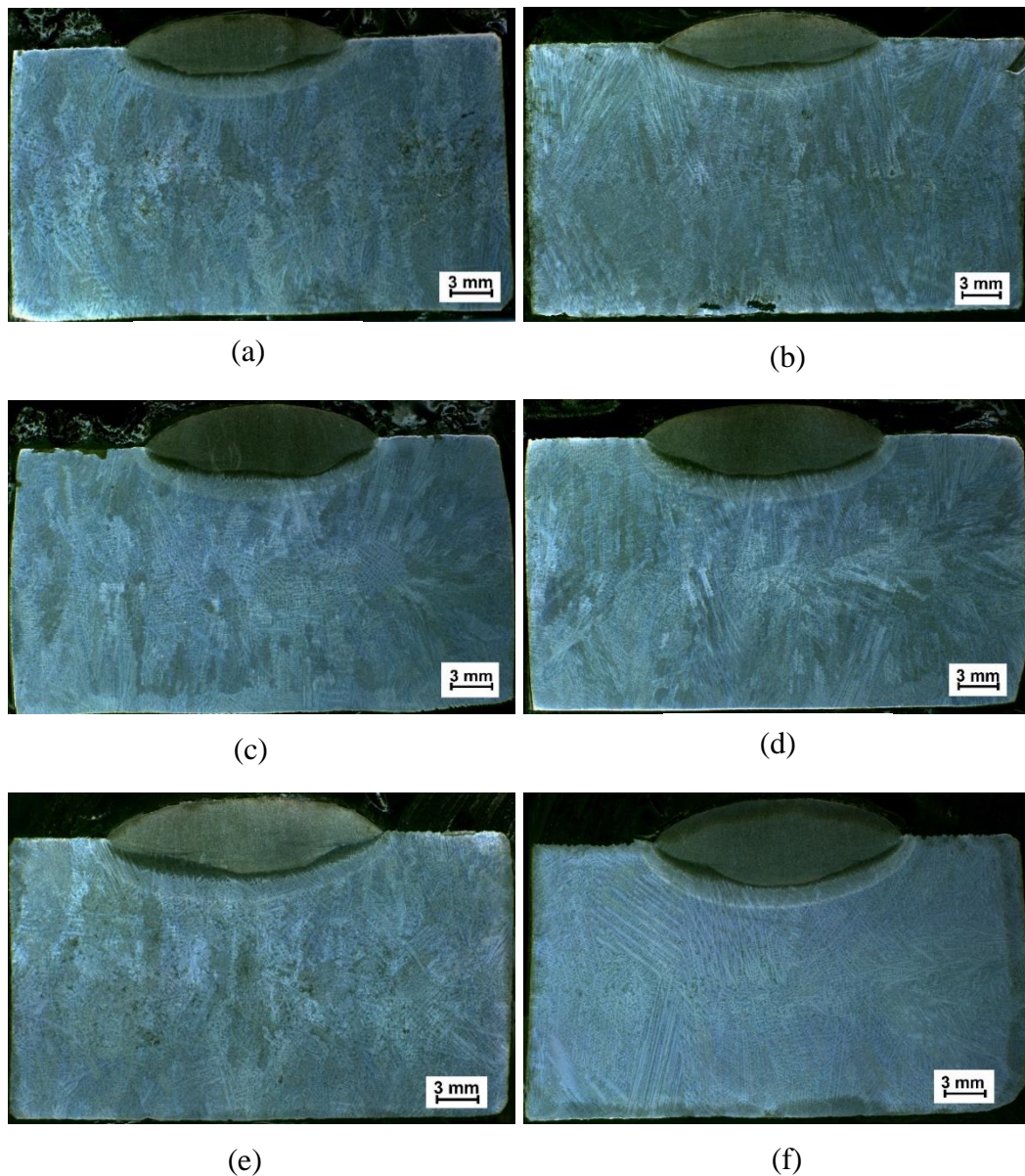


Fig.4.29 Single pass macrographs for measuring percent dilution (a) 1B 3H 500A AC (b) 1B 3H 500A DC+ (c) 1B 3H 600A AC (d) 1B 3H 600A DC+ (e) 1B 3H 700A AC (f) 1B 3H 700A DC+

Table 4.4 Percent dilution for all experiments

Conditions	Area A (mm ²)	Area B (mm ²)	Dilution (%)
500A AC	100.5052	85.335	44.8219
500A DC+	77.547	70.736	47.7034
600A AC	70.095	61.079	46.5633
600A DC+	91.922	99.9938	52.0891
700A AC	39.565	31.76	45.5285
700A DC+	41.932	42.453	50.3087

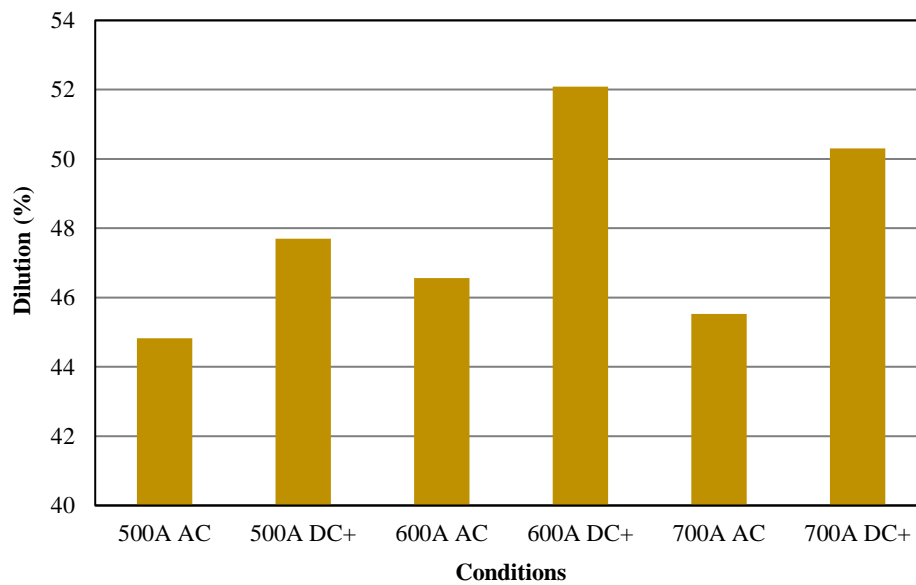
**Fig 4.30** Welding dilution (%)

Fig 4.30 and Table 4.4 show the per cent dilution result for all welded samples. Based on the results, the samples welded using AC polarity had lower dilution. There is a wide gap in dilution results of dissimilar polarities for the samples deposited using 600A and 700A. The per cent dilution of the sample welded using 600A and 700A with dissimilar polarities highly shows differences. Dilution percentage has a correlation with single layer of hardfacing's microstructure, hardness and abrasive wear resistance.

4.8 Hardness Distributions

4.8.1 Cross-sectional hardness

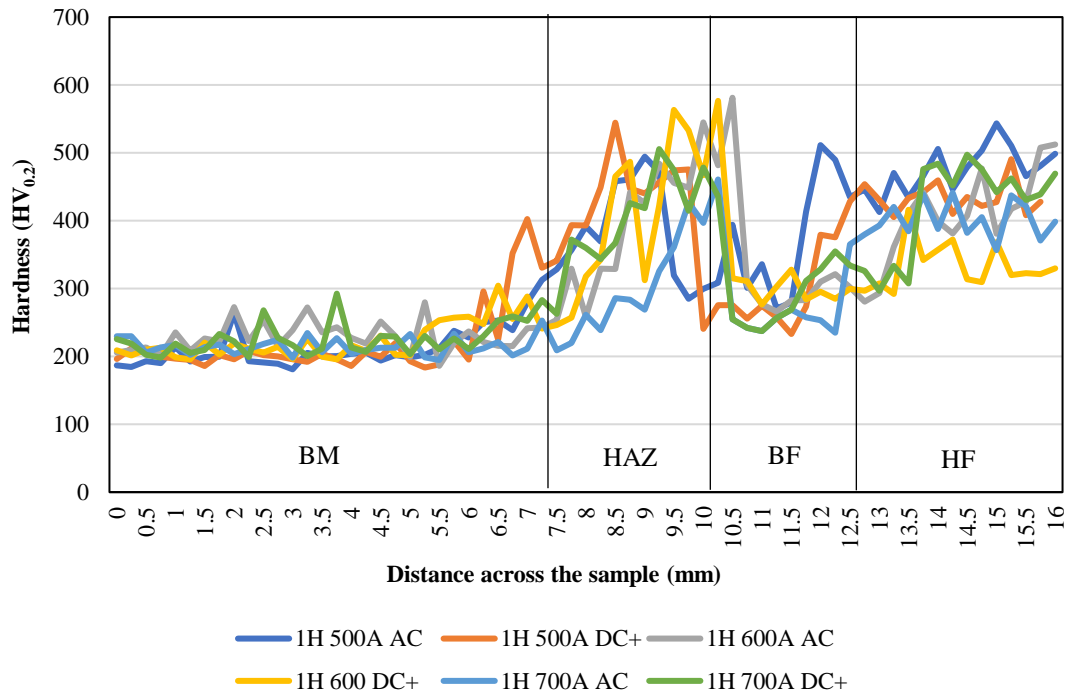


Fig 4.31 Cross-sectional hardness values across single layer hardfacing

The cross-sectional hardness values across single layer hardfacing for all experiments present in Fig 4.31. Normally, the hardness values of the base metal (3.5% Cr steel) is about 190-220 HV. Hardness values of the heat affected zone region of the base metal showing higher hardness values (about 390-550 HV) because this region contains the needle shape martensite structure due to the fast cooling effect. The average hardness of buffer layer is about 250-280 HV and the microstructure of this layer shows austenite phase with coarse grain, which tends to lower hardness. The hardness values of single layer hardfacing result in between 350 HV and 550 HV. According to the following results, the highest hardness value is found on the sample welded with 500A using AC polarity, while the sample welded with 600A using DC+ polarity results in the lowest hardness values.

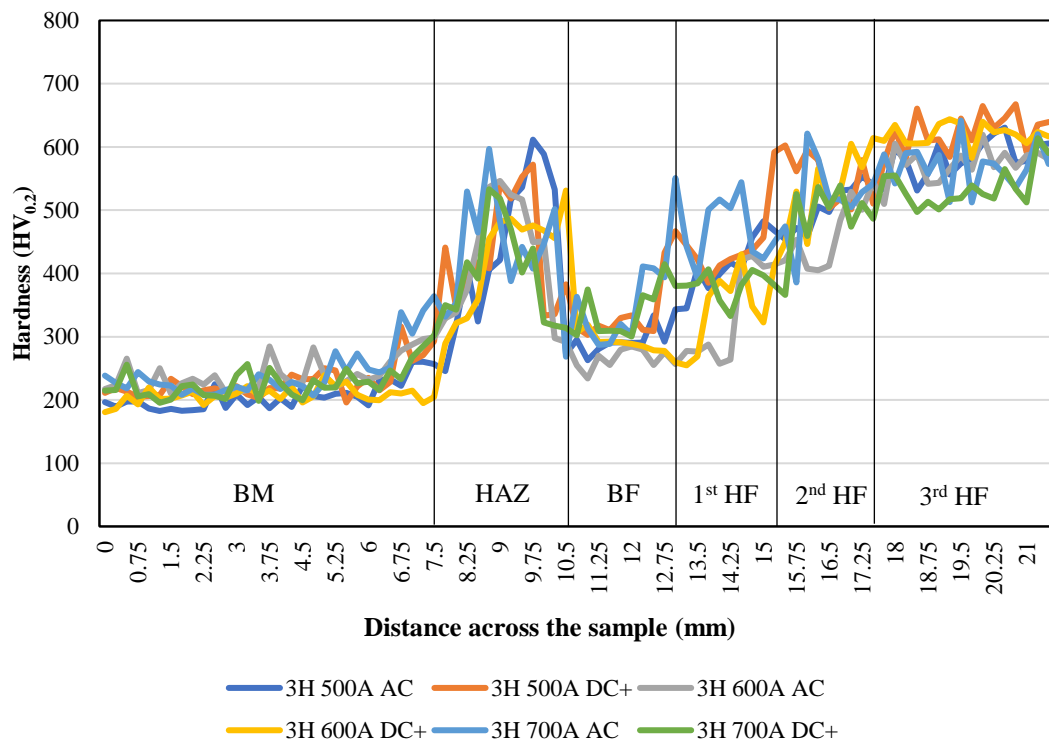


Fig 4.32 Cross-sectional hardness values across three layers hardfacing

The hardness profiles of the cross-sectional three layers hardfacing deposited with different currents and polarities are compared in Fig 4.32. The average hardness values of the base metal and buffer layer are same as that of single layer hardfacing. The hardness values of the heat affected zone and a buffer layer of three layers hardfacing are between 350 HV and 610 HV because the microstructure of three layers hardfaced samples' heat affected zone contains the coarser martensite phase than that of single layer hardfacing. In the first hardfacing layer, the sample welded with 700A using AC polarity shows the highest hardness and the sample welded with 600A using DC+ polarity presents the lowest hardness in this area. The hardness of second hardfacing layer presents many fluctuating values but the sample welded with 600A using AC polarity shows the lowest values. The hardness values of third hardfacing layer result in the overlapped evolutions except for the values of the sample deposited with 700A using DC+ polarity, which give the lowest values.

4.8.2 Top surface hardness

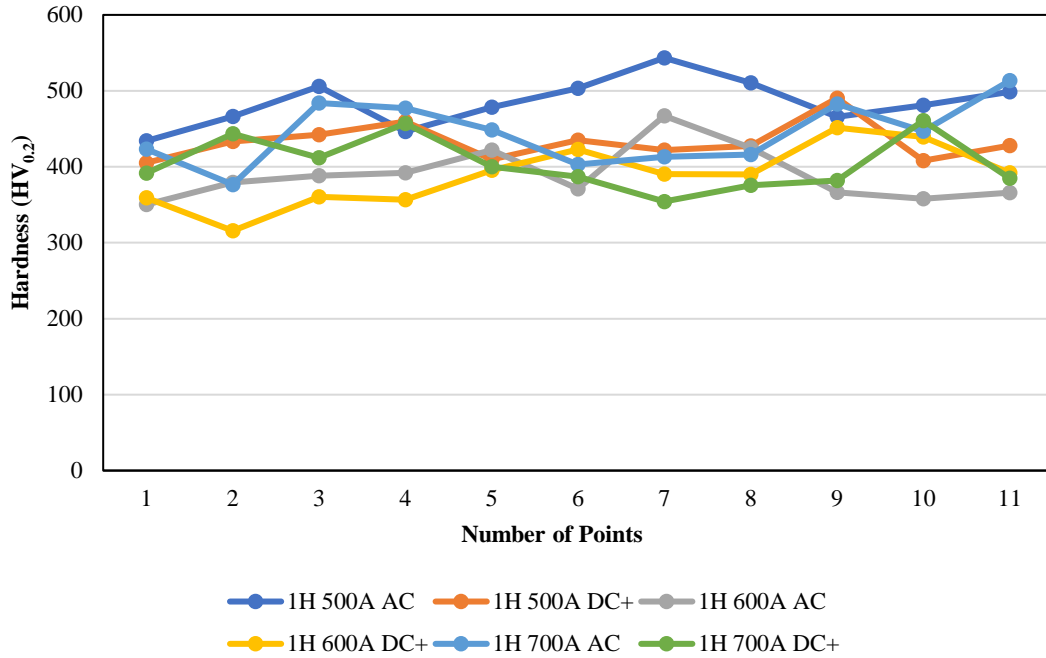


Fig 4.33 Top surface hardness of single layer hardfacing

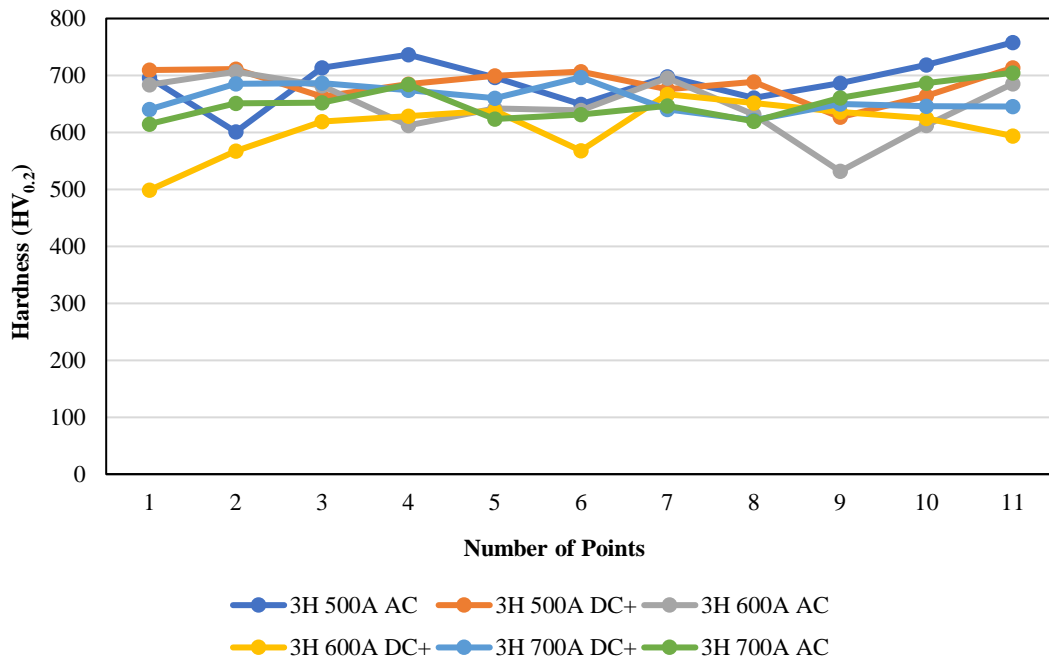


Fig 4.34 Top surface hardness of three layers hardfacing

The microhardness data of top surface obtained under different currents and polarities were randomly analysed at 11 points on each sample. The results of hardness values for 11 points of single layer and three layers hardfacing are illustrated in Fig 4.33 and Fig 4.34. The top surface hardness values of single layer hardfacing are between 315 HV and 550 HV. The top surface hardness evolutions of three layers hardfacing range from 500 HV to 750 HV. The lowest top surface hardness value among the illustration of single layer hardfacing (about 315 HV) and three layers hardfacing (about 500HV) is picked from the sample welded with 600A using DC+ polarity, whereas the highest top surface hardness value about 550 HV from single layer hardfacing and about 750 HV from three layers hardfacing can be seen in the results of the samples welded with 500A using AC polarity. Comparing with the cross-sectional hardness, the top surface hardness values are generally higher for both single and three layers hardfacing.

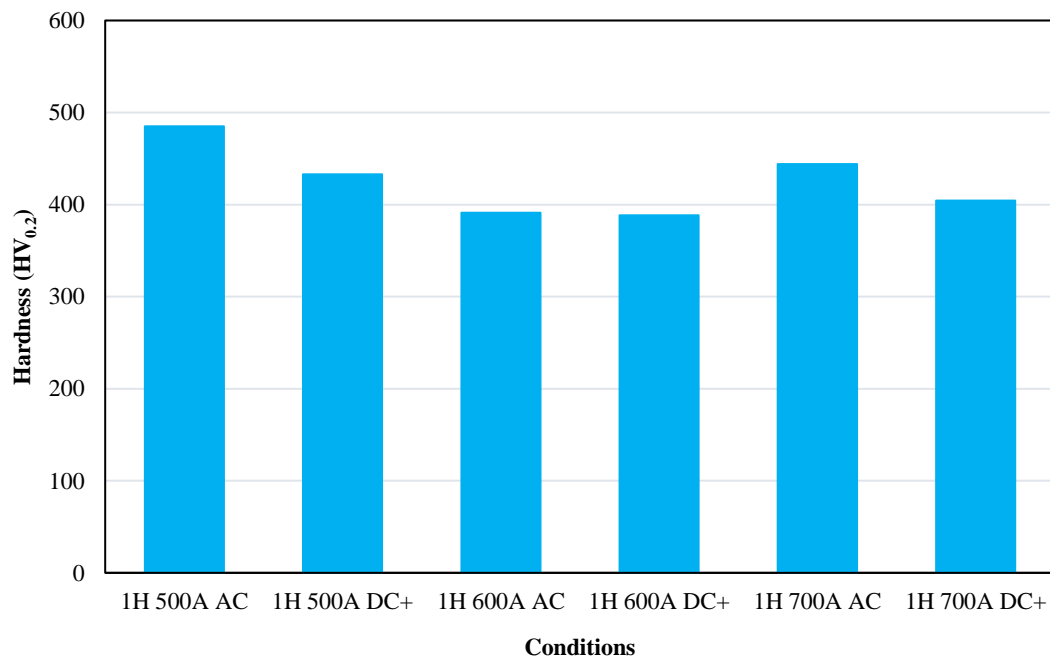


Fig 4.35 Average top surface hardness of single layer hardfacing

The average hardness values of 11 points analysis on the top surface of all experiments for both single layer and three layers hardfacing are shown in Fig 4.35 and Fig 4.36. The clear results of the top surface hardness can be seen in the following chart. The highest average top surface hardness of single layer hardfacing is found on the sample welded with 500A using AC polarity. The highest hardness value of the average top surface of single layer hardfacing is about 484.9 HV. The samples welded with 600A using different polarity result in the lowest hardness values about 388.4 HV. The samples welded with 500A using dissimilar polarity show the highest average top surface hardness by far. The average hardness values of 3H 500A AC sample and 3H 500A DC+ sample are about 692.3 HV and 685.8 HV. On the other hand, the lowest average hardness values on top surface of three layers hardfacing are found on 3H 600A DC+ sample and the significant result of the lowest values is about 608.4 HV. The hardness values reflect the amount of martensite phase formed.

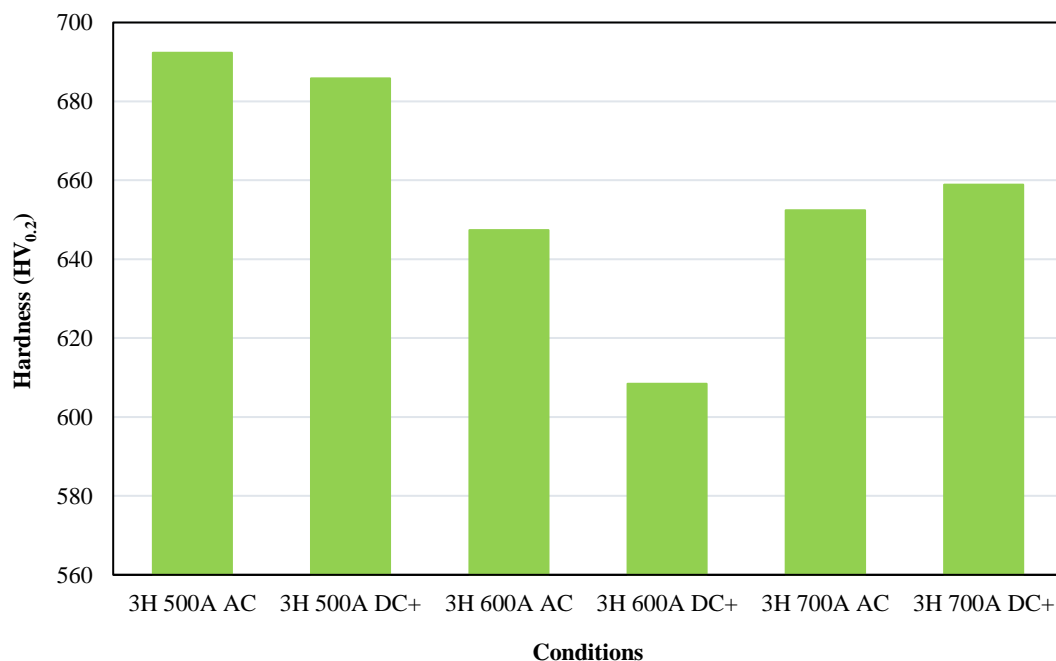


Fig 4.36 Average top surface hardness of three layers hardfacing

4.9 Abrasive mass loss

Wear resistance of the hardfacing layers is determined by measuring the abrasive mass loss of the samples. This abrasive mass loss is given by differences in weight between the original weight of abrasive specimens and the weight of wear tested specimens. Of course, the higher abrasive mass loss reflects lower wear resistance. Table 4.5 compares the abrasive mass loss of both single and three layers hardfacing welded with 500A, 600A and 700A using AC and DC+ polarity. In Table 4.5, the initial weight of the sample before testing the wear mass loss, the final weight after the samples have been tested, the different weight loss between before and after testing, wear resistance of the samples and an average hardness of the samples can be seen.

Table 4.5 Abrasive wear test results of all experimental conditions

Conditions	Initial weight (g)	Final weight (g)	Abrasive mass loss (g)	Abrasive wear resistance (m/mg)
BM	181.9646	179.2033	2.7613	1.56
1H 500A AC	187.3722	184.5586	2.8136	1.53
3H 500A AC	184.4880	182.3625	2.1370	2.02
1H 500A DC+	182.9022	180.0294	2.8728	1.50
3H 500A DC+	180.7942	178.4359	2.3583	1.83
1H 600A AC	189.5675	186.7358	2.8314	1.52
3H 600A AC	190.3556	188.1204	2.2352	1.92
1H 600A DC+	191.4432	188.2508	3.1924	1.34
3H 600A DC+	192.4543	189.9619	2.4958	1.73
1H 700A AC	197.6258	194.5651	3.0607	1.40
3H 700A AC	153.1673	151.0203	2.1470	2.01
1H 700A DC+	206.7446	203.7133	3.0313	1.42
3H 700A DC+	205.4332	203.0438	2.3894	1.80

The abrasive mass loss results of all samples comparing single layer and three layers hardfacing welded with different currents and polarities are presented in Fig 4.37. According to the following chart, the abrasive mass loss of three layers hardfacing is higher than that of single layer hardfacing for all conditions because three layers hardfacing showed more amount of martensite phase in the microstructure and higher hardness in both the cross-sectional and top surface than single layer hardfacing. Although the welding parameters and materials are same for both single and three layers hardfacing, single layer hardfacing has the effect of dilution with the austenitic buffer layer. The effect of dilution with austenitic buffer layer influences the microstructure, hardness and abrasive wear resistance of the hardfacing. Almost all the single layer mass loss results are higher than the base metal because of its dilution. Therefore, welding of single layer hardfacing in this project is one of the reasons to prove the effect of welding dilution. Three layers hardfacing can get the expected microstructure, hardness and wear resistance of the actual properties of hadfacing deposited with the martensitic steel type electrode.

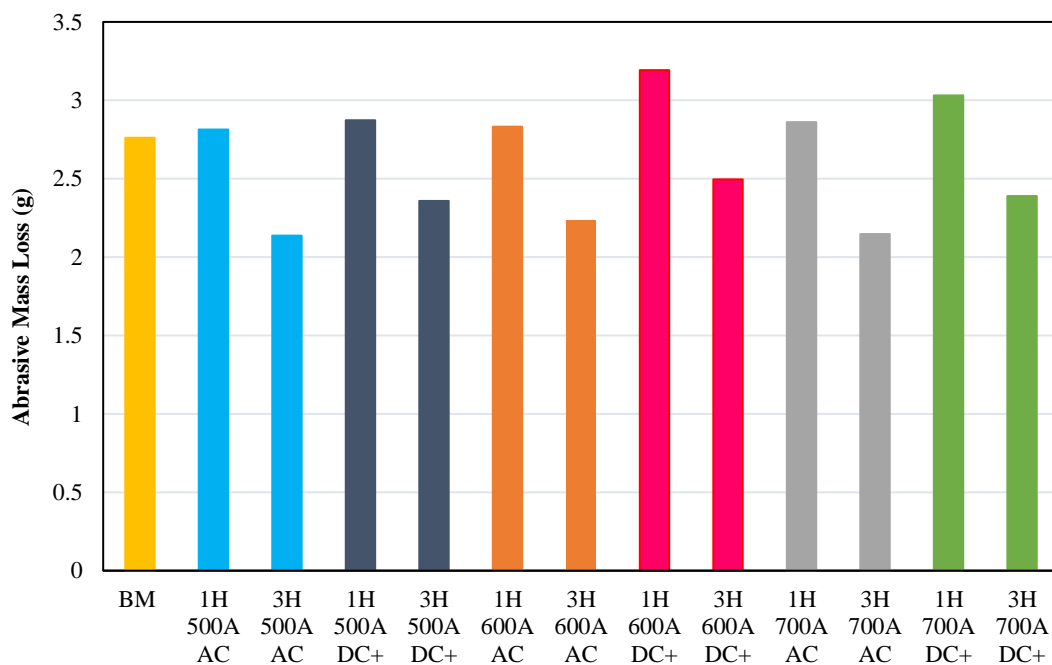


Fig 4.37 Abrasive mass loss result comparing different layers (single and three)

The effect of welding polarity on the abrasive mass loss of both single layer and three layers hardfacing is shown in Fig 4.38. In this project, two different welding polarities (AC and DC+) are used to analyze. In accordance with Fig 4.35, the abrasive mass loss of both single layer and three layers hardfacing welded using AC (Alternating Current) is lower than that of the sample used DC+ (Direct Current Electrode Positive). The sample welded with 500A using AC polarity goes to the highest wear resistance for both single and three layers hardfacing. The lowest wear resistance for both single and three layers hardfacing is the sample welded with 600A using DC+ polarity. The lowest abrasive mass loss among all welding conditions in this project is the sample three-layer hardfaced with 500A using AC polarity and the sample single layer hardfaced with 600A using DC+ polarity results in the highest abrasive mass loss.

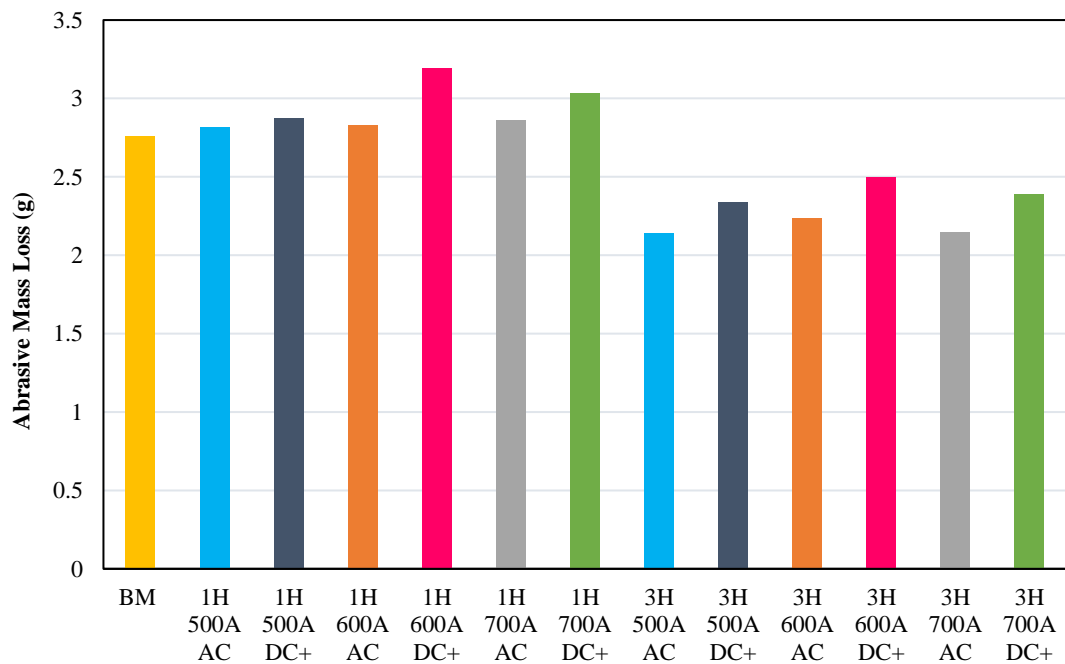


Fig 4.38 Abrasive mass loss result comparing different polarities (AC and DC+)

Chapter 5

Conclusions and recommendations

The study is designed to investigate the effect of welding currents and polarities on microstructures, hardness, dilution and wear resistance of the 3.5% Cr steel hardfaced by submerged arc welding process. Twelves different variable conditions were investigated.

5.1 Conclusions

1. All the hardfaced samples showed microstructures that are mixtures of martensite and retained austenite that gave higher hardness and superior resistance to wear.
2. Single layer hardfacing showed higher weld dilution with the austenitic buffer layer, thus decreasing the hardness and wear resistance of the hardfaced layer.
3. The wear resistance of three layers hardfacing was higher than that of the samples hardfaced with only a single layer and greater than the wear resistance of the base metals.
4. Alternating current (AC) welding polarity is the most suitable for the hardfacing welding with submerged arc welding. Comparing effects of AC and DC+ polarity show that the sample welded with AC polarity gave a lower percentage of dilution and a higher amounts of martensite phase; this led to increased hardness and wear resistance of the hardfaced layers above that seen in samples welded with DC+ polarity.
5. In comparing the results obtained in the samples welded with 500 A and 700 A, the samples deposited with the lower 500 A, and using different polarities gave larger amount of martensite phase than those welded using 700 A because the higher heat input give slower cooling rate, thus retained more austenite.
6. According to the experimental results obtained in this study, the sample deposited with 500 A using AC polarity for three layers hardfacing is the best condition for repairing single roll coal crusher at Mae Moh Mine in the project.

5.2 Recommendations

1. The base metal that was made by 3.5% Cr should be preheated before welding at least 350 °C for submerged arc welding surfacing because this temperature was calculated using the carbon equivalent equation, and to ensure higher heat generation to melt the electrode. Preheating also avoids welding defects, such as cracking due to heat shock.

2. Preheating of the workpiece is critical in this hardfacing welding process. It is very important not to allow the temperature of the workpiece after applying the buffer layer to decrease below the preheating temperature or at least below 200-250°C as that will increase the high cooling rate of the hardfaced layers. This will also avoid cracking of the workpiece.

3. The single buffer layer is used to ensure good bonding between the hardfacing layer and base metal, and it increases impact wear resistance.

4. The hardfaced layer should be deposited at least two layers to reduce the problem of dilution with the underlying buffer layer as that decreases hardness and wear resistance of hardfaced layers.

5. When the third layer hardfacing is completely worn, wear will increase rapidly in the second and first layer, respectively. Therefore, the condition of hardfaced surfaces should be monitored and plans to mitigate wear problem is necessary.

References

- [1] Payal, P., Jainy, B., Kajal, D., Sheela, Z., Nayak, R., (2015). Coal crushing and conveyor system. *International journal of engineering research and reviews*, 3(1), 60-65.
- [2] American Welding Society (2013). *Welding handbook: Welding Processes Part 2*, Volume 3, 9th edition.
- [3] Davis, J. R. (Ed.). (2001). *Surface engineering for corrosion and wear resistance*. ASM international.
- [4] Yamamoto, S. (2008). Third edition, Arc welding of specific steels and cast irons. *Shinko Welding Service, Japan*.
- [5] Chattopadhyay, R. (2007). *Advanced thermally assisted surface engineering processes*. Springer Science & Business Media.
- [6] Avner, S. H. (1964). *Introduction to physical metallurgy*, New York: McGraw-Hill.
- [7] Burnell-Gray, J. S., & Datta, P. K. (Eds.). (1996). *Surface Engineering Casebook: Solutions to Corrosion and Wear-related Failures*. Elsevier.
- [8] Bastien Gerard. (2016) *Fundamentals of hardfacing by arc welding*. Welding Alloys Group, France.
- [9] American Welding Society (2013). *Welding Handbook: Welding Processes Part 1*, Volume 2, 9th edition.
- [10] Hobart Brothers Company (2015). *Submerged arc welding consumable*. 4th edition.
- [11] Weman, K. (2003). First edition. *Welding processes handbook*. Elsevier.
- [12] Bailey, N. (1994). *Weldability of ferritic steels*. Woodhead Publishing. Cambridge.
- [13] Easterling, K. (2013). *Introduction to the physical metallurgy of welding*. Elsevier.
- [14] ESAB, (2008). *Repair, and Maintenance Welding Handbook*, 2nded, Sweden.
- [15] Kobe Steel Ltd., (2015), Arc welding of specific steels and cast iron, Tokyo, The Institute.

References (Continued)

- [16] Tsai, H. L., Tarn, Y. S., & Tseng, C. M. (1996). Optimization of submerged arc welding process parameters in hardfacing. *The International Journal of Advanced Manufacturing Technology*, 12(6), 402-406.
- [17] Mellor, B. G. (Ed.). (2006). *Surface coatings for protection against wear*. Taylor & Francis, USA.
- [18] Kobelco, (2015). The ABC's of Arc Welding and Inspection. Kita-Shinagawa, Shinagawa-Ku, Tokyo, Japan.
- [19] Weman, K., (2012). Second edition. *Welding processes handbook*. Elsevier.
- [20] Herring, D. H., (2005). A Discussion of Retained Austenite. *Industrial Heating*, 72(3), 14–16.
- [21] ASTM International, (1997), Standard Test Method for Vickers Hardness of Metallic Materials, E92, ASTM standards, pp 1-10.
- [22] Udomphol, T. (2007) Laboratory 2, Hardness Testing. *Mechanical metallurgy laboratory 431303*.
- [23] Kenchi Reddy K. M. and Jayadeva C. T., (2014). The Effect of Microstructure on 3 Body Abrasive Wear Behavior of Hardfacing Alloys, Bonfring International Journal of Industrial Engineering and Management Science, Vol. 4, No. 1, pp 14-23.
- [24] ASTM International, (2013). Standard Test Method for Measuring Abrasion using the Dry Sand Rubber Wheel, G65-A, ASTM Standards, pp 1–12.
- [25] Chang, C. M., Chen, Y. C., & Wu, W. (2010). Microstructural and abrasive characteristics of high carbon Fe–Cr–C hardfacing alloy. *Tribology international*, 43(5-6), 929-934.
- [26] Buchely, M. F., Gutierrez, J. C., Leon, L. M., & Toro, A. (2005). The effect of microstructure on abrasive wear of hardfacing alloys. *Wear*, 259(1-6), 52-61.
- [27] Zahiri, R., Sundaramoorthy, R., Lysz, P., & Subramanian, C. (2014). Hardfacing using ferro-alloy powder mixtures by submerged arc welding. *Surface and Coatings Technology*, 260, 220-229.

References (Continued)

- [28] Günther, K., Bergmann, J. P., & Suchodoll, D. (2018). Hot wire-assisted gas metal arc welding of hypereutectic FeCrC hardfacing alloys: Microstructure and wear properties. *Surface and Coatings Technology*, 334, 420-428.
- [29] Tušek, J., & Suban, M. (2003). High-productivity multiple-wire submerged-arc welding and cladding with metal-powder addition. *Journal of materials processing technology*, 133(1-2), 207-213.
- [30] Chakraborty, G., Das, C. R., Albert, S. K., Bhaduri, A. K., Murugesan, S., & Dasgupta, A. (2016). Effect of Alloy 625 Buffer Layer on Hardfacing of Modified 9Cr-1Mo Steel Using Nickel Base Hardfacing Alloy. *Journal of Materials Engineering and Performance*, 25(4), 1663-1672.
- [31] Morsy, M., & El-Kashif, E. (2014). The effect of microstructure on high-stress abrasion resistance of Fe-Cr-C hardfacing deposits. *Welding in the World*, 58(4), 491-497.
- [32] Kiran, V. B., Krishna, M., Natraj, J. R., & Kumar, S. (2012). Development and characterization of a electrode deposition procedure for crack-free hardfacing of low carbon steel. *International Journal of Engineering and Technology*, 4(1), 18.
- [33] Coronado, J. J., Caicedo, H. F., & Gómez, A. L. (2009). The effects of welding processes on abrasive wear resistance for hardfacing deposits. *Tribology International*, 42(5), 745-749.
- [34] Prasad, K., & Dwivedi, D. K. (2008). Some investigations on microstructure and mechanical properties of submerged arc welded HSLA steel joints. *The international journal of advanced manufacturing technology*, 36(5-6), 475-483.
- [35] Chatterjee, S., & Pal, T. K. (2006). Weld procedural effect on the performance of iron based hardfacing deposits on cast iron substrate. *Journal of Materials Processing Technology*, 173(1), 61-69.
- [36] Chotěborský, R., Hrabě, P., Müller, M., Savková, J., & Jirka, M. (2008). Abrasive wear of high chromium Fe-Cr-C hardfacing alloys. *Research in Agricultural Engineering*, 54(4), 192-198.

References (Continued)

- [37] Toma, R. E., Brandi, S. D., Souza, A. C., & Morais, Z. (2011). Comparison between DC (+) and Square Wave AC SAW Current Outputs to Weld AISI 304 for Low-Temperature Applications. *Welding Journal*, 90(9), 153S-160S.
- [38] American Welding Society (2013). *Welding Handbook: Materials and Application Part 1*, Volume 4, 9th edition.
- [39] Boccalini, M., & Goldenstein, H. (2001). Solidification of high speed steels. *International Materials Reviews*, 46(2), 92-115.
- [40] Arias, J., Cabeza, M., Castro, G., Feijoo, I., Merino, P., & Pena, G. (2010). Microstructural characterization of laser surface melted AISI M2 tool steel. *Journal of microscopy*, 239(3), 184-193.
- [41] Dilawary, S. A. A., Motallebzadeh, A., Houdková, Š., Medlin, R., Haviar, S., Lukáč, F., ... & Cimenoglu, H. (2018). Modification of M2 hardfacing: Effect of molybdenum alloying and laser surface melting on microstructure and wear performance. *Wear*, 404, 111-121.
- [42] John, L., & Damian, J. K. (2005). *Welding metallurgy and weldability of stainless steels*, John Wiley and Sons, Hoboken, New Jersey, USA.

APPENDIX A:
Single Layer Hardness Data

Table A1 1H 500A AC

Distance (mm)	Hardness (HV)	Distance (mm)	Hardness (HV)
0.00	187	6.00	228.1
0.25	184.7	6.25	250.6
0.50	193.1	6.50	252.7
0.75	190.1	6.75	238.7
1.0	213.5	7.0	280
1.25	192.3	7.25	312.8
1.5	199.2	7.5	328.5
1.75	199.7	7.75	356.8
2.00	263.8	8.00	391.7
2.25	192.8	8.25	369.5
2.50	191.1	8.50	458.2
2.75	189.4	8.75	460.7
3.0	181	9.0	494.3
3.25	205.2	9.25	471.7
3.5	200.2	9.5	319.3
3.75	200.4	9.75	285.1
4.00	203.6	10.00	299.4
4.25	205.6	10.25	308.4
4.50	193.9	10.50	394
4.75	202	10.75	301.1
5.0	198.5	11.0	335.8
5.25	202.4	11.25	271
5.5	211.8	11.5	279.1
5.75	238	11.75	413.4

Table A1 1H 500A AC (Continued)

Distance (mm)	Hardness (HV)	Distance (mm)	Hardness (HV)
12.00	511.3	14.25	446.5
12.25	489.8	14.50	478.6
12.50	434.9	14.75	503.5
12.75	446	15.0	543.4
13.0	412.6	15.25	510.6
13.25	470.3	15.5	465.7
13.5	434	15.75	480.9
13.75	466.3	16.00	498.7
14.00	505.7		

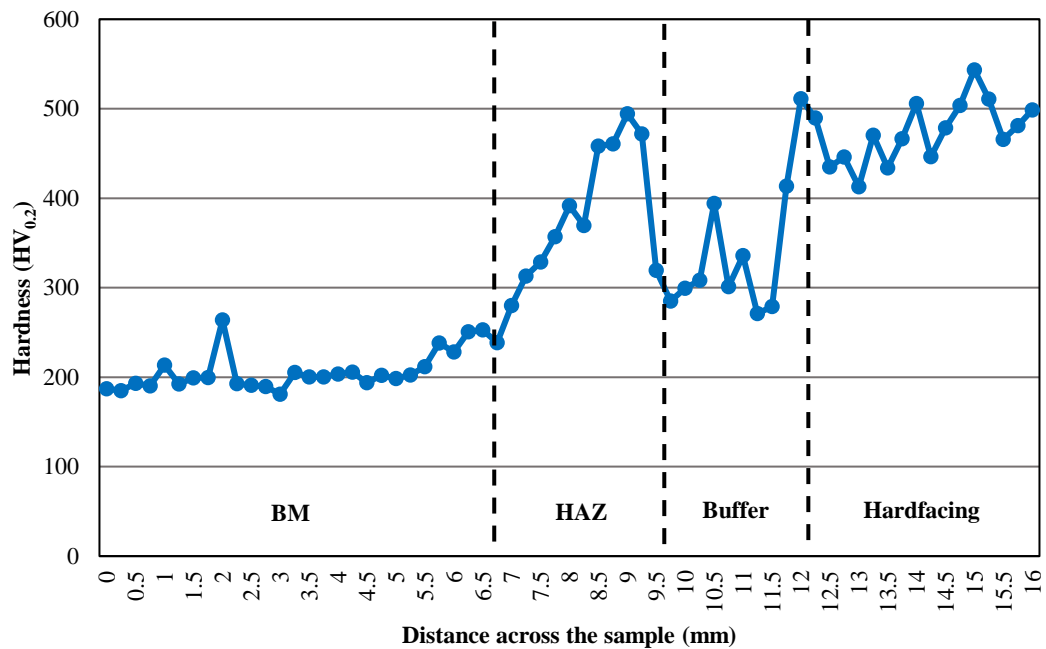
**Fig A1** Hardness values of 1H 500A AC

Table A2 1H 500A DC+

Distance (mm)	Hardness (HV)	Distance (mm)	Hardness (HV)
0.00	196.1	6.00	195.2
0.25	211.9	6.25	295.6
0.50	206.2	6.50	225.1
0.75	199.7	6.75	351.9
1.0	196.9	7.0	402.3
1.25	194.7	7.25	330.6
1.5	185.9	7.5	341.1
1.75	201.9	7.75	393.3
2.00	195.9	8.00	392.9
2.25	208	8.25	449.3
2.50	201.8	8.50	544.4
2.75	199.9	8.75	447.4
3.0	195.6	9.0	440.2
3.25	192	9.25	456.6
3.5	203.6	9.5	474.2
3.75	195.9	9.75	475.4
4.00	185.7	10.00	240.6
4.25	206.7	10.25	275.3
4.50	199.6	10.50	275.5
4.75	219.9	10.75	255.6
5.0	192.9	11.0	274.7
5.25	183.6	11.25	257.6
5.5	188.3	11.5	233.2
5.75	222.9	11.75	273.7

Table A2 1H 500A DC+ (Continued)

Distance (mm)	Hardness (HV)	Distance (mm)	Hardness (HV)
12.00	379.4	14.25	409.8
12.25	375.6	14.50	434.9
12.50	428.4	14.75	421.8
12.75	453.8	15.0	427.6
13.0	430.2	15.25	490.4
13.25	405.3	15.5	407.9
13.5	433.4	15.75	427.9
13.75	442.2	16.00	428
14.00	459.5		

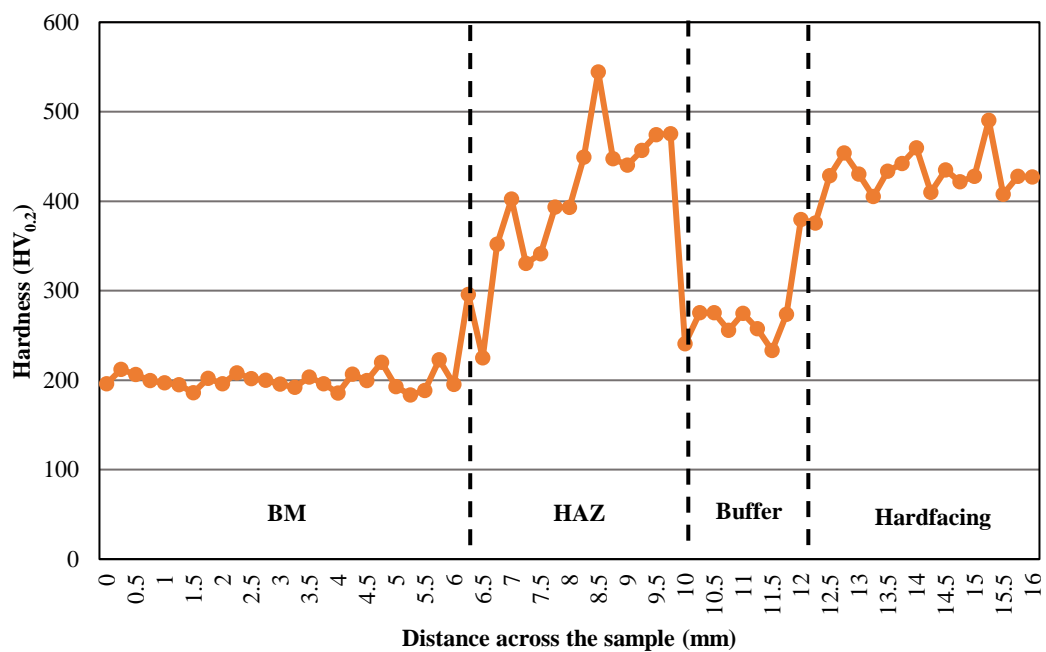
**Fig A2** Hardness values of 1H 500A DC+

Table A3 1H 600A AC

Distance (mm)	Hardness (HV)	Distance (mm)	Hardness (HV)
0.00	205.6	6.00	236.7
0.25	209.4	6.25	221.2
0.50	213.4	6.50	215.4
0.75	201.5	6.75	215.2
1.0	235.4	7.0	241.7
1.25	208.4	7.25	242.3
1.5	226.4	7.5	254
1.75	222.2	7.75	329.4
2.00	272.6	8.00	258.7
2.25	222.6	8.25	329.4
2.50	253.3	8.50	328.7
2.75	215.3	8.75	441.6
3.0	238.6	9.0	426.1
3.25	272	9.25	483.8
3.5	235.3	9.5	455.6
3.75	243	9.75	448.7
4.00	227.6	10.00	544.8
4.25	218.7	10.25	481.6
4.50	251.7	10.50	581.2
4.75	230	10.75	305.1
5.0	199.3	11.0	277
5.25	279.6	11.25	266
5.5	186.1	11.5	282.7
5.75	219.9	11.75	283.1

Table A3 1H 600A AC (Continued)

Distance (mm)	Hardness (HV)	Distance (mm)	Hardness (HV)
12.00	309.9	14.25	381.2
12.25	321.2	14.50	407.1
12.50	301.8	14.75	477.1
12.75	280.6	15.0	380.5
13.0	293.6	15.25	417.4
13.25	361.2	15.5	427.9
13.5	410.3	15.75	507.8
13.75	441.6	16.00	512.5
14.00	398.9		

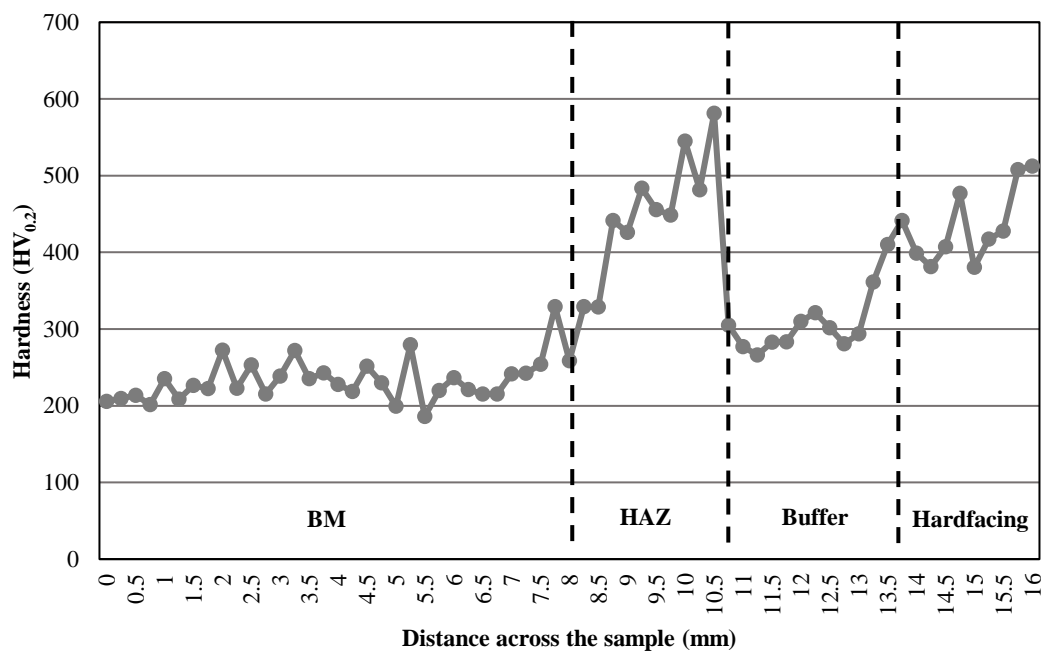
**Fig A3** Hardness values of 1H 600A AC

Table A4 1H 600A DC+

Distance (mm)	Hardness (HV)	Distance (mm)	Hardness (HV)
0.00	208.8	6.00	258.7
0.25	201.6	6.25	247.6
0.50	210.1	6.50	304.4
0.75	212.9	6.75	255.4
1.0	198.7	7.0	288.1
1.25	195.9	7.25	240.9
1.5	220.5	7.5	246.5
1.75	202.9	7.75	257
2.00	219	8.00	318.2
2.25	211.5	8.25	342.5
2.50	205.9	8.50	465
2.75	214.3	8.75	486.8
3.0	196.3	9.0	312.5
3.25	226	9.25	422.4
3.5	199.7	9.5	563.2
3.75	195.7	9.75	533.3
4.00	216.7	10.00	467
4.25	207.9	10.25	576.6
4.50	230.9	10.50	315
4.75	202.5	10.75	311.1
5.0	201.8	11.0	276.4
5.25	239.3	11.25	302.7
5.5	253.4	11.5	327.9
5.75	257.1	11.75	283.8

Table A4 1H 600A DC+ (Continued)

Distance (mm)	Hardness (HV)	Distance (mm)	Hardness (HV)
12.00	295.2	14.25	372.3
12.25	285	14.50	313.5
12.50	299.4	14.75	309.7
12.75	296.6	15.0	368.6
13.0	307.4	15.25	319.9
13.25	292.1	15.5	322.6
13.5	416.2	15.75	321.2
13.75	341.8	16.00	329.8
14.00	356.9		

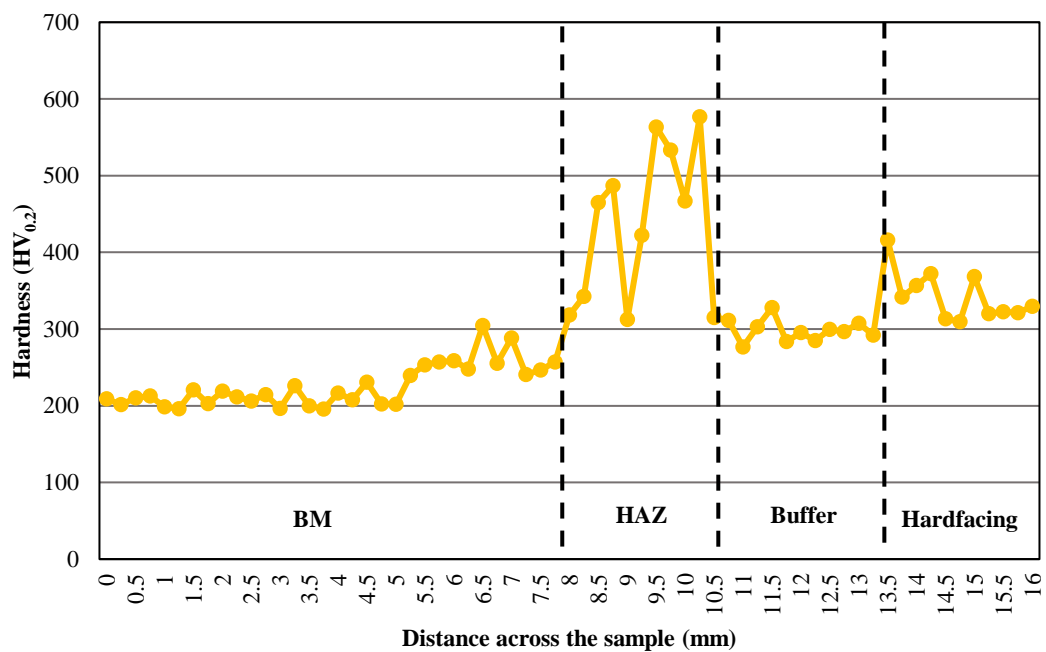
**Fig A4** Hardness values of 1H 600A DC+

Table A5 1H 700A AC

Distance (mm)	Hardness (HV)	Distance (mm)	Hardness (HV)
0.00	229.7	6.00	206.4
0.25	230	6.25	211.9
0.50	205.7	6.50	221.4
0.75	213.2	6.75	201.3
1.0	217	7.0	211.3
1.25	202.3	7.25	253
1.5	213.9	7.5	209.2
1.75	217.6	7.75	219.8
2.00	203.3	8.00	261.6
2.25	210.7	8.25	238.8
2.50	218.3	8.50	285.8
2.75	224.8	8.75	283.5
3.0	198	9.0	268.8
3.25	234.5	9.25	325.7
3.5	206.4	9.5	360.8
3.75	227.1	9.75	426.5
4.00	204.1	10.00	396.7
4.25	209.7	10.25	460.8
4.50	212.6	10.50	254.6
4.75	213	10.75	242
5.0	233.2	11.0	237.5
5.25	198.5	11.25	256.8
5.5	194.7	11.5	269.1
5.75	233.5	11.75	257.6

Table A5 1H 700A AC (Continued)

Distance (mm)	Hardness (HV)	Distance (mm)	Hardness (HV)
12.00	253.4	14.25	440.9
12.25	235.1	14.50	497.4
12.50	365.1	14.75	468.5
12.75	379.7	15.0	481.9
13.0	392.9	15.25	437.3
13.25	420.3	15.5	421.3
13.5	384.4	15.75	509.6
13.75	438.5	16.00	433.4
14.00	387.9		

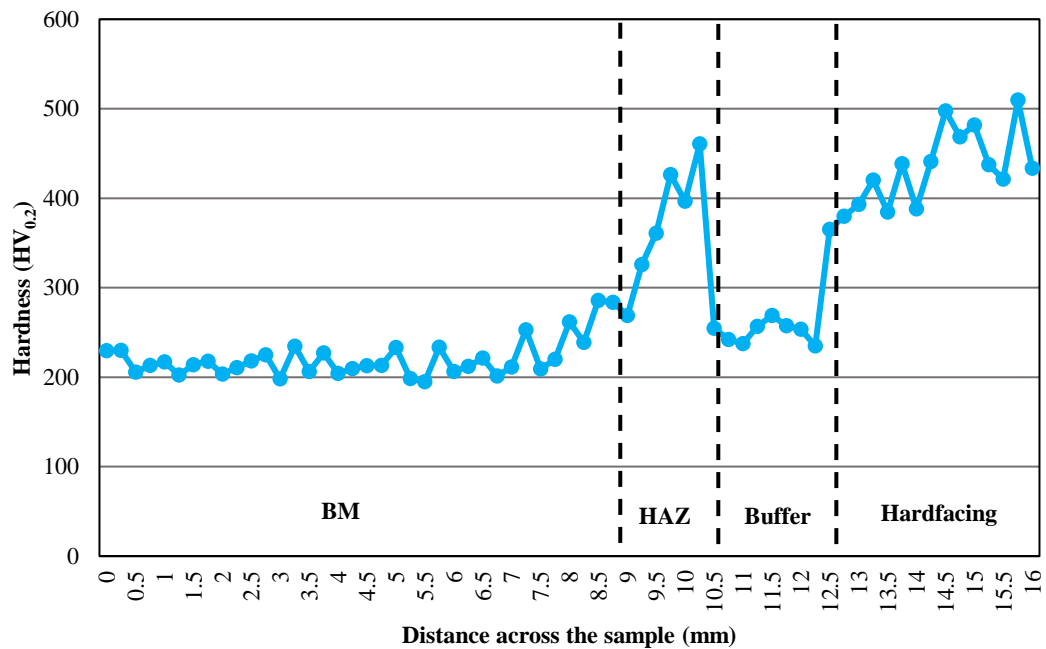
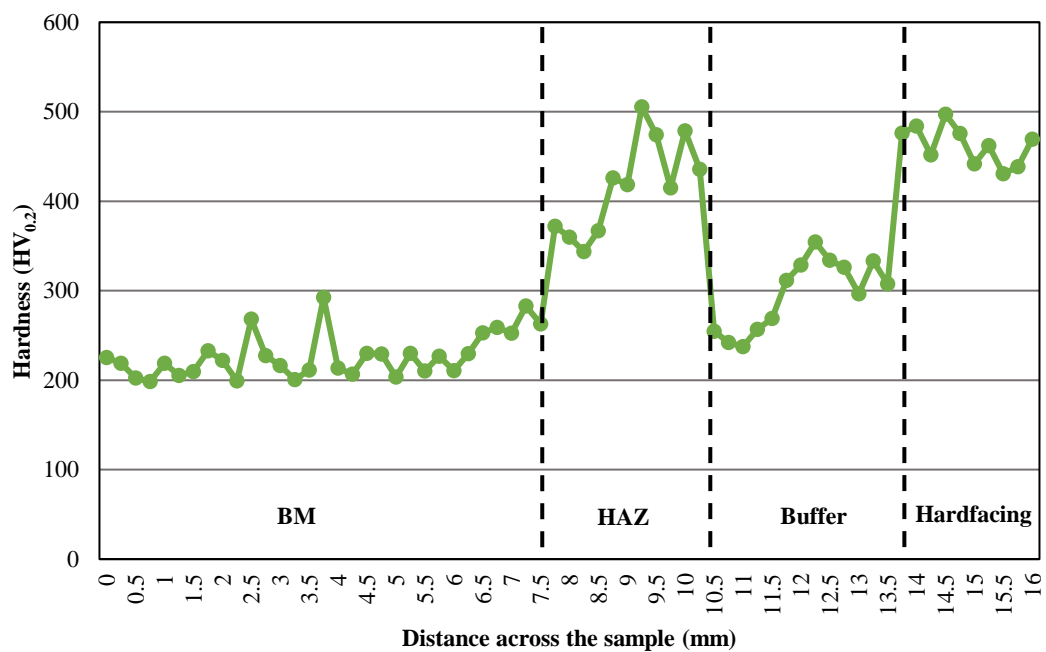
**Fig A5** Hardness values of 1H 700A AC

Table A6 1H 700A DC+

Distance (mm)	Hardness (HV)	Distance (mm)	Hardness (HV)
0.00	225.4	6.00	210.7
0.25	218.7	6.25	229.6
0.50	202.3	6.50	252.7
0.75	198.3	6.75	259
1.0	218.7	7.0	252.4
1.25	205.1	7.25	283
1.5	209.7	7.5	262.7
1.75	232.9	7.75	372.1
2.00	222.2	8.00	359.9
2.25	199	8.25	343.6
2.50	268.1	8.50	366.9
2.75	227.4	8.75	426.1
3.0	216.4	9.0	418.3
3.25	200.5	9.25	505.5
3.5	211.4	9.5	474.4
3.75	292.4	9.75	414.8
4.00	213.4	10.00	478.5
4.25	206.6	10.25	435.8
4.50	230.1	10.50	254.6
4.75	229.3	10.75	242
5.0	203.3	11.0	237.5
5.25	230.1	11.25	256.8
5.5	210.4	11.5	269.1
5.75	226.7	11.75	311.5

Table A6 1H 700A DC+ (Continued)

Distance (mm)	Hardness (HV)	Distance (mm)	Hardness (HV)
12.00	328.5	14.25	451.8
12.25	354.6	14.50	497.2
12.50	334.2	14.75	475.7
12.75	326.1	15.0	441.9
13.0	296.6	15.25	462.1
13.25	333.4	15.5	430.5
13.5	307.7	15.75	438.5
13.75	476.1	16.00	469.3
14.00	484		

**Fig A6** Hardness values of 1H 700A DC+

APPENDIX B:
Three Layers Hardness Data

Table B1 3H 500A AC

Distance (mm)	Hardness (HV)	Distance (mm)	Hardness (HV)
0.00	196.3	6.00	191.6
0.25	189.3	6.25	231.5
0.50	197.6	6.50	232.6
0.75	197.4	6.75	222.4
1.0	186.5	7.0	260.1
1.25	182.5	7.25	260.2
1.5	185.7	7.5	256.9
1.75	183.1	7.75	245.5
2.00	184	8.00	318.7
2.25	185.4	8.25	409.6
2.50	224.8	8.50	324.2
2.75	187.6	8.75	406.3
3.0	208.6	9.0	421.3
3.25	192.1	9.25	517.1
3.5	204.8	9.5	536.1
3.75	186.8	9.75	611.8
4.00	202.6	10.00	588.6
4.25	188.9	10.25	532.5
4.50	222.1	10.50	272.7
4.75	206.2	10.75	295.1
5.0	203.7	11.0	262.7
5.25	209.7	11.25	280.3
5.5	211.4	11.5	290.5
5.75	205.2	11.75	291.1

Table B1 3H 500A AC (Continued)

Distance (mm)	Hardness (HV)	Distance (mm)	Hardness (HV)
12.00	290.2	18.00	596.7
12.25	290.8	18.25	579.8
12.50	333.6	18.50	531.3
12.75	292.1	18.75	558
13.0	343.4	19.0	605.4
13.25	344.7	19.25	556.3
13.5	407.7	19.5	573.9
13.75	376.8	19.75	581.4
14.00	398.9	20.00	605.4
14.25	417	20.25	621.4
14.50	407.5	20.50	630.6
14.75	457.2	20.75	574.4
15.0	482.3	21.0	578
15.25	468	21.25	603
15.5	454.2	21.5	605.7
15.75	472		
16.00	458.2		
16.25	505.7		
16.50	497		
16.75	530.9		
17.0	532.7		
17.25	553.3		
17.5	540.7		
17.75	532.9		

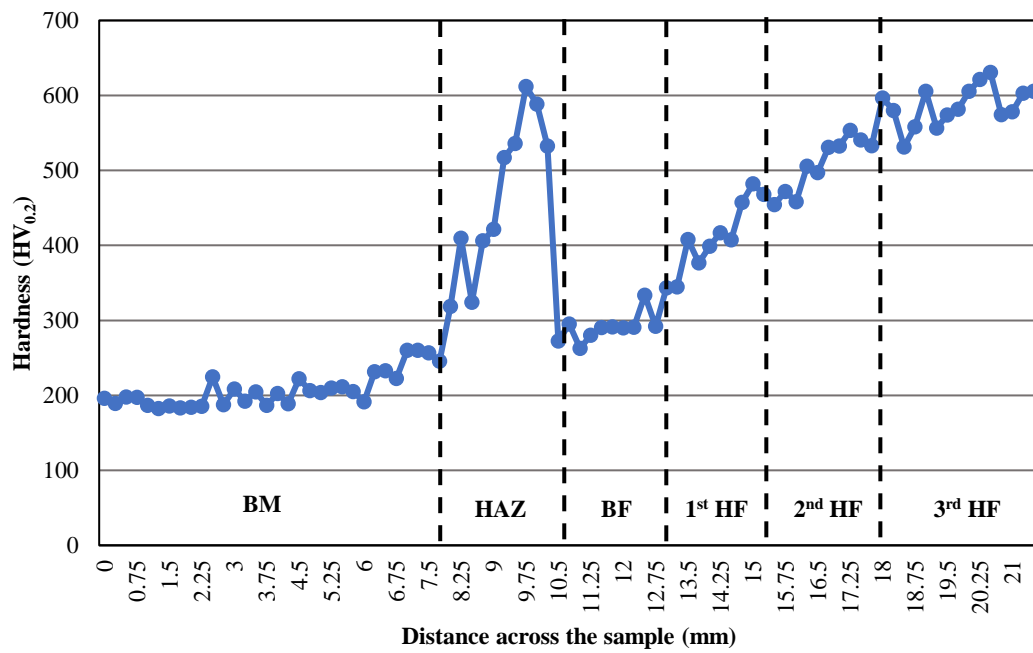


Fig B1 Hardness value of 3H 500A AC

Table B2 3H 500A DC+

Distance (mm)	Hardness (HV)	Distance (mm)	Hardness (HV)
0.00	211.3	6.00	234.8
0.25	218.8	6.25	215
0.50	213.3	6.50	228.3
0.75	204.7	6.75	315.8
1.0	206	7.0	261.9
1.25	207.5	7.25	270.8
1.5	233.4	7.5	292.8
1.75	221.6	7.75	440.9
2.00	209.1	8.00	346.8
2.25	215.3	8.25	392.4
2.50	218.5	8.50	417.3
2.75	213.7	8.75	407.9
3.0	221.7	9.0	542.8
3.25	208.6	9.25	518.3
3.5	203.2	9.5	552.6
3.75	218.8	9.75	572.3
4.00	218.3	10.00	333
4.25	240	10.25	335.6
4.50	233.1	10.50	382.7
4.75	233	10.75	313.9
5.0	250.3	11.0	302.6
5.25	246.7	11.25	317.4
5.5	196	11.5	310.3
5.75	221.1	11.75	329.8

Table B2 3H 500A DC+ (Continued)

Distance (mm)	Hardness (HV)	Distance (mm)	Hardness (HV)
12.00	333.7	18.00	626.5
12.25	310.8	18.25	582.6
12.50	308.9	18.50	660.8
12.75	432.9	18.75	610.2
13.0	466.8	19.0	612.3
13.25	444.5	19.25	584.4
13.5	422.4	19.5	644.9
13.75	385.4	19.75	610.3
14.00	412.5	20.00	664.7
14.25	422.7	20.25	630.1
14.50	429.3	20.50	645.7
14.75	436.7	20.75	667.5
15.0	456.6	21.0	591.9
15.25	591.9	21.25	635.5
15.5	602.5	21.5	639.2
15.75	561.5		
16.00	594.1		
16.25	579.8		
16.50	503.1		
16.75	517.9		
17.0	501.1		
17.25	579.4		
17.5	510.5		
17.75	576.6		

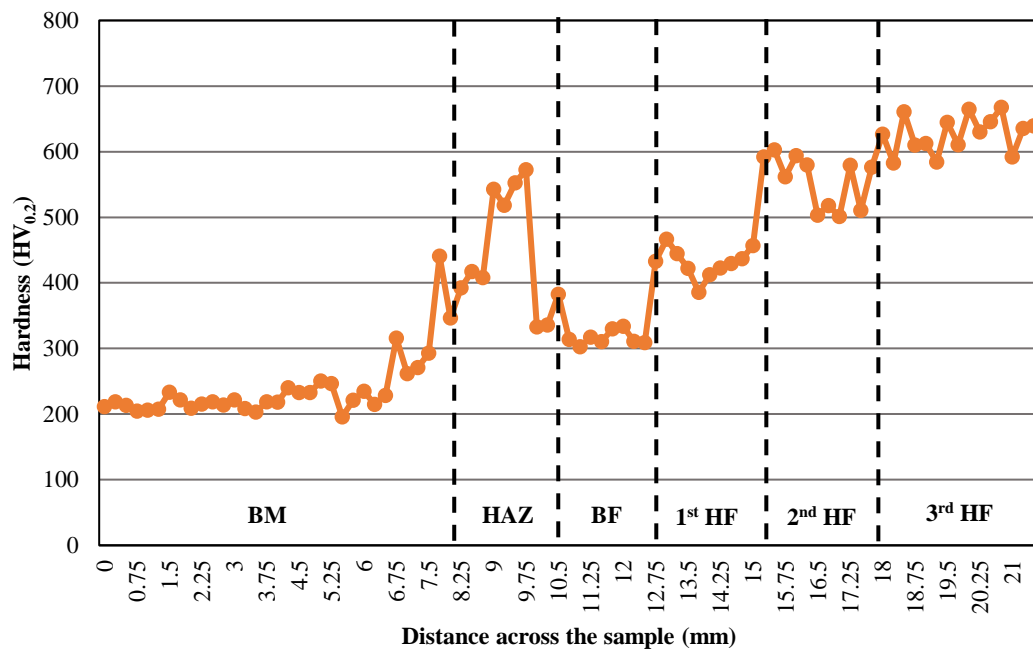


Fig B2 Hardness value of 3H 500A DC+

Table B3 3H 600A AC

Distance (mm)	Hardness (HV)	Distance (mm)	Hardness (HV)
0.00	217.1	6.00	232.2
0.25	223.5	6.25	238.1
0.50	265.1	6.50	260.9
0.75	210.7	6.75	277.8
1.0	215.7	7.0	287.6
1.25	250.4	7.25	296.2
1.5	210.1	7.5	298.9
1.75	226.2	7.75	329.1
2.00	233.6	8.00	338.4
2.25	224.2	8.25	374.4
2.50	239	8.50	449
2.75	211.8	8.75	536.6
3.0	211.9	9.0	546.5
3.25	216	9.25	524.3
3.5	220.3	9.5	516.7
3.75	284.4	9.75	449.6
4.00	241.1	10.00	450.4
4.25	226.1	10.25	297.9
4.50	227.5	10.50	291.8
4.75	283.3	10.75	254.6
5.0	239.3	11.0	233.9
5.25	220	11.25	269.8
5.5	230	11.5	255.4
5.75	240.9	11.75	279.5

Table B3 3H 600A AC (Continued)

Distance (mm)	Hardness (HV)	Distance (mm)	Hardness (HV)
12.00	284.5	18.00	605.2
12.25	279.7	18.25	571.7
12.50	255.4	18.50	588.2
12.75	275.5	18.75	541.5
13.0	256.7	19.0	543.1
13.25	277.7	19.25	565.4
13.5	276.4	19.5	586.3
13.75	287.8	19.75	564.1
14.00	257.1	20.00	619.3
14.25	263.8	20.25	568.1
14.50	421.8	20.50	591
14.75	427.7	20.75	567.2
15.0	410.7	21.0	586.8
15.25	414.2	21.25	591
15.5	420.7	21.5	580.7
15.75	453		
16.00	407.4		
16.25	405		
16.50	412.1		
16.75	484.1		
17.0	528.9		
17.25	500.9		
17.5	545.2		
17.75	509.8		

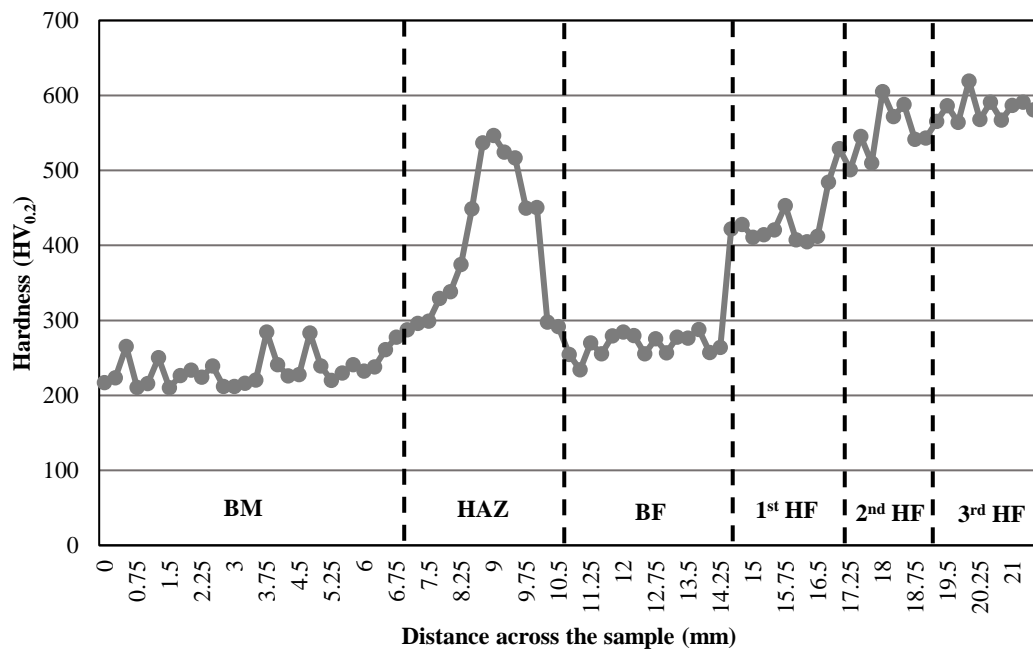


Fig B3 Hardness value of 3H 600A AC

Table B4 3H 600A DC+

Distance (mm)	Hardness (HV)	Distance (mm)	Hardness (HV)
0.00	180.7	6.00	200.5
0.25	185.9	6.25	199.4
0.50	206.4	6.50	212.4
0.75	193	6.75	210
1.0	220	7.0	214.9
1.25	201.5	7.25	194.9
1.5	202.2	7.5	204.6
1.75	206.9	7.75	289.3
2.00	213.3	8.00	321.7
2.25	192.2	8.25	328.9
2.50	206.3	8.50	358.5
2.75	203.4	8.75	454.6
3.0	210.1	9.0	481.7
3.25	221.7	9.25	486.4
3.5	207.4	9.5	469.1
3.75	214.6	9.75	476.1
4.00	201.8	10.00	467.6
4.25	220.7	10.25	455.6
4.50	195.8	10.50	530.9
4.75	205.7	10.75	307.1
5.0	239.1	11.0	318.9
5.25	221.6	11.25	291.9
5.5	229.1	11.5	292.2
5.75	208.1	11.75	291.1

Table B4 3H 600A DC+ (Continued)

Distance (mm)	Hardness (HV)	Distance (mm)	Hardness (HV)
12.00	288.4	18.00	634.8
12.25	284.9	18.25	605.4
12.50	278.5	18.50	605.4
12.75	277.6	18.75	606.4
13.0	259.4	19.0	636.4
13.25	254.7	19.25	643.8
13.5	268.7	19.5	637
13.75	363.3	19.75	582.6
14.00	388.1	20.00	640.1
14.25	372.1	20.25	623.2
14.50	430.3	20.50	626.7
14.75	347.6	20.75	619.4
15.0	322.3	21.0	605.9
15.25	411.9	21.25	623.9
15.5	449.3	21.5	616.5
15.75	529.7		
16.00	446.5		
16.25	565.7		
16.50	508.7		
16.75	530.9		
17.0	604.9		
17.25	567.9		
17.5	614.3		
17.75	609.3		

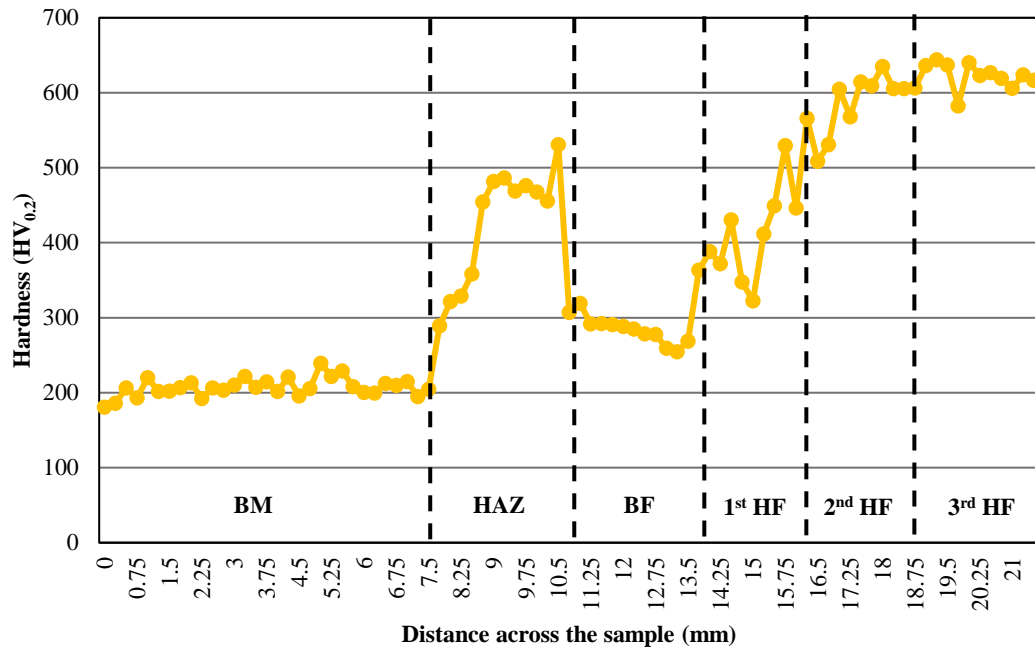


Fig B4 Hardness value of 3H 600A DC+

Table B5 3H 700A AC

Distance (mm)	Hardness (HV)	Distance (mm)	Hardness (HV)
0.00	238.3	6.00	248.3
0.25	226.8	6.25	243.7
0.50	218.3	6.50	251.1
0.75	244	6.75	338.9
1.0	229.3	7.0	304.6
1.25	224.6	7.25	341.3
1.5	222.7	7.5	364.1
1.75	208.3	7.75	331.8
2.00	217.6	8.00	352.8
2.25	208.2	8.25	529.7
2.50	208.1	8.50	464.7
2.75	215.9	8.75	596.7
3.0	220.8	9.0	482.6
3.25	215.3	9.25	387.9
3.5	240.4	9.5	441.9
3.75	232.2	9.75	407.4
4.00	217.1	10.00	446.5
4.25	228.3	10.25	501.6
4.50	221.8	10.50	268.5
4.75	206.9	10.75	362.8
5.0	227.6	11.0	313
5.25	276.8	11.25	286.9
5.5	245.8	11.5	288.5
5.75	273.5	11.75	320.2

Table B5 3H 700A AC (Continued)

Distance (mm)	Hardness (HV)	Distance (mm)	Hardness (HV)
12.00	303.1	18.00	542.3
12.25	410.9	18.25	590.5
12.50	408.1	18.50	592.4
12.75	393.7	18.75	558
13.0	550.7	19.0	587.2
13.25	442.5	19.25	512.9
13.5	392.8	19.5	641.7
13.75	500.9	19.75	512.5
14.00	517.1	20.00	577.1
14.25	503.1	20.25	573.5
14.50	544	20.50	556.5
14.75	434.9	20.75	535.7
15.0	423.8	21.0	564.1
15.25	449.6	21.25	620.4
15.5	474.4	21.5	573
15.75	385.9		
16.00	621		
16.25	581.2		
16.50	518.6		
16.75	516.7		
17.0	504.6		
17.25	528.5		
17.5	541.7		
17.75	588.1		

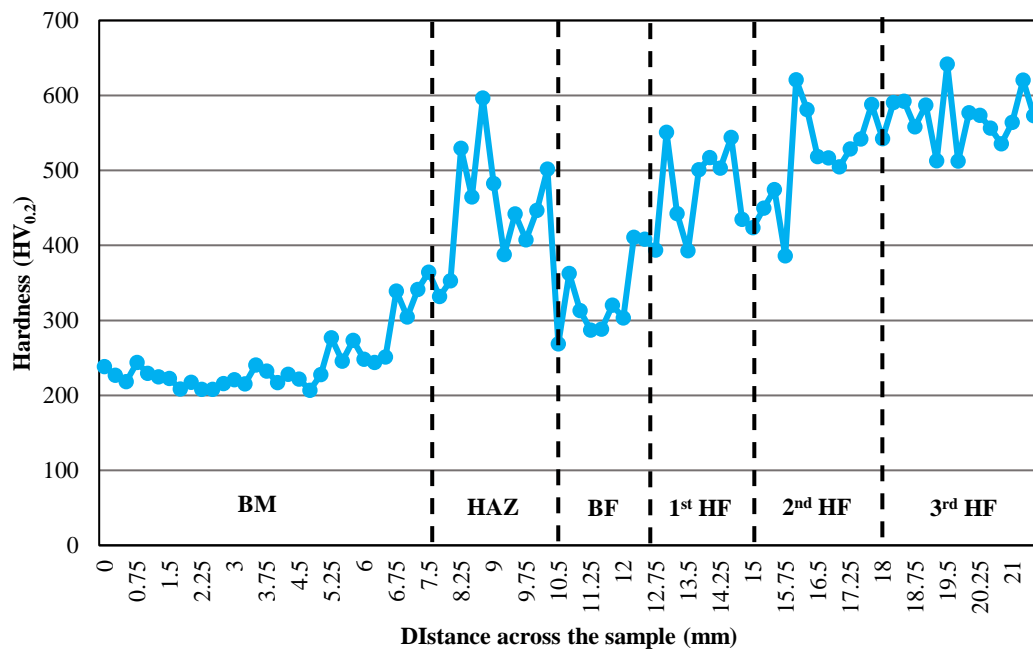


Fig B5 Hardness value of 3H 700A AC

Table B6 3H 700A DC+

Distance (mm)	Hardness (HV)	Distance (mm)	Hardness (HV)
0.00	214.7	6.00	228.8
0.25	215.8	6.25	215.9
0.50	255.9	6.50	246.4
0.75	205.4	6.75	232.9
1.0	209.4	7.0	268
1.25	195.5	7.25	284.9
1.5	200.8	7.5	302
1.75	221.8	7.75	350
2.00	224.2	8.00	343
2.25	207.5	8.25	417.9
2.50	206.6	8.50	391.9
2.75	201.5	8.75	532.9
3.0	239.7	9.0	518.6
3.25	256.7	9.25	470
3.5	198.3	9.5	401.3
3.75	250.5	9.75	439.7
4.00	227	10.00	322.5
4.25	208.6	10.25	317.6
4.50	199.5	10.50	314
4.75	231.4	10.75	302.5
5.0	219.2	11.0	374.9
5.25	219.8	11.25	308.7
5.5	249	11.5	309.6
5.75	226.2	11.75	308.9

Table B6 3H 700A DC+ (Continued)

Distance (mm)	Hardness (HV)	Distance (mm)	Hardness (HV)
12.00	300.3	18.00	554.8
12.25	365.6	18.25	525.3
12.50	358.8	18.50	497
12.75	414.8	18.75	513.3
13.0	380.2	19.0	501.4
13.25	380.9	19.25	517.5
13.5	384.4	19.5	519
13.75	406.6	19.75	539.4
14.00	357.4	20.00	525.3
14.25	332.8	20.25	518.6
14.50	381.9	20.50	564.8
14.75	405.4	20.75	533.7
15.0	397.1	21.0	512.1
15.25	381.8	21.25	613.8
15.5	366.2	21.5	590.5
15.75	525.3		
16.00	459.1		
16.25	536.6		
16.50	504		
16.75	539		
17.0	473.9		
17.25	511.3		
17.5	486.5		
17.75	553.7		

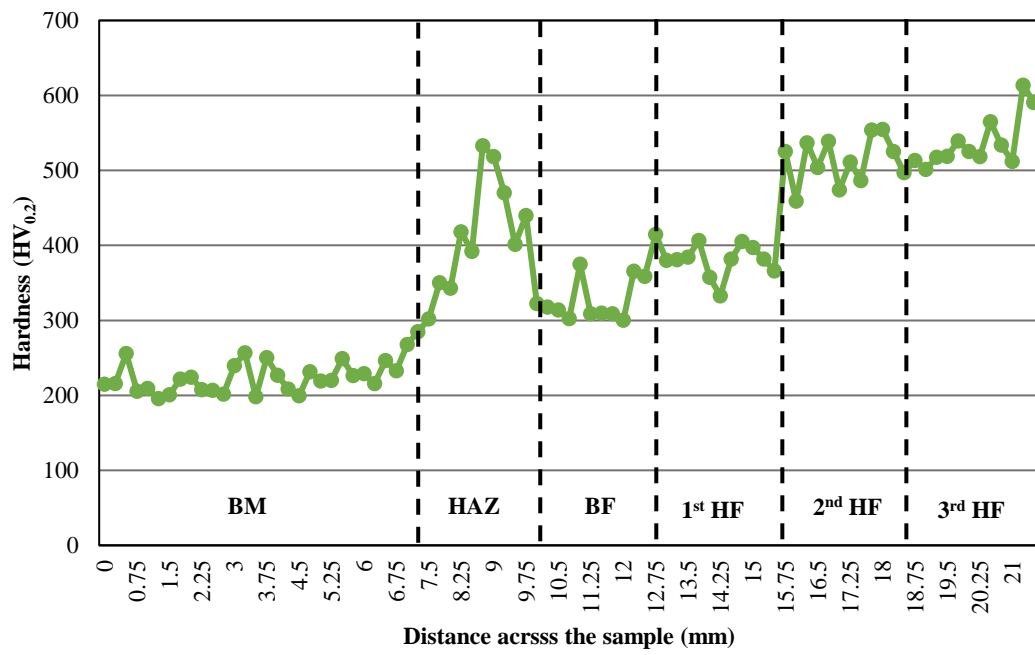


Fig B6 Hardness value of 3H 700A DC+

APPENDIX C:

**Emission-dispersive x-ray spectroscopy results of Single and Three layers
hardfacing**

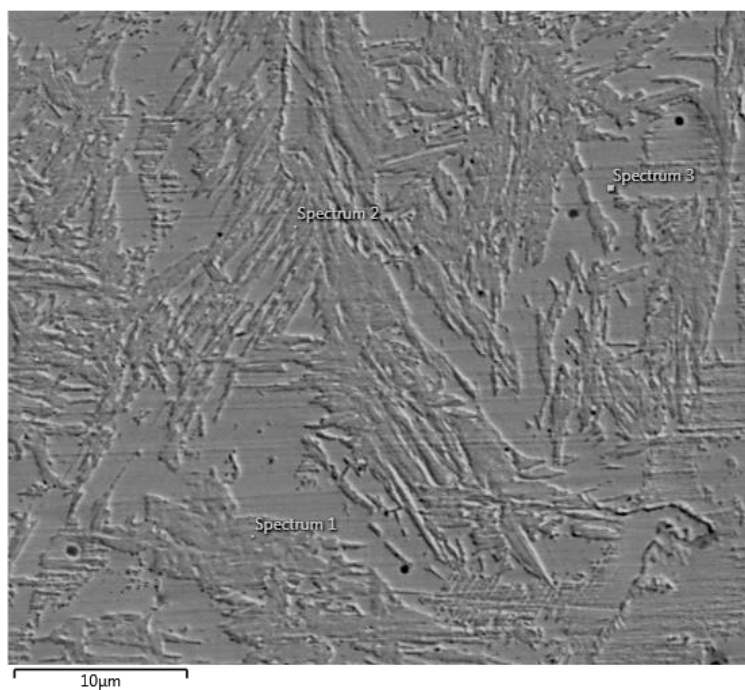


Fig C1 Scanning electron micrograph of three layers hardfacing analyzed by emission-dispersive x-ray spectroscopy

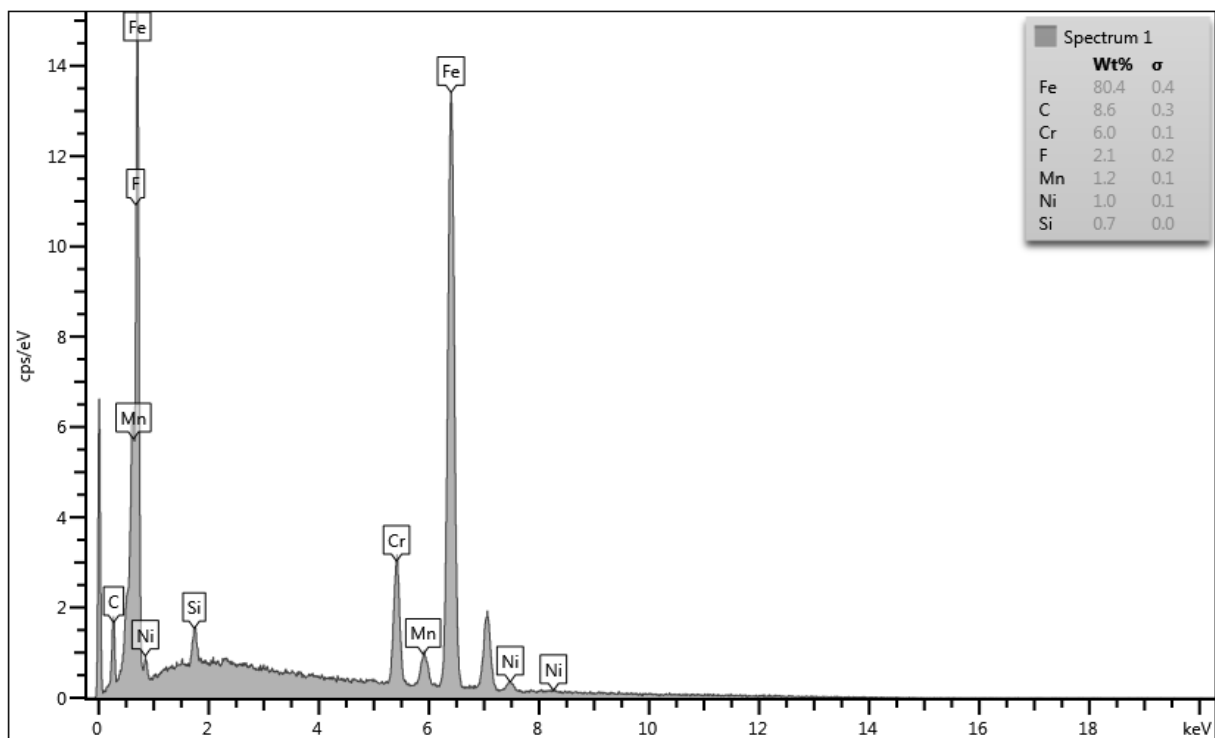


Fig C2 Emission-dispersive x-ray spectroscopy result of Spectrum 1 for single layer hardfacing

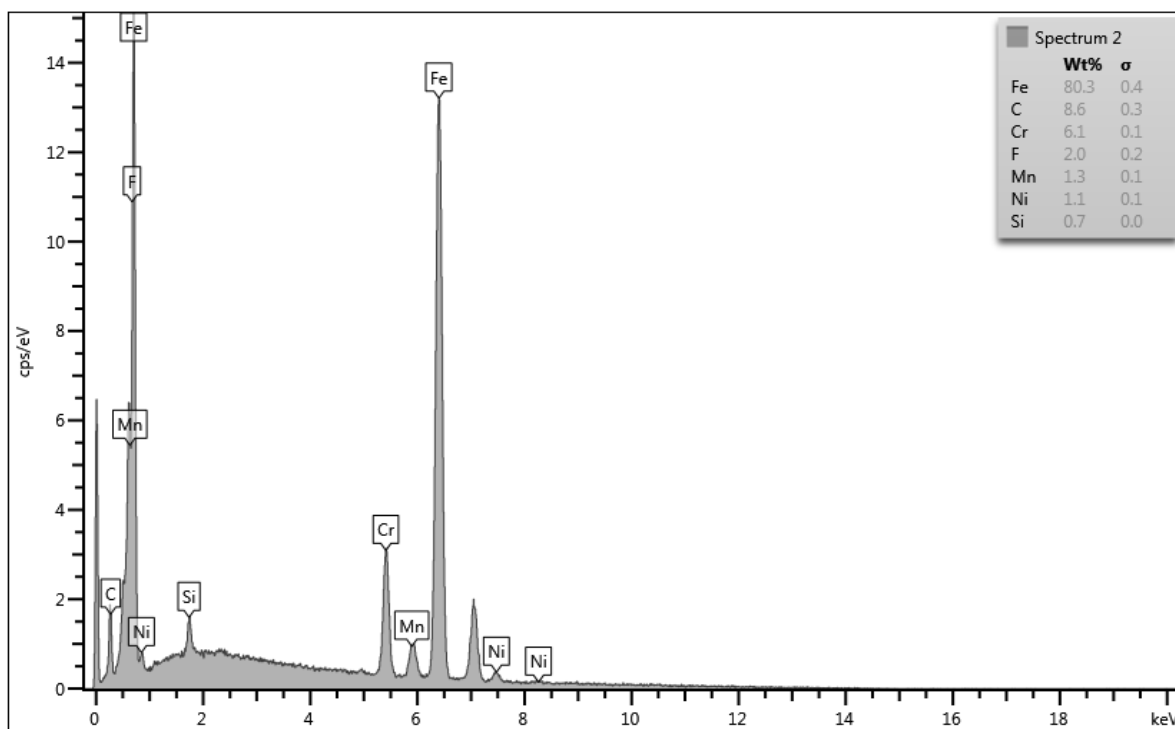


Fig C3 Emission-dispersive x-ray spectroscopy result of Spectrum 2 single layer hardfacing

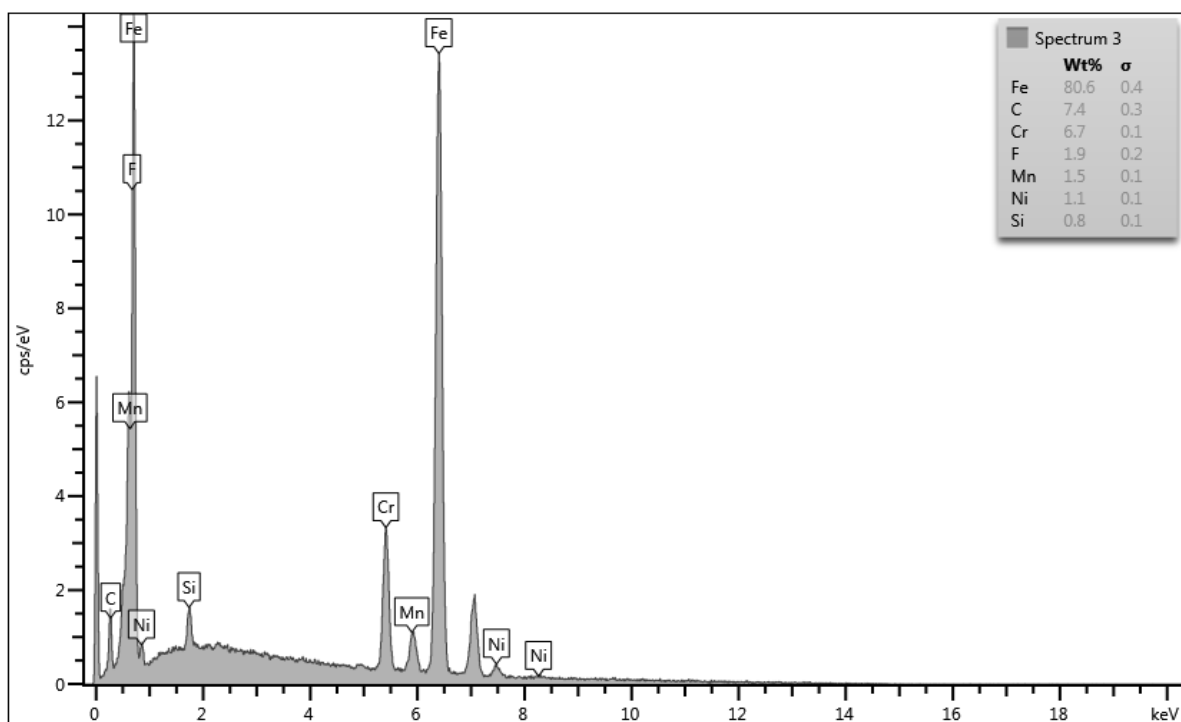


Fig C4 Emission-dispersive x-ray spectroscopy result of Spectrum 3 single layer hardfacing

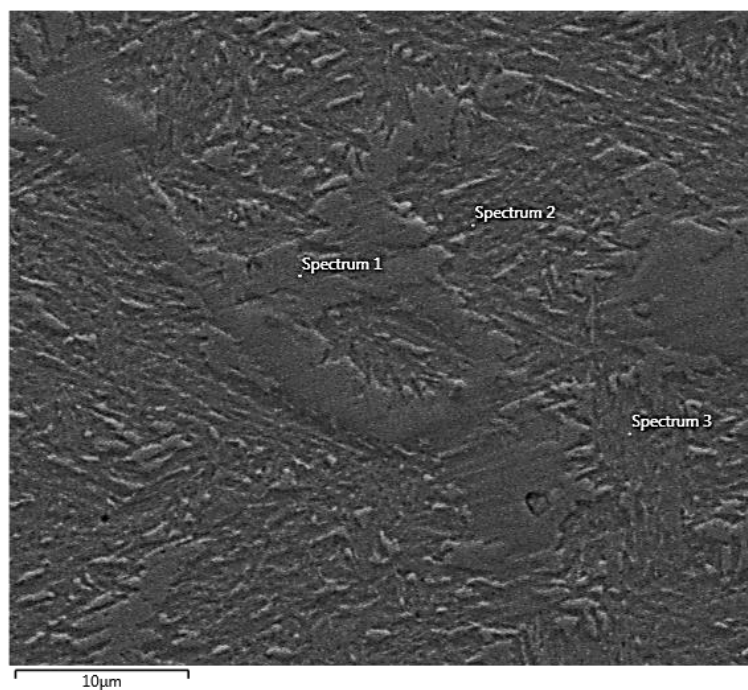


Fig C5 Scanning electron micrograph of three layers hardfacing analyzed by emission-dispersive x-ray spectroscopy

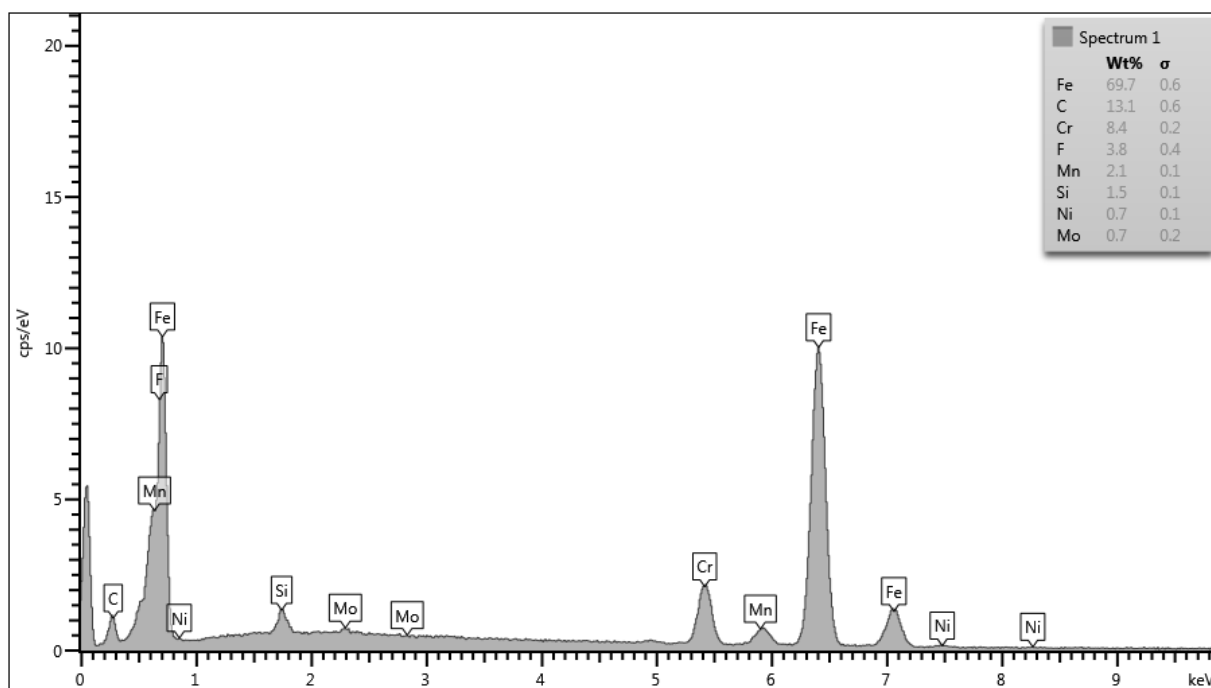


Fig C6 Emission-dispersive x-ray spectroscopy result of Spectrum 1 for three layers hardfacing

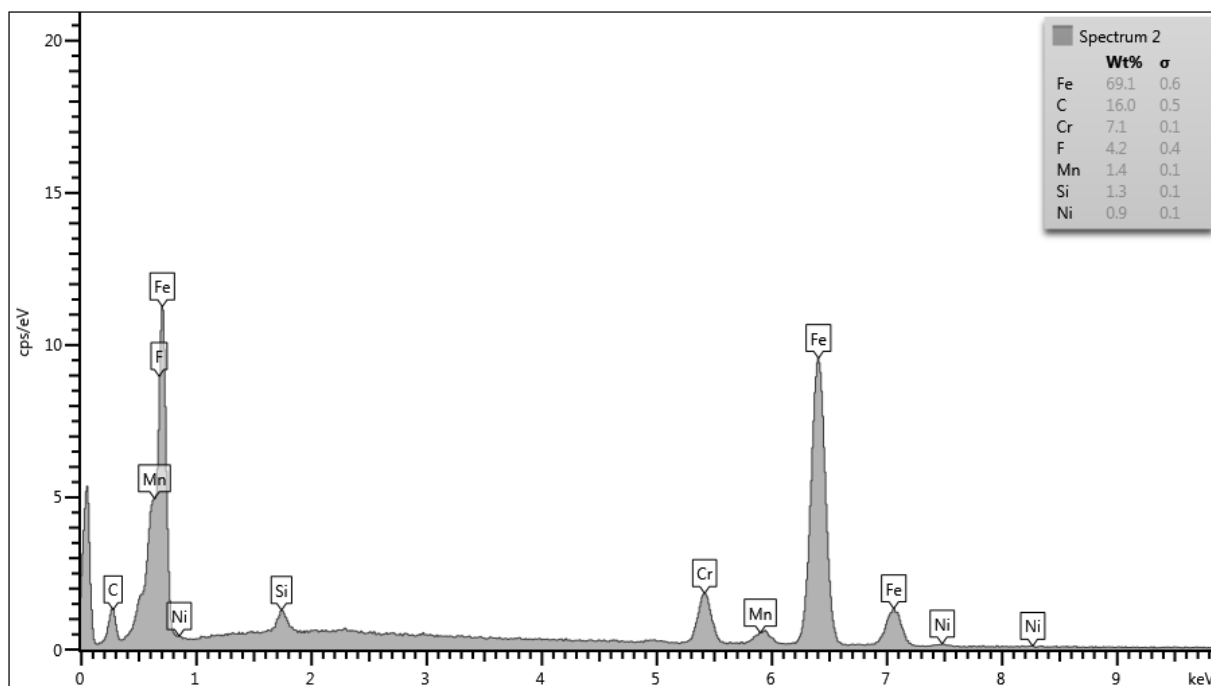


Fig C7 Emission-dispersive x-ray spectroscopy result of Spectrum 2 three layers hardfacing

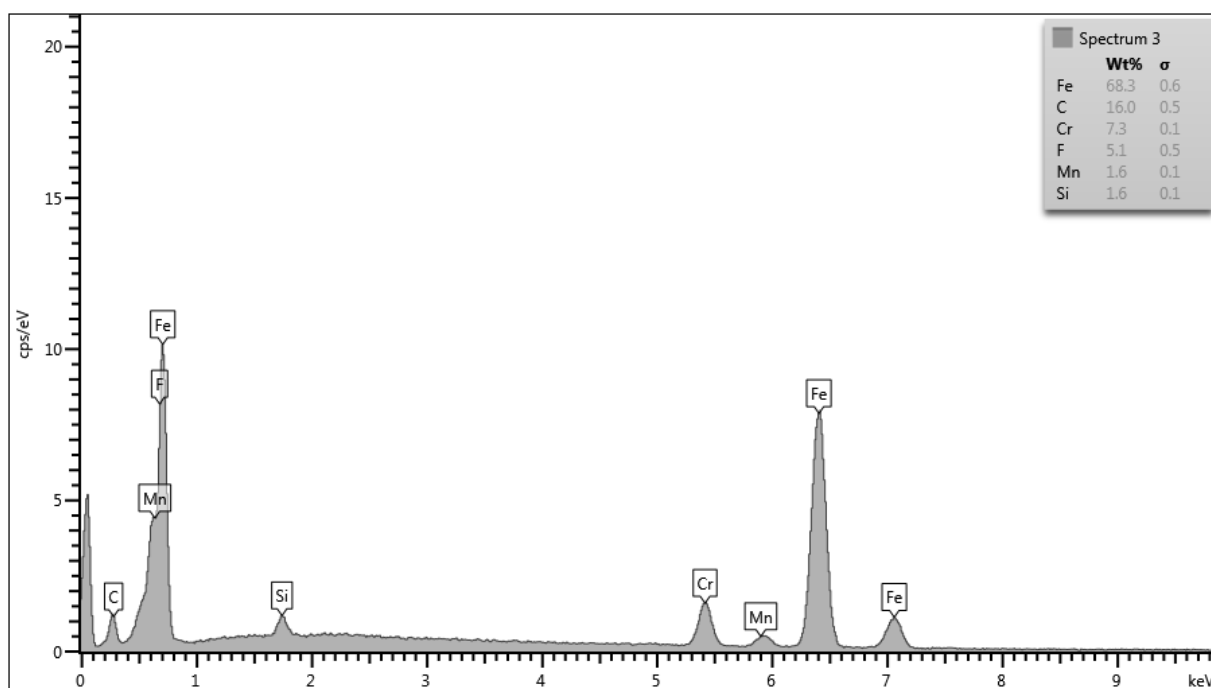



Fig C8 Emission-dispersive x-ray spectroscopy result of Spectrum 3 three layers hardfacing

LIST OF PUBLICATIONS

Springer for Research & Development Search Home Contact us Log in



Metallurgist
March 2018, Volume 61, Issue 11-12, pp 1033-1037 | [Cite as](#)

Correlating Hardness and Welding Dilution with the Abrasion Mass Loss of Hardfacings Welded with Different Currents and Polarities

Authors Authors and affiliations

<p>Hein Zaw Oo ¹ ✉ Email author</p> <p>B. Srikarun ¹</p> <p>P. Muangjunburee ¹</p>	<p>1. Department of Mining and Materials Engineering, Faculty of Engineering, Prince of Songkla University, Hat Yai, Thailand</p>
-----------------------------------------------------------------------------------------------------------------------------------------	-----------------------------------------------------------------------------------------------------------------------------------

Article
First Online: 12 April 2018

176 Downloads

- Download PDF
- Cite article
- Share article
- Article
- Notes
- References
- Copyright information
- About this article

Web of Science InCites Journal Citation Reports Essential Science Indicators EndNote Publons Sign In Help English

Web of Science Clarivate Analytics

Search My Tools Search History Marked List

Results: 1
(from Web of Science Core Collection)

You searched for: AUTHOR: (Oo hein zaw) ...More
Create Alert

Refine Results

Search within results for...

Publication Years
2018 (1)
Refine

Sort by: **Date** Times Cited Usage Count Relevance More

Page 1 of 1

1. **Correlating Hardness and Welding Dilution with the Abrasion Mass Loss of Hardfacings Welded with Different Currents and Polarities**

By: **Oo, Hein Zaw**; Srikarun, B.; Muangjunburee, P.
METALLURGIST Volume: 61 Issue: 11-12 Pages: 1033-1037 Published: MAR 2018

Full Text from Publisher View Abstract

Times Cited: 0
(from Web of Science Core Collection)

Usage Count

Sort by: **Date** Times Cited Usage Count Relevance More

Show: 10 per page

Page 1 of 1

DOI 10.1007/s11015-018-0604-3
Metallurgist, Vol. 61, Nos. 11–12, March, 2018

**CORRELATING HARDNESS AND WELDING DILUTION
 WITH THE ABRASION MASS LOSS OF HARDFACINGS
 WELDED WITH DIFFERENT CURRENTS AND POLARITIES**

Hein Zaw Oo, B. Srikarun, and P. Muangjunburee

UDC 621.7

The correlation of hardness, microstructure, and dilution with the abrasion mass loss of hardfaced samples deposited using different currents (500 and 600 A) and polarities (AC and DC+) was studied. Four different welding conditions were considered for submerged arc welding using a martensitic hardfacing electrode and austenitic buffer electrode. Single-layer hardfacing was applied over the single-layer buffer. The microstructure of hardfacing was observed by an optical microscope. The micro-Vickers hardness across a single-layer hardfacing and dilution percentage were also measured. A dry-sand-rubber wheel abrasion test was conducted according to ASTM G65 procedure A to record the abrasive mass loss of the samples. The use of higher current and DC+ polarity resulted in the highest mass loss because of the deepest dilution and lowest hardness. Dilution affects the hardness and microstructure of hardfacing. The lowest abrasive mass loss, shallowest dilution, and highest hardness were obtained for the sample welded with lower current and AC polarity.

Keywords: *hardfacing, martensitic, austenitic buffer, welding dilution, submerged arc welding.*

Introduction. The wearing of machinery components is a common problem in engineering applications [1]. Tool materials interact with hard and sharp particles or rocks in the mining and agriculture industries. This interaction removes material from the tools such that they eventually stop working effectively. Tools must therefore be replaced or rebuilt [2]. The surfaces of components are damaged by heavy impacts and scratching of the tool by hard abrasives trapped between the contacting surfaces when a machine is used [3].

Hardfacing is a useful and economical technique employed to mitigate the severe wear of tools and machines [4]. Hardfacing applies hard and durable surface layers to base metals to impart abrasion resistance, impact wear resistance and erosion resistance [5, 6]. The hardfaced coatings are frequently deposited by welding (either during maintenance or in the manufacture of new components) in many industries [7]. Submerged arc welding is an effective welding process that produces hardfacing deposits because it provides several ways to increase the welding efficiency [8].

The choice of suitable hardfacing alloys mainly depends on the microstructure, chemical composition, and hardness of the alloy [9]. Iron-based hardfacing materials are commonly used because they are inexpensive and easy to use. There are many types of microstructures and compositions that provide different abrasion resistances available for iron-based hardfacings [10–12]. Martensitic steel is a popular hardfacing material because of its combination of good wear and corrosion resistances [13]. Buffer layers are often employed between a substrate and hardfacing deposits [14].

At the Mae Moh Lignite Coal Mine of the Electricity Generating Authority of Thailand, the surface of a single-roll coal crusher made from low-alloy steel was hardfaced to mitigate wear. The present study investigated the correlation of the microstructure, dilution percentage, and microhardness with wear resistance for single-layer hardfacing applied to the low-alloy steel coal crusher by submerged arc welding using different welding currents (500 and 600 A) and polarities (AC and DC+).

Department of Mining and Materials Engineering, Faculty of Engineering, Prince of Songkla University, Hat Yai, Songkhla, 90112, Thailand; e-mail: prapas.m@psu.ac.th.

TABLE 1. Chemical Composition of the Base Metal (wt.%)

C	Si	Mn	Ni	Cr	Mo	Cu	Fe
0.38	0.40	0.52	0.17	3.42	0.30	0.04	Bal

TABLE 2. Chemical Composition of the Electrodes Used for Hardfacing and Buffer Layer (wt.%)

Electrode	C	Si	Mn	Cr	Ni	Fe
Hardfacing	0.5	2.5	1.5	8.5	–	Bal
Buffer	0.1	0.5	6	19	9	Bal

TABLE 3. Fixed Parameters of the Research

Parameters	
Welding process	SAW
Number of layers	1
Voltage, V	30
Travel speed, cm/min	60
Wire diameter, mm	2.4
Wire extension, mm	25.4
Preheating temperature, °C	350

Experimental. An austenitic stainless-steel electrode (EN 14700: T Fe10) and martensitic-steel electrode (EN 14700: T Fe8) were used to deposit onto a low-alloy steel base metal plate and thus create a buffer layer and hardfacing layer. The chemical compositions of the base metal and wire electrodes used for the hardfacing and buffer are given in Tables 1 and 2. An agglomerated basic flux having a basicity index of 2.3 was used for submerged arc welding. Buffer and hardfacing layers with six beads were deposited for a flat position employing twin-wire submerged arc welding. The overlap between the beads was approximately 30%. All samples were cooled at room temperature after welding.

Hardfaced deposits were applied to four 20-mm-thick base metal steel coupons having dimensions of 250 × 75 mm using twin-wire submerged arc welding equipment. Each sample was hardfaced using current of 500 or 600 A and AC or DC+ welding polarity. Before welding, the base metal plate was preheated at 350°C. A single-layer buffer deposit was first applied, and a single hardfacing layer was then deposited over the buffer layer. Other parameters were kept constant. The welding parameters used in this work are given in Table 3.

Results and discussion. Cross-sectional optical micrographs of the hardfacing layer for different conditions are shown in Fig. 1. The hardfacing microstructures for different conditions are almost uniform. These microstructures present martensite (dark regions) and austenite (white regions) phases at the grain boundaries. Despite using an electrode made from martensitic steel for the hardfacing layer, a greater amount of austenite phase appears in the microstructure of the hardfacing because of dilution with the austenitic buffer layer. Generally, the microstructures of both samples welded with 500 A had slightly more martensite, which is a hard and strong phase, than the microstructures of samples welded with 600 A because of higher dilution. Lower dilution is achieved by setting a lower current [15]. The microstructure of the sample welded with 600 A using AC polarity had the most austenite phase, which is soft and ductile.

The average micro-Vickers hardness distributions across single-layer hardfacings for all conditions are illustrated in Fig. 2. The samples welded using AC polarity for both high and low current were harder than the samples welded using DC+ polarity. The hardest and softest samples had a difference in hardness of about 100 HV. The highest hardness of about 430 HV

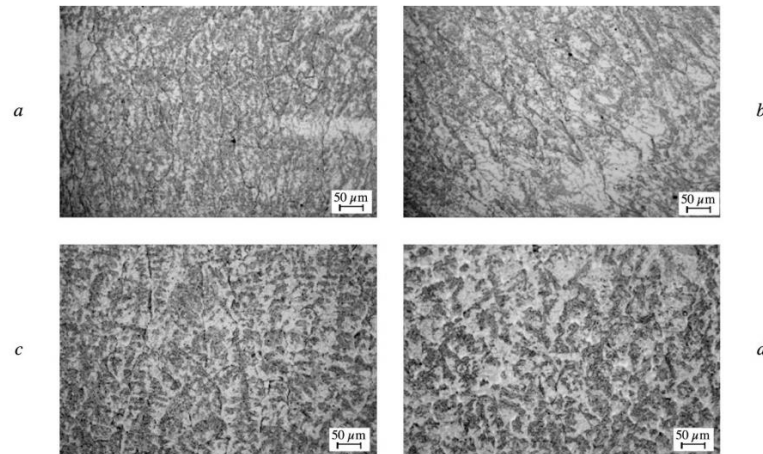


Fig. 1. Microstructure of the cross-sectional hardfaced layer: *a)* 500 A AC; *b)* 500 A DC+; *c)* 600 A AC; *d)* 600 A DC+.

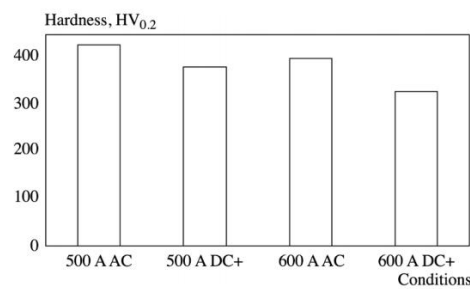


Fig. 2. Average hardness values of the different hardfacing samples.

was obtained for the sample welded with 500 A and AC polarity, whereas the sample welded with 600 A and DC+ polarity had the lowest hardness of about 330 HV. The average hardness values of the 600-A AC sample and 500-A DC+ sample were almost identical, differing by approximately 15 HV.

The welding dilution percentage is defined by the ratio of the area of melted parent metal to the total area of deposition [16]. Dilution critically affects the mechanical and metallurgical properties of overlays [17]. For hardfacing application, the welding dilution should be as low as possible because the surface properties of more diluted samples are not sufficiently improved owing to the presence of a higher amount of adjacent layer [18]. The welding dilution of each sample was calculated by image analysis software. The dilution percentages are given in Table 4 for all conditions. The sample welded with 500 A using AC polarity had the lowest dilution, while the highest dilution (nearly 7% more) was obtained for the sample welded using DC+ polarity. Greater dilution can be observed by increasing the current and using DC+ polarity.

TABLE 4. Welding Dilution of the Samples

Conditions	Dilution, %
500A AC	44.8219
500A DC+	47.7034
600A AC	46.5633
600A DC+	52.0891

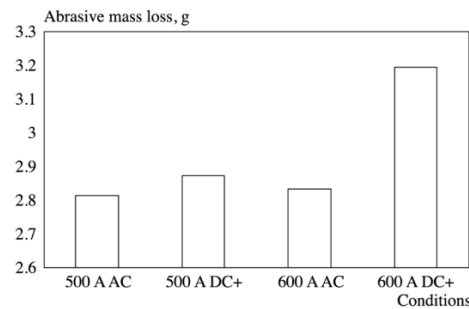


Fig. 3. Abrasive mass losses of hardfacing samples.

The abrasive mass loss of the samples was tested using a dry sand–rubber wheel abrasion machine according to ASTM G65 procedure A [19]. After running the machine, the abrasive mass loss of specimens was recorded with accuracy of ± 0.1 mg by measuring the original weight of specimens and the weight of tested specimens on an electric balance, and taking the difference. Higher abrasive mass loss leads to lower wear resistance. The abrasive mass losses of the four samples are compared in Fig. 3. The samples obtained using AC polarity had a lower abrasion mass loss than the samples obtained using DC+ polarity. The abrasive mass losses of the two samples obtained using AC polarity were nearly the same, with the sample welded with 500 A having the lowest abrasive mass. The abrasive mass loss was highest for the sample welded with 600 A using DC+ polarity because this sample had the most austenite phase present in the microstructure, lowest hardness, and highest dilution. The abrasion mass loss and dilution results of the other three samples were not greatly different, with the sample welded with 600 A using DC+ polarity having the highest abrasion mass loss and dilution. According to Wang et al. [20], the wear resistance of hardfacing layers depends on the combination of the microstructure and hardness. The microstructure and hardness of hardfacing generally relate to the welding dilution [16].

Conclusions. The correlation of hardness and welding dilution with the abrasive mass loss of samples welded with different welding currents and polarities was studied. The abrasive mass loss was lowest for the sample obtained with 500 A using AC polarity. This sample had the lowest austenite phase in its microstructure, highest hardness, and lowest dilution. Welding dilution can affect the microstructure of the welded sample. The dilution percentage and hardness values have a direct correlation with the wear resistance of single-layer hardfacing because higher abrasion mass loss follows from higher dilution and lower hardness. An increasing welding current leads to higher abrasive mass loss. Comparing between different polarities, it was found that the samples obtained using DC+ polarity had higher abrasive mass loss and welding dilution and lower hardness.

Acknowledgments. This work was supported by the Higher Education Research Promotion and the Thailand's Education Hub for Southern Region of ASEAN Countries Project Office of the Higher Education Commission. The authors

would like to acknowledge the Department of Mining and Materials Engineering, Faculty of Engineering, Prince of Songkla University, Hat Yai Campus, Thailand for supporting equipment, and the Electricity Generating Authority of Thailand (EGAT), Mae Moh Lignite Mine, Thailand for some data of this research.

REFERENCES

1. A. Saha and S. C. Mondal, "Multi-objective optimization of manual metal arc welding process parameters for nano-structured hardfacing material using hybrid approach," *Measurement*, **102**, 80–89 (2017).
2. K. G. Budinski and S. T. Budinski, "On replacing three-body abrasion testing with two-body abrasion testing," *Wear*, **376**, 1859–1865 (2017).
3. C. Wang, X. Li, Y. Chang, S. Han, and H. Dong, "Comparison of three-body impact abrasive wear behaviors for quenching–partitioning–tempering and quenching–tempering 20Si2Ni3 steels," *Wear*, **362**, 121–128 (2016).
4. E. Correa, N. Alcântara, L. Valeriano, et al., "The effect of microstructure on abrasive wear of a Fe–Cr–C–Nb hardfacing alloy deposited by the open arc welding process," *Surf. Coat. Technol.*, **276**, 479–484 (2015).
5. N. Yüksel and S. Şahin, "Wear behavior–hardness microstructure relation of Fe–Cr–C and Fe–Cr–C–B based hardfacing alloys," *Mater. Des.*, **58**, 491–498 (2014).
6. X. Wang, F. Han, and S. Qu, "Microstructure of the Fe-based hardfacing layers reinforced by TiC–VC–Mo₂C particles," *Surf. Coat. Technol.*, **202**, No. 8, 1502–1509 (2008).
7. American Society for Metals, *Welding, Brazing and Soldering: Metals Handbook*, Metals Park, Ohio (1983), 9th ed., Vol. 6, p. 2873.
8. R. Bendikiene and L. Kavaliauskiene, "The effect of plastic deformation rate on the wear performance of hardfaced coatings," *Weld. World*, **61**, No. 5, 1–8 (2017).
9. J. H. Bulloch and J. L. Henderson, "Some considerations of wear and hardfacing materials," *Int. J. Press. Vess. Piping*, **46**, No. 3, 251–267 (1991).
10. M. Morsy and E. El-Kashif, "The effect of microstructure on high-stress abrasion resistance of Fe–Cr–C hardfacing deposits," *Weld. World*, **58**, No. 4, 491–497(2014).
11. C. Fang, Y. Chen, Z. Yang, et al., "Cable-type welding wire submerged arc surfacing," *J. Mater. Process. Technol.*, **249**, 25–31 (2017).
12. M. Kirchgaßner, E. Badisch, and F. Franek "Behaviour of iron-based hardfacing alloys under abrasion and impact," *Wear*, **265**, No. 5–6, 772–779 (2008).
13. K. Yang, S. Yu, Y. Li, and C. Li, "Effect of carbonitride precipitates on the abrasive wear behaviour of hardfacing alloy," *Appl. Surf. Sci.*, **254**, No. 16, 5023–5027 (2008).
14. S. Chatterjee and T. K. Pal, "Weld procedural effect on the performance of iron based hardfacing deposits on cast iron substrate," *J. Mater. Process. Technol.*, **173**, No. 1, 61–69 (2006).
15. A. C. Crespo, A. Scotti, and M. R. Pérez, "Operational behavior assessment of coated tubular electrodes for SMAW hardfacing," *J. Mater. Process. Technol.*, **199**, No. 1, 265–273 (2008).
16. H. L. Tsai, Y. S. Tarn, and C. M. Tseng, "Optimisation of submerged arc welding process parameters in hardfacing," *Int. J. Adv. Manuf. Technol.*, **12**, No. 6, 402–406 (1996).
17. K. Siva, N. Murugan, and R. Logesh, "Optimization of weld bead geometry in plasma transferred arc hardfaced austenitic stainless-steel plates using genetic algorithm," *Int. J. Adv. Manuf. Technol.*, **41**, No. 1, 24–30 (2009).
18. K. Marimuthu and N. Murugan, "Prediction and optimisation of weld bead geometry of plasma transferred arc hardfaced valve seat rings," *Surf. Eng.*, **19**, No. 2, 143–149 (2003).
19. ASTM International, *G65-16: Standard Test Method for Measuring Abrasion Using the Dry Sand/Rubber Wheel*, ASTM Standards 04 (2013), pp. 1–12.
20. X. Wang, F. Han, and S. Qu, "Microstructure of the Fe-based hardfacing layers reinforced by TiC–VC–Mo₂C particles," *Surf. Coat. Technol.*, **202**, No. 8, 1502–1509 (2008).



ISSN: 2214-7853

- [View Articles](#)
- [Guide for Authors](#)
- [Abstracting/ Indexing](#)
- [Track Your Paper](#)

Materials Today: Proceedings

- > Supports Open Access
- Publisher: [S. Bland](#)
- > View Editorial Board

Materials Today is proud to introduce *Materials Today: Proceedings*. A new journal specializing in the publication of conference proceedings.

Materials Today: Proceedings provides the materials science community with a fast and flexible route to the publication of research presented at leading scientific...

[Read more](#)

Feedback

Download full text in PDF [Export](#)

Search ScienceDirect [Advanced](#)

- Outline
- Abstract
- Keywords
- References

materialstoday:
PROCEEDINGS
Volume 5, Issue 3, Part 2, 2018, Pages 9281-9289



Wear behaviour of hardfacing on 3.5% chromium cast steel by submerged arc welding

Hein Zaw Oo, Prapas Muangjumburee

Department of Mining and Materials Engineering, Faculty of Engineering, Prince of Songkla University, Hat Yai, Songkhla 90112, Thailand.

Available online 17 April 2018.

[Show less](#)

<https://doi.org/10.1016/j.matpr.2017.10.101>

[Get rights and content](#)

Abstract

The principal objectives of this research are to improve the wear behaviour of

Part of special issue:

The 10th Thailand International Metallurgy Conference, March 30-31, 2017

Edited by Piyorose Promdirek, Suchart Siengchin, Somrerk Chandra-ambhorn, Sureerat Patsilpa, Yuttanant Boonyongmaneerat, Rajarshi Banerjee, ..., Vitoon Uthaisangsuk

Other articles from this issue

[Effect of SnO₂ reinforcement on creep propert...](#)

Materials Today: Proceedings, Volume 5, Issue 3, ...

Download PDF [View details](#)

[Physical water model and CFD studies of fluid...](#)

Materials Today: Proceedings, Volume 5, Issue 3, ...

Download PDF [View details](#)

[Flow prediction in the multi-strand continuous ...](#)

Materials Today: Proceedings, Vo...

Download PDF [View detail](#) [Feedback](#)



Available online at www.sciencedirect.com

ScienceDirect

Materials Today: Proceedings 5 (2018) 9281–9289

materialstoday:
PROCEEDINGS

www.materialstoday.com/proceedings

The 10th Thailand International Metallurgy Conference (The 10th TIMETC)

Wear behaviour of hardfacing on 3.5% chromium cast steel by submerged arc welding

Hein Zaw Oo, Prapas Muangjunburee*

** Department of Mining and Materials Engineering, Faculty of Engineering, Prince of Songkla University, Hat Yai, Songkhla, Thailand, 90112.*

Abstract

The principal objectives of this research are to improve the wear behaviour of hardfacing deposits made onto 3.5% chromium cast steel plate using submerged arc welding (SAW) process and discover the wear behaviour of hardfacing deposits. Austenitic stainless steel type and martensitic steel type electrodes were chosen as buffer and hardfacing electrodes respectively. In this study, four different kinds of welding parameters were conducted. Preheating temperature of the base metal before welding was fixed 350°C for all samples. In both AC and DC+ polarity welded samples, the microstructure in the single layer hardfacing showed a combination of massive austenite phases and a small amount of martensite phase because of dilution effect of the austenitic buffer layer, whereas that of three layers hardfacing resulted in fully martensitic phase with some retained austenite. Abrasive wear resistance of three layers hardfacing deposits was totally higher than that of the single layer for both AC and DC+ polarity. The best condition of hardness and wear resistance was observed three layers hardfacing sample welded with AC polarity.

© 2018 Elsevier Ltd. All rights reserved.

Selection and/or Peer-review under responsibility of The 10th Thailand International Metallurgy Conference.

Keywords: Hardfacing; Submerged arc welding; 3.5% Chromium steel; Abrasive wear

1. Introduction

Hardfacing has become an issue of powerful advancement related to wear resistant application as it can boost the service life of the engineering components. Welding hardfacing has been usually employed to improve the wear

* Corresponding author. Tel.: +66 7 428 7322; fax: +66 7 455 8834.

E-mail address: prapas.m@psu.ac.th

2214-7853 © 2018 Elsevier Ltd. All rights reserved.

Selection and/or Peer-review under responsibility of The 10th Thailand International Metallurgy Conference.

resistance in the sugar industry, agricultural, mining and other to increase hardness and wear resistance of the mechanical components [1]. Several welding techniques such as oxyacetylene gas welding (OAW), gas metal arc welding (GMAW), shielded metal arc welding (SMAW) and submerged arc welding (SAW) can be used for hardfacing. The important differences among these techniques lie in the welding efficiency, the weld plate dilution and the manufacturing cost of welding consumables [2]. The submerged arc welding process is commonly used for repairing surface by welding hardfacing due to its easy applicability, high current density and its ability to deposit multiple filler wire at the same time, especially in restoration of worn parts, which is of great importance to manufacturers [3]. The successful application of a welding the process mainly depends on the effective understanding of the temperature distribution in the weldment that can be helpful to estimate the evolution of the metallurgical microstructures and its subsequent influence on the mechanical properties [4].

Choice of the welding consumables and a welding procedure are first done in preparing the hardfacing deposits [5]. Iron-based hardfacing alloys are widely applied because they are reasonably inexpensive and easy to use. In the iron-based hardfacings, there are many microstructures and wide differences in composition that provide different abrasion wear resistance [6]. Kotecki and Ogborn [7] claimed that microstructure is the most important factor for wear resistance. According to John J. Coronado et al [1], the high welding dilution levels reduced wear resistance of hardfacing when only one layer was deposited and abrasion resistance increased with the number of hardfacing layers applied. In addition, a buffer layer that is used as intermediate deposits between the base material and the actual hardfacing weld metal is very important for bonding with base metal, reducing stress and avoiding cracks [8].

The surfaces of components are damaged by heavy impacts and scratching of hard abrasives trapped between the contacting surfaces during the wear [9]. Generally, worn tool and machine surfaces due to impact and abrasive wear are refurbished using austenitic stainless-steel type buffer layer with good ductility and toughness to withstand impact wear, and martensitic steel type hardfacing which is hard and strong enough to resist abrasive wear. Therefore, the wear resistance of a hardfaced 3.5% Cr steel single roll coal crusher from Mae Moh lignite mine was investigated by determining the metallurgical properties (macro/microstructural analysis), mechanical properties (microhardness) and wear behaviour (abrasive wear test) in different layers of hardfacing (single and three layers), applied using different types of polarity: (AC and DC+) in submerged arc welding process.

2. Experimental

2.1. Materials and welding procedures

Austenitic stainless-steel type wire electrode for buffer and martensitic steel type electrode for hardfacing were used onto 3.5% Cr steel plate as the base metal. The dimensions of base metal plates in this research measured 250 mm × 75 mm × 20 mm for all conditions. The chemical composition of base metal can be seen in Table 1. The chemical composition of wire electrodes and flux used for submerged arc welding are given in Table 2 and 3. The buffer and hardfacing layers were deposited in the flat position using twin-wire submerged arc welding process. Welding voltage, travel speed, the diameter of the electrode, electrode stick-out and preheating temperature of base metal before welding were fixed in all conditions. After welding, the samples for all conditions were cooled in air.

Table 1. Chemical composition of 3.5% Cr steel plate (wt.%).

C	Si	Mn	Ni	Cr	Mo	Cu	Fe	Hardness
0.38	0.40	0.52	0.17	3.42	0.30	0.04	Bal	200HV

Table 2. Chemical composition of Hardfacing electrode (Martensitic) and buffer electrode (Austenitic) (wt.%).

Electrode	C	Si	Mn	Cr	Ni	Fe	Hardness
Hardfacing	0.5	2.5	1.5	8.5	-	Bal	520HV
Buffer	0.1	0.5	6	19	9	Bal	235HV

Table 3. Chemical composition of Flux for Submerged Arc Welding (EN 760: S A FB 2 65 DC H5).

SiO ₂ +TiO ₂	CaO + MgO	Al ₂ O ₃ + MnO	CaF ₂
18	35	23	22

Four different kinds of 3.5% Cr steel coupons were designed to weld hardfacing deposits by twin-wire submerged arc welding (SAW - Twin wire) equipment, as illustrated in Fig. 1. Each sample was varied in number of hardfacing layers (single layer and three layers) and type of welding polarity (AC/DC+). Single layer buffer deposit was used for all conditions. The buffer layer and hardfacing layers are only different from the type of welding electrode used and the other parameters were completely same. Preheating temperature of the base metal before welding was fixed 350°C for all conditions. The diameter of tubular wire electrode and wire electrode stick out were 2.4 mm and 25.4 mm. The variable conditions and important fixed parameters of this work are presented in Fig 1 and Table 4.

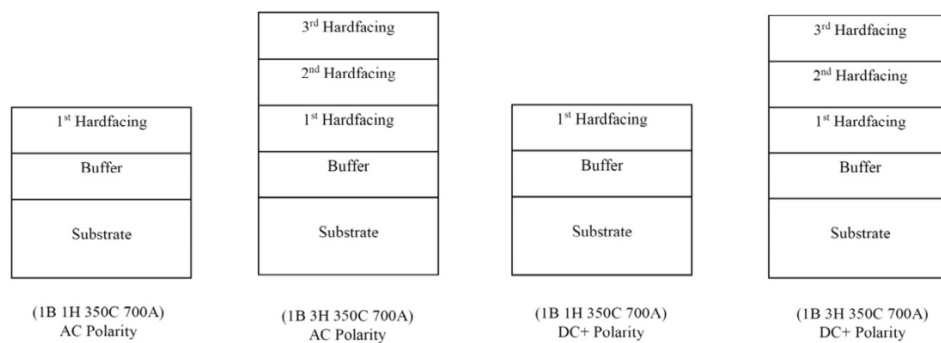


Fig. 1. Design of experiment for four coupons.

2.2. Macrostructural and microstructural characterization

Specimens for macro/microstructural examination were cut out from the hardfacing steel plate and then grounded and polished. After being metallographically polished, the specimens were all etched base metal and HAZ with 2% Nital solution for 6 sec. Hardfacing layers and buffer layer were etched with Villera's reagent for 15 secs and 30 secs respectively. The macroscopy and microscopy characterization for all conditions were performed using an Optical microscope (OM). For microscopic examination, both the cross-section and top surface of hardfacing samples were observed.

2.3. Hardness testing

The microhardness distribution across the cross section of samples between the base metal and hardfacing layers, including base metal, heat affected zone (HAZ), the buffer layer and hardfacing layers were recorded by using a Vickers hardness tester. For the hardness testing, the load was 0.2 kg (1961 N), dwell time was 10 secs and the distance between each point was 0.25 mm. Comparison between the microhardness evolution of AC and DC+ polarity for single layer and three layers were studied.

2.4. Abrasive wear test

The dry sand rubber wheel apparatus according to Procedure "A" of ASTM G65 was used for testing and measuring the abrasive mass loss of hardfacing layers. In accordance with that ASTM standard, the standard size specimens with 14 mm × 25.4 mm × 74.6 mm dimensions were cleaned and weighted on an electric balance with an accuracy of ± 0.1 mg. Round quartz sand size of range from 212 to 300 μm was applied as abrasive particles. The applied load and flow rate of sand were fixed 130N and 300 g/min. Rubber wheel rotation speed during running the

machine, the diameter of the wheel and a total distance of wheel rotation were 200 rpm, 228.6 mm and 4309 m respectively. After running the machine, the mass loss of specimens was measured and recorded on an electric balance again, and then compared to the original weight of specimens and weight of tested specimens.

Table 4. Fixed parameters of the research.

Wire	Current (A)	Voltage (V)	Travel speed (cm/mm)	Heat Input (KJ/cm)
Hardfacing	700	30	60	21
Buffer	700	30	60	21

3. Results and discussion

3.1. Macroscopy and microscopy analysis results

The microstructure of base metal (3.5% Cr Steel) is shown in Fig. 2. Ferrite, pearlite and bainite microstructure are involved.



Fig. 2. Microstructure of base metal (3.5% Cr Steel).

The macrostructural and microstructural evolution of heat affected zone (HAZ), the buffer layer and hardfacing layer for both AC and DC+ polarity are shown in Fig 3 and 4. The macrostructure of all specimens shows no welding defects inside the cross-section of weld metal and good bonding of each layer. The microstructure of the heat affected zones revealed needle shape martensite with austenite phase in both single and three layers hardfacing applied using different polarities, see Fig 3 (C) and Fig 4 (C), Fig 3 (H) and Fig 4 (H). Heat affected zone (HAZ) microstructure of three layers hardfacing revealed the bigger martensite phase than that of the single layer. Fig 3 (B) and Fig 4 (B) show microstructure of buffer layer for single layer hardfacing and Fig 3 (G) and Fig 4 (G) showed microstructure of buffer layer for three layer hardfacing. The buffer microstructure for all conditions exhibited austenite phase with grain boundaries because austenitic stainless-steel wire electrode was used for this layer. For first hardfacing layer, Fig 3 (A) and Fig 3 (F) show microstructure of the sample welded with DC+ polarity and then Fig 4 (A) and Fig 4 (F) show microstructure of the sample welded with AC polarity as well. Although martensitic steel type electrode was used for all hardfacing layers, the microstructure of the first hardfacing layer showed huge austenite phase (white region) with a small amount of martensite (black region), as the first hardfacing layer had higher welding dilution with the austenitic buffer layer. Comparison of the microstructure of single layer and the first hardfacing from three layers hardfacing with different polarities, grain boundaries of the first hardfacing from three layers' micrograph were a bit coarser than single layer micrograph owing to the different cooling rate. Fig 3 (E) and Fig 4 (E) are microstructure of second hardfacing layer for AC and DC+. Fig 3 (D) presents micrograph of the third hardfacing for the sample welded with DC+ polarity and Fig 4 (D) shows third hardfacing micrograph for the sample welded with AC polarity. Both AC and DC+ polarity, the microstructure of third hardfacing layer revealed the large martensite phase with a small amount of retained austenite in the grain boundary. The reason why retained austenite grain was produced in the martensite microstructure is that the third layer was deposited onto the second layer, which was still at high temperature and formed a slow cooling rate. Despite preheating before welding, this process was only done on the base metal plates because the preheating temperature was calculated by the

chemical composition of the base metal used. Therefore, in this research, the preheating process cannot control the temperature and cooling rate of hardfacing layers. Comparing to the microstructure of AC with DC+ polarity, second and third hardfacing microstructure of AC resulted in the slight larger martensite phase than that of DC+.

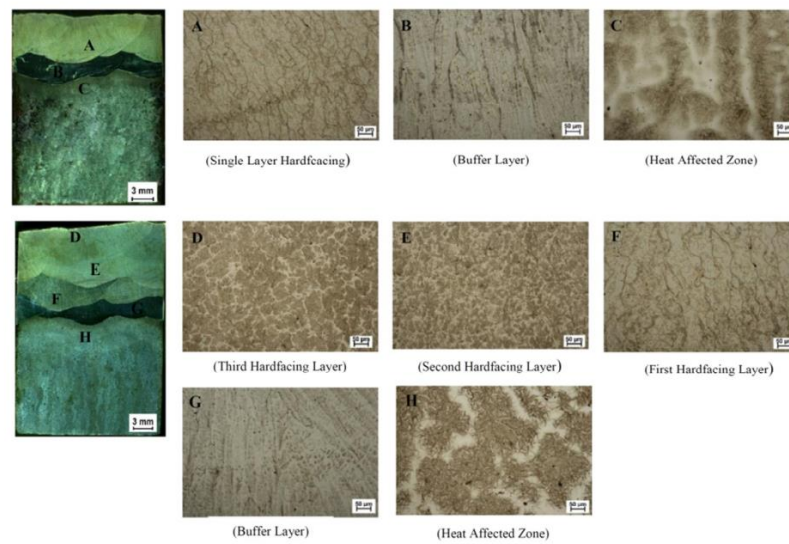


Fig. 3. Macrostructure and Microstructure of single layer and three layers hardfacing welded with DC+.

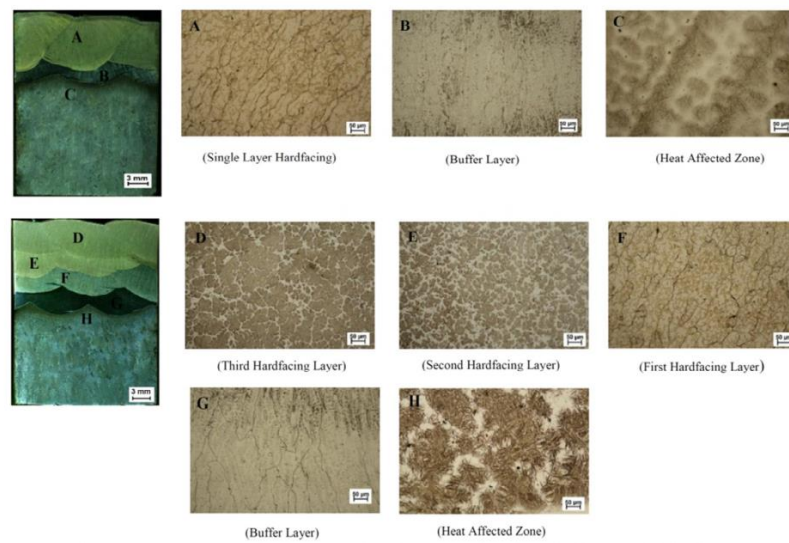


Fig. 4. Macrostructure and Microstructure of single layer and three layers hardfacing welded with AC.

In Fig 5 and Fig 6, the microstructure of hardfacing top surface for single and three layers are presented. Fig 5 (a) and Fig 6 (a) show single and three layers hardfacing top surface micrograph of the sample welded with DC+ polarity, while Fig 5 (b) and Fig 6 (b) show microstructure of top surface for the sample applied in AC polarity for single and three layers. For the single layer hardfacing surface, Fig 5 (a) shows microstructure of the sample welded with DC+ and Fig 5 (b) shows microstructure of the sample welded with AC. The microstructure of single layer top surface for both AC and DC+ polarity is very similar and shows massive austenite phase with a small amount of martensite in the grain boundaries. Fig 6 (a) and (b) represent three layers hardfacing top surface microstructure for DC+ and AC. A couple of microstructure for three hardfacing top surface show martensite microstructure surrounded by retained austenite phase. However, the martensite phase in the top surface microstructure of the sample welded with AC is coarser than that of DC+ sample like the microstructural results of the cross section.

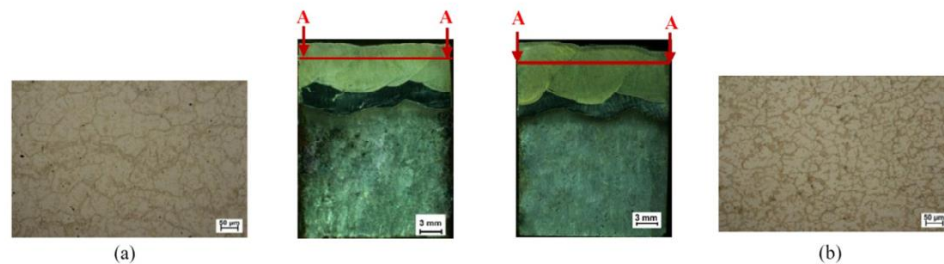


Fig. 5. Microstructure of top surface for single layer (a) for DC+ and (b) for AC.

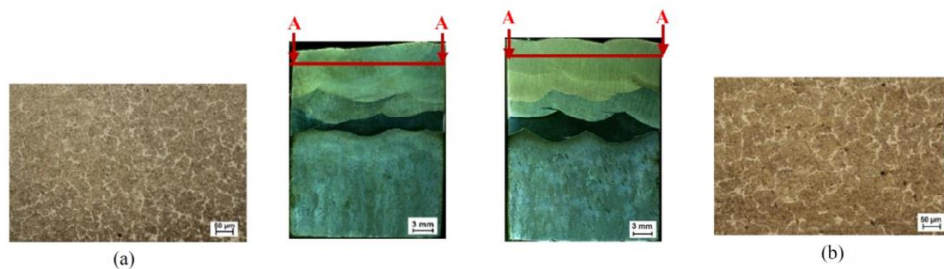


Fig. 6. Microstructure of top surface for three layers (a) for DC+ and (b) for AC.

3.2. Hardness profile

Single layer hardness evolution through base metal, heat affected zone (HAZ), the buffer layer and hardfacing layer comparing AC and DC+ polarity is shown in Fig 7. The hardness value of the base metal is about 200 HV. Though the average hardness value of heat affected zone for samples welded with AC is as high as that of the sample welded with DC+ because of containing the needle shape martensite phase, a single layer hardness value of HAZ in the DC+ welded sample is higher than that of AC sample. Moreover, the buffer layer hardness value of the sample welded with DC+ is higher and wider distance (about more 1mm than AC sample) in the graph. It means that single layer hardfacing of DC+ sample has higher dilution with buffer. In general, it can be conjectured that some points of hardness profile for the upper part of single layer welded with AC are higher hardness than that of the other, but the overall trend of single layer hardness distribution for both samples are nearly identical with many fluctuations nonetheless. Additionally, hardness distribution of three layers hardfacing for different polarities between the base metal and the third hardfacing layer is also given. In three layers, hardness value of the base metal, heat affected zone (HAZ), the buffer layer and the third hardfacing layer is virtually similar. However, hardness

profile of first layer and second layer of three layers hardfacing for AC and DC+ is slightly dissimilar. As can be clearly seen in Fig 8, the all-round hardness values of first layer, second layer and some points of third layer for the sample welded with AC are higher than that of the sample welded with DC+.

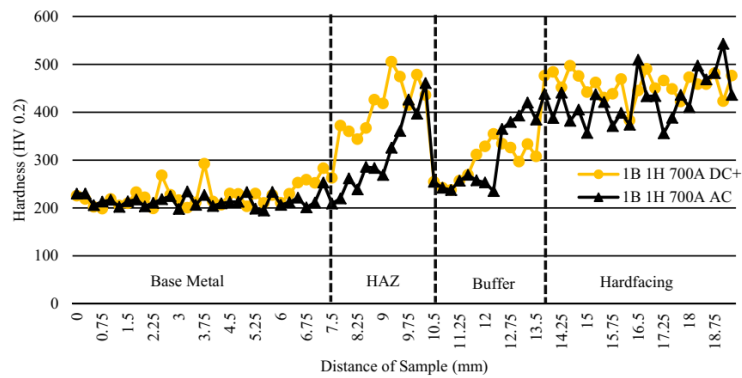


Fig. 7. Hardness distribution for single layer hardfacing.

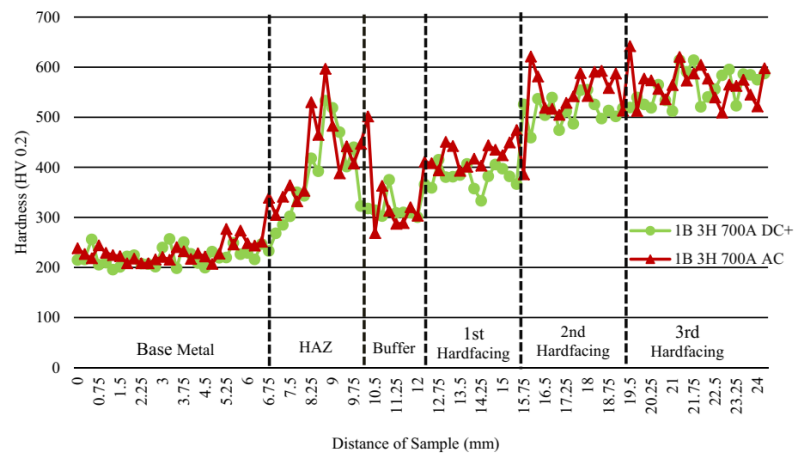


Fig. 8. Hardness distribution for three layers hardfacing.

3.3. Abrasive wear test results

Fig 9 shows the average mass loss value of the four specimens with a different number of layers and different type of polarity used. In this study, the wear resistance is determined by the average mass loss of the specimens, which means the difference between the weight of original specimens and the tested specimens. In the specimens, higher the mass loss indicates lower the wear resistance. Wear resistance of single layer hardfacing is obviously

lower than three layers hardfacing because the mass loss data for single layer hardfacing is completely higher than three layers hardfacing. This is because all single layer micrographs indicate the larger austenite phase, which has lower hardness and soft property, on the one hand, each three layers micrograph shows the huge martensite phase with small amount of retained austenite phase, which is hard and strong enough. Single layer hardfacing causes higher dilution with austenitic buffer layer and three layers hardfacing may only dilute with the martensitic second hardfacing layer. Therefore, single layer hardfacing shows bigger austenite phase than three layers hardfacing for both polarities. This reason can clearly explain that the three layers revealed lower mass loss than the single layer. Furthermore, John J. Coronado et al [1] also concluded that no relation was found between hardness and the abrasive wear resistance because microstructure was more important than hardness in the abrasion resistance of the deposits. Abrasive mass loss of single layer hardfacing of each specimen is quite alike. Comparing to wear resistance of three layers hardfacing for dissimilar polarity used, mass loss of the sample welded with AC is lower than that of the sample welded with DC+; in other words, wear resistance of three layers hardfacing welded with AC is a peak among the others. It means that the wear resistance of the three-layered sample welded with AC polarity is the best condition because of its microstructure, which shows the huge martensite phase. Chatterjee et al [10] studied that hardness can only give a rough estimation but not an exact prediction of chemical composition and microstructure of the hardfacing deposits are more relevant to the improvement of abrasion resistance than hardness is. Therefore, the hardness value of three layers hardfacing for both samples shows almost equal. Nevertheless, wear resistance of three layers hardfacing sample with AC presents apparent quality comparing to the sample with DC+.

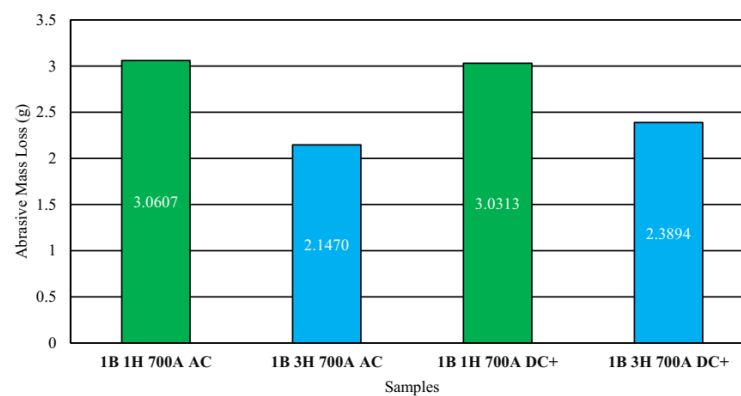


Fig. 9. Wear resistance of four samples.

4. Conclusions

The following conclusions are drawn from the above study:

1. Microstructural results are almost similar, but microstructure of three layers hardfacing welded with AC polarity shows a slight bigger martensite phase than that of DC+ polarity for both cross-section and top surface.
2. Hardness values of AC polarity are slightly higher than that of DC+ polarity in both single and three hardfaced layers.
3. Mass loss data of three layers welded with AC is lower than that of three layers welded with DC+.
4. Based on the overall results, three layers hardfacing welded with AC polarity (1B 3H 350 AC 700A) is the best condition in the research.

Acknowledgments

The authors would like to be grateful to Scholarship Award of Thailand's Education Hub for Southern Region of ASEAN Countries (TEH-AC) for fully financial aid, and then, Department of Mining and Materials Engineering, Faculty of Engineering, Prince of Songkhla University, Hat Yai Campus, Thailand for supporting equipment and many facilities, and finally, Electricity Generating Authority of Thailand (EGAT), Mae Moh Lignite Mine, Thailand for some data of this research.

References

- [1] J. J. Coronado, H. F. Caicedo, A. L. Gómez. The Effect of Welding Process on Abrasive Wear Resistance for Hardfacing Deposits. *Tribology International*. 42 (2009) 745-749
- [2] W. Wo, L.T. Wu. The Wear Behavior Between Hardfacing Materials. *Metall. Mater. Trans. A* 27A (1996) 3639–3648.
- [3] B Gulenc, N Kahraman. Wear Behaviour of Bulldozer Rollers Welded using a Submerged Arc Welding Process. *Materials and Design*. 24 (2003) 537–542.
- [4] D. V. Kiran, J. Cheon, N. Arif, H. Chung, S. J. Na. Three-dimensional Finite Element Modelling of Pulsed AC Gas Metal Arc Welding Process. *Int. J. Adv. Manuf. Technol.* 86 (2016) 1453–1474.
- [5] R.J. Dawson, S. Shewchuk, J.E. Pritchard. Selection and Use of Hardfacing Alloys. *Weld. J.* 61 (11) (1982) 15–23.
- [6] M. Morsy, E. El-Kashif. The Effect of Microstructure on High-Stress Abrasion Resistance of Fe-Cr-C- Hardfacing Deposits. *Weld World*. 58 (2014) 491-497.
- [7] D. J. Kotecki, J. S. Ogborn. Abrasion Resistance of Iron-Based Hardfacing Alloys. *Welding Journal* 74(8) (1995) 269-288.
- [8] *Repair and Maintenance Welding Handbook*. second ed., ESAB.
- [9] C. Wang, X. Li, Y. Chang, S. Han, H. Dong. Comparison of Three-body Impact Abrasive Wear Behavior for Quenching-Partitioning-Tempering and Quenching-Tempering 20Si2Ni3 steels. *Wear*. 362-363 (2016) 121-128.
- [10] S. Chatterjee, T.K. Pal. Wear behaviour of Hardfacing Deposits on Cast Iron. *Wear*. 255 (2003) 417 -425.

2018 5th International Conference
on Business and Industrial Research

ICBIR 2018

Smart Technologies

for Next Generation
of Informatics, Engineering, Business and Social Sciences

17-18 MAY, 2018

Thai-Nichi Institute of Technology, Bangkok, Thailand

TOYOTA
mobility of happiness

SCG

POWER OF INNOVATION
FOUNDATION

DENSO
Crafting the Core

amazing
THAILAND

www.tni.ac.th

ISBN : 978-1-5386-5253-4

Effects of The Austenitic Buffer Layer on Abrasive Mass Losses of Alloys Hardfaced with A Martensitic Layer Using Submerged Arc Welding

Hein Zaw Oo

Department of Mining and Materials Engineering
Faculty of Engineering, Prince of Songkla University
Songkhla, Thailand
heinzawoo93@gmail.com

Prapas Muangjumburee

Department of Mining and Materials Engineering
Faculty of Engineering, Prince of Songkla University
Songkhla, Thailand
prapas.m@psu.ac.th

Abstract— The focus of this research is to investigate the effects of the buffer layer on the wear resistance of hardfaced alloys. Martensitic steel wire electrode was used for the hardfacing layer and austenitic steel wire electrode was applied to the buffer layer. Four samples with or without buffer layer were deposited using twin-wire submerged arc welding process with two-different currents. All samples were preheated to 350°C prior to welding, and a single layer of hardfacing was applied. An optical microscope was used to examine the microstructure of deposits. The hardness distributions were determined using a Vickers' hardness tester and wear tests were done following ASTM G65 Standard (Dry sand rubber wheel machine). Data showed that the austenitic buffer layer was mixed with martensitic hardfacing due to the weld dilution. The abrasive mass losses of the samples without buffer layer were higher than that of the samples with the buffer layer.

Keywords—buffer; hardfacing; abrasive mass loss; ASTM G65; submerged arc welding

I. INTRODUCTION

Wear is one of the most commonly encountered problems in the industry which requires frequent replacement of components [1]. Hardfacing is commonly employed to increase the wear and corrosion resistance of components exposed to severe service conditions, thus extending their service lives. [2-4]. Hardfacing is widely used to improve hardness and wear resistant of engineering components in numerous industries [5]. The hardfacing technique is the best effective method to protect against wear problem [6]. The application of a hard, wear-resistant surface coating of various metals or alloys on a metallic substrate by weld deposition is one of the versatile and inexpensive techniques, especially when these components are large or expensive [7].

Welding is a key technology to apply hardfacing alloys [8]. Several welding techniques such as oxyacetylene gas welding (OAW), gas metal arc welding (GMAW), shielded metal arc welding (SMAW) and submerged arc welding (SAW) can be deposited with a solid or cored wire electrode for hardfacing. [9]. The submerged arc welding process is commonly used for repairing surface by welding hardfacing due to its easy applicability, high current density and its ability to deposit multiple filler wires at the same time, especially in the restoration of worn parts, which is of great importance to

manufacturers [10,11]. A twin-wire arc mode is generally applied to increase deposition rate of hardfacing layer [11].

The surfaces of components are damaged by heavy impacts and scratching by hard abrasives trapped between the contacting surfaces during the wear [12]. Generally, worn tool and machine surfaces due to impact and abrasive wear are refurbished using austenitic stainless-steel type buffer layer with good ductility to withstand impact wear, and martensitic steel type hardfacing which is hard and strong enough to resist abrasive wear. The concern is the effect of weld dilution on the austenitic buffer. The objective of this paper is to study the effect of the austenitic buffer layer on a martensitic hardfacing layer by determining microstructures, hardness and abrasive wear mass loss.

II. EXPERIMENTAL

A. Materials and welding procedures

Martensitic steel type wire electrode was used in the submerged arc welding to deposit a hardfacing layer onto the low alloy base steel plate. For the samples with the buffer layer, austenitic stainless-steel type wire electrode was welded onto the base steel plates prior to application of the hardfacing layer. The dimension of all base metal plates used in this research was 12.5 cm × 7.5 cm × 2 cm. The chemical composition of the base steel plate and wire electrodes are given in Table I. All welded layers were deposited in the flat position using twin-wire submerged arc welding process. Welding voltage, travel speed, the diameter of the electrode, electrode stick-out and preheating temperature of base metal before welding were identical for all samples. After welding, all the samples were cooled in air.

Four coupons of low alloy steel base metal were hardfaced, with and without buffer layer using twin-wire submerged arc welding equipment. Preheating temperature of the base metal before welding was kept constant at 350 °C for all welding conditions. The diameter of tubular wire electrode and wire electrode stick out were 2.4 mm and 25.4 mm.

Direct current electrode positive (DCEP) polarity was applied in all experiments. Welding voltage and travel speed during welding were fixed at 30 V and 60 cm/min respectively.

TABLE I. THE CHEMICAL COMPOSITION OF BASE METAL AND ELECTRODES (WT%)

Elements	Base Metal	Hardfacing	Buffer
C	0.38	0.5	0.1
Si	0.40	2.5	0.5
Mn	0.52	1.5	6
Ni	0.17	-	9
Cr	3.42	8.5	19
Mo	0.30	-	-
Cu	0.04	-	-
Fe	Bal	Bal	Bal

TABLE II. STANDARD PARAMETERS OF ASTM G65 (DRY SAND RUBBER WHEEL MACHINE)

ASTM G65 Parameters	Values
Procedure	A
Round quartz sand size (μm)	212-300
Applied load (N)	130
Sand flow rate (g/min)	300
Rubber wheel rotation speed (rpm)	200
Wheel diameter (mm)	228.6
Wheel rotation distance (m)	4309

B. Microstructural characterization

Microstructural specimens were prepared from the welded samples. After grinding and polishing with metallographic sandpapers from 80 grits to 800 grits and final polishing with 5-micron alumina solution, the hardfacing layer was etched for 15 seconds and buffer layer for 30 seconds using Villera's reagent. The microstructures obtained in all the samples were examined using an optical microscope (OM). The structures seen on both the cross-sections and top surfaces of the hardfaced samples were recorded.

C. Hardness testing

Vickers' hardness tester was used. The load was set at 0.2 kg, dwell time was set at 10 seconds with the distances between each point was set at 0.25 mm. The microhardness profiles were obtained across the cross sections of samples from base metal, heat affected zone (HAZ), the buffer layer and the hardfacing layers were recorded. The cross-sectional microhardness values of the samples welded with and without a buffer layer applied to different welding currents were compared.

D. Abrasive wear test

The dry sand rubber wheel test following ASTM G65 standard was carried out using standard size specimens of 14 mm \times 25.4 mm \times 74.6 mm. First, wear specimens were

cleaned and weighted on an electric balance with an accuracy of ± 0.1 mg. After the tests, the mass loss of specimens was measured and recorded on an electric balance again, and then compared to their original weight to get the abrasive mass loss of hardfacing layers to determine the wear resistance of applied hardfacing. Details of the wear test procedure used are presented in Table 2.

III. RESULTS AND DISCUSSION

A. Microstructural characterization

The transverse cross-sectional microstructures of the hardfacing layer obtained from the samples welded using different currents with and without buffer layer are shown in "Fig. 1". "Fig. 1(a)" and "Fig. 1 (b)" depict hardfacing microstructure of the samples deposited without a buffer. Fully martensite phase with a small amount of retained austenite phase can be seen in the microstructure of the sample without buffer, while the microstructure of the sample with buffer revealed a large amount of austenite phase with a matrix of martensite phase in "Fig. 1(c)" and "Fig. 1 (d)". It indicates that the austenitic buffer layer mixed with martensitic hardfacing layer due to significant high dilution of austenite into martensite. This weld dilution is defined as the percent ratio of the area of melted base metal to the area of weld metal. [13]. The microstructure of buffer layer shows austenite phase in the grain boundaries in "Fig. 2", as austenitic steel type filler was deposited for this layer. "Fig. 2(a)" shows the microstructure of the sample welded using 500A and "Fig. 2(b)" shows the microstructure of the sample welded using 600A. The austenite phase in "Fig. 1(c)" and "Fig. 1 (d)" displays due to the dilution effect of "Fig. 2(a)" and "Fig. 2(b)".

B. Hardness

Hardness distributions between the base metal and hardfacing layer comparing with four different conditions are presented in "Fig 3". The hardness of low alloy steel base metal presents about 190 HV. Buffer layer hardness shows the values between 230 HV and 330 HV. Hardness values of the sample without buffer showed higher than that of the sample with buffer. These two samples revealed fully martensite phase in the hardfacing microstructure and martensite microstructure gives very high hardness [14]. On the other hands, lower hardness values have presented the results of the sample with buffer. The rate of dilution significantly influences the chemical composition of the hardfacing [15]. The average hardness values for the samples without buffer layer presented about 730 HV and the average hardness profiles of the samples with buffer layer showed about 430 HV. The different hardness between the sample with buffer layer and without buffer is approximately 300 HV and this gap of hardness is very high. Hardness values vary in the amount of martensite revealed in micrographs. Among them, the sample welded using 500A without buffer showed the highest hardness values, whereas the lowest hardness results can be seen in the samples deposited using 600A with buffer.

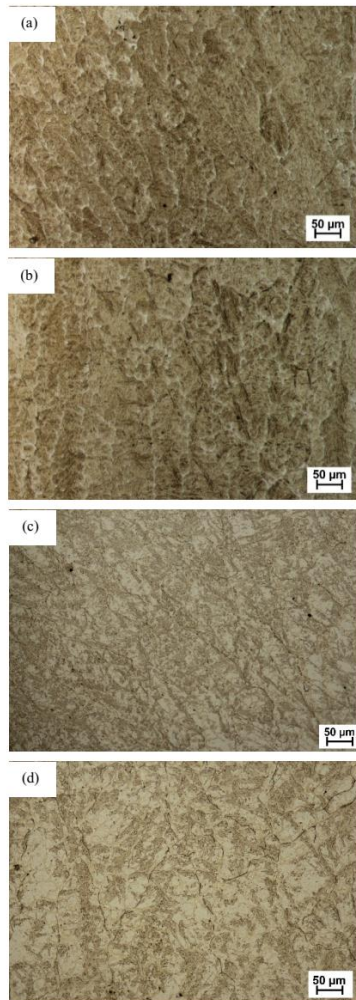


Fig. 1. Microstructure of the cross-sectional hardfacing layer (a) 0B 1H 500A (b) 0B 1H 600A (c) 1B 1H 500A (d) 1B 1H 600A

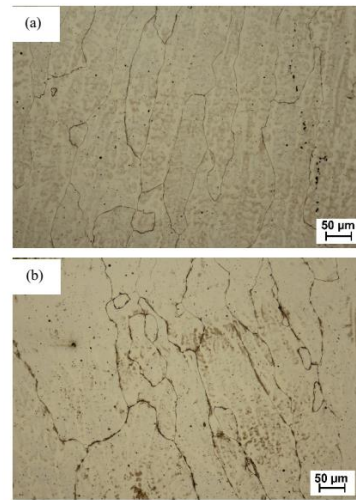


Fig. 2. Microstructure of the buffer layer (a) 1B 1H 500A (b) 1B 1H 600A

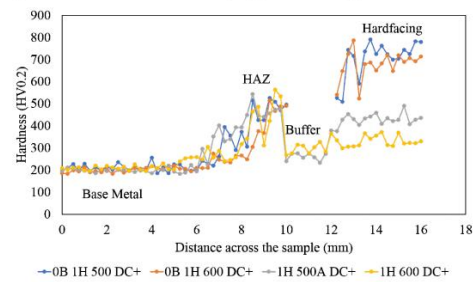


Fig. 3. Hardness profiles across the samples

C. Abrasive wear mass loss

Abrasive wear mass loss results of all experiments are shown in Table 4. Abrasive mass loss of the sample without a buffer is very lower and the different mass loss between the sample with and without a buffer is about 1 gram.

The highest weight loss was tested in the sample welded using 600A with buffer because this sample showed the highest amount of retained austenite phase contained in the micrograph and lowest hardness. The retained austenite is a ductile phase that can easily be cut by abrasive particle [16]. It can clearly say that the amount of martensite and hardness reflect the abrasive mass of hardfacing. The lowest mass loss values can be seen in the results of the sample welded using 500A without a buffer.

TABLE III. ABRASIVE MASS LOSS OF THE SAMPLES

Name of Specimens	Initial Weight (g)	Final Weight (g)	Mass Loss (g)
0B 1H 500A	179.7484	177.8266	1.9218
0B 1H 600A	181.9372	180.0036	1.9336
1B 1H 500A	182.9022	180.0294	2.8728
1B 1H 600A	183.3483	180.1559	3.1924

IV CONCLUSIONS

The microstructure, hardness and abrasive wear mass loss were investigated. The following conclusions are drawn from the experimental results:

1. Martensite microstructure influences the hardness and wears resistance.
2. Welding dilution affects the microstructure of hardfacing deposits.
3. The amount of martensite phase in the microstructure and hardness of deposits are very important factors to investigate the abrasive wear mass loss.
4. Austenitic buffer layer was diluted with the martensitic hardfacing and to reduce hardness and wear resistance. On the other hands, austenitic steel has a good impact wear resistance.
5. Using two or more hardfacing layers is the best way to avoid the dilution effect of buffer and to get the expected microstructure, hardness and wear resistance.

ACKNOWLEDGMENTS

This work was supported by the Higher Education Research Promotion and Thailand's Education Hub for Southern Region of ASEAN Countries Project Office of the Higher Education Commission. The authors are grateful to Department of Mining and Materials Engineering, Faculty of Engineering, Prince of Songkhla University, Hat Yai Campus, Thailand.

REFERENCES

- [1] M. Shamanian, S.M.R. Mousavi Abarghouie, and S.R. Mousavi Pour, "Effects of surface alloying on microstructure and wear behavior of ductile iron." *Mater. Des.*, vol. 31, pp. 2760-2766, June 2010.
- [2] Hong-Xia Deng, Hui-Ji Shi, Seiji Tsuruoka, Hui-Chen Yu, and Bin Zhong, "Influence of welding technique and temperature on fatigue properties of steel deposited with Co-based alloy hardfacing coating." *Int. J. Fatigue*, vol. 35, pp. 63-70, January 2012.
- [3] R. Puli, and G.J. Ram, "Microstructures and properties of friction surfaced coatings in AISI 440C martensitic stainless steel." *Surf. Coat. Technol.*, vol. 207, pp. 310-318, August 2012.
- [4] K. Yang, Y. Gao, K. Yang, Y. Bao, and Y. Jiang, "Microstructure and wear resistance of Fe-Cr13-C-Nb hardfacing alloy with Ti addition." *Wear*, vol. 376, pp. 1091-1096, April 2017.
- [5] X. Shule, Y. Shengfu, D. Yu, D. Minghui, and Y. Lu, "Effect of cerium on abrasive wear behaviour of hardfacing alloy." *J. Rare Earths*, vol. 30, pp. 69-73, January 2012.
- [6] D. Li, Y. Yang, L. Liu, J. Zhang, and Q. Yang, "Effects of RE oxide on the microstructure of hardfacing metal of the large gear." *Mater. Sci. Eng., A*, vol. 509, pp. 94-97, May 2009.
- [7] X. H. Wang, Z. D. Zou, S. Y. Qu, and S. L. Song, "Microstructure and wear properties of Fe-based hardfacing coating reinforced by TiC particles." *J. Mater. Process. Technol.*, vol. 168, pp. 89-94, January 2005.
- [8] M. Kirchgäßner, E. Badisch, and F. Franek, "Behaviour of iron-based hardfacing alloys under abrasion and impact." *Wear*, vol. 265, pp. 772-779, August 2008.
- [9] R. Zahiri, R. Sundaramoorthy, P. Lysz, and C. Subramanian, "Hardfacing using ferro-alloy powder mixtures by submerged arc welding." *Surf. Coat. Technol.*, vol. 260, pp. 220-229, December 2014.
- [10] B. Gülenç, and N. Kahraman, "Wear behaviour of bulldozer rollers welded using a submerged arc welding process." *Mater. Des.*, vol. 24, pp. 537-542, July 2003.
- [11] R.S. Chandel, H.P. Seow, and F.L. Cheong, "Effect of increasing deposition rate on the bead geometry of submerged arc welds." *J. Mater. Process. Technol.* vol. 72, no. 1, pp. 124-128, December 1997.
- [12] C. Wang, X. Li, Y. Chang, S. Han, and H. Dong, "Comparison of three-body impact abrasive wear behaviors for quenching-partitioning-tempering and quenching-tempering 20Si2Ni3 steels." *Wear*, vol. 362, pp. 121-128, September 2016.
- [13] S.D. Borle, I. Le Gall, and P. F. Mendez, "Primary chromium carbide fraction control with variable polarity SAW." *Weld. J.*, vol. 94, pp. 1s-7s, January 2015.
- [14] S. Yamamoto, Arc welding of specific steels and cast irons, Shinko Welding Service, Japan, 2008.
- [15] K. Günther, J. P. Bergmann, and D. Suchodoll, "Hot wire-assisted gas metal arc welding of hypereutectic FeCrC hardfacing alloys: Microstructure and wear properties." *Surf. Coat. Technol.*, vol. 334, pp. 420-428, January 2018.
- [16] J.J. Coronado, H.F. Caicedo, and A.L. Gómez, "The effects of welding processes on abrasive wear resistance for hardfacing deposits." *Tribol. Int.*, vol. 42, no. 5, pp. 745-749, May 2009.

VITAE

Name Mr. Hein Zaw Oo

Student ID 5910120006

Educational Attainment

Degree	Name of Institution	Year of Graduation
Bachelor of Engineering (Metallurgy)	West Yangon Technological University	2015

Scholarship Awards during Enrolment

The Scholarship Awards for Master and Ph.D. Studies Thailand's Education Hub for Southern Region of ASEAN Countries (TEH-AC)

List of Publication and Proceeding

1. Hein Zaw Oo, Buntoeng Srikarun, and Prapas Muangjunburee, (2018). Correlating Hardness and Welding Dilution with the Abrasion Mass Loss of Hardfacings Welded with Different Currents and Polarities. *Metallurgist*, 1033-1037. <https://doi.org/10.1007/s11015-018-0604-3>
2. Hein Zaw Oo, and Prapas Muangjunburee, (2018). Wear behaviour of hardfacing on 3.5% chromium cast steel by submerged arc welding. *Materials Today: Proceedings*, 5(3), 9281-9289. <https://doi.org/10.1016/j.matpr.2017.10.101>
3. Hein Zaw Oo, and Prapas Muangjunburee, (2018). Effects of The Austenitic Buffer Layer on Abrasive Mass Losses of Alloys Hardfaced with A Martensitic Layer Using Submerged Arc Welding. *The 5th International Conference on Business and Industrial Research (ICBIR)*.